EXPERIMENTALLY AND THERMODYNAMIC ANALYSIS OF PV/T SYSTEMS USING HYBRID AND GRAPHENE NANOFLUIDS

Omran M. H. ALSHIKHI

2021
PhD THESIS
ENERGY SYSTEMS ENGINEERING

Thesis Advisor
Prof. Dr. Muhammet KAYFECİ

EXPERIMENTALLY AND THERMODYNAMIC ANALYSIS OF PV/T SYSTEMS USING HYBRID AND GRAPHENE NANOFLUIDS

Omran M. H. ALSHIKHI

T.C
Karabuk University
Institute of Graduate Programs
Department of Energy Systems Engineering
Prepared As
PhD Thesis

Thesis Advisor
Prof. Dr. Muhammet KAYFECİ

KARABUK
November 2021

I certify that in my opinion the thesis submitted by Omran M. H. ALSHIKHI titled "EXPERIMENTALLY AND THERMODYNAMIC ANALYSIS OF PV/T SYSTEMS USING HYBRID AND GRAPHENE NANOFLUIDS" is fully adequate in scope and in quality as a thesis for the degree of Doctor of Philosophy.

Prof. Dr. Muhammet KAYFECİ ……
Thesis Advisor, Department of Energy Systems Engineering

This thesis is accepted by the examining committee with a unanimous vote in the Department of Energy Systems Engineering as a Ph.D. thesis. November 9, 2021

Examining Committee Members (Institutions)		Signature
Chairman	: Prof. Dr. Fevzi BEDİR (GTU)	……..….....
Member	: Prof. Dr. Sezayi YILMAZ (KBU)	……...
Member	: Prof. Dr. Ali KEÇEBAŞ (MSKU)	……...
Member	: Prof. Dr. Kamil ARSLAN (KBU)	……...
Member	: Prof. Dr. Muhammet KAYFECI (KBU)	……...

The degree of Doctor of Philosophy by the thesis submitted is approved by the Administrative Board of the Graduate School of Natural and Applied Sciences, Karabük University.

Prof. Dr. Hasan SOLMAZ ……...
Head of Institute of Graduate Programs

"I declare that all the information within this thesis has been gathered and presented in accordance with academic regulations and ethical principles and I have according to the requirements of these regulations and principles cited all those which do not originate in this work as well."

Omran M. H. ALSHIKHI

ABSTRACT

Ph. D. Thesis

EXPERIMENTALLY AND THERMODYNAMIC ANALYSIS OF PV/T SYSTEMS USING HYBRID AND GRAPHENE NANOFLUIDS

Omran M. H. ALSHIKHI

Karabük University
Institute of Graduate Programs
Department of Energy Systems Engineering

Thesis Advisors:
Prof. Dr. Muhammet KAYFECİ
November 2021, 98 pages

Although significant studies and worthy achievements of utilized nanofluids in solar thermal systems, there is a need for more practical and theoretical studies to increase the general knowledge of the importance of using nanofluids specifically in solar systems. After reviewing many scientific researches, it became clear that increasing the performance of PV/T systems using nanofluids as coolant working fluids has gained the interest of researchers in about recent decades. However, there is a need to increase studies, especially experimental studies, in order for them to contribute to enriching investigations related to PV/T collectors. One sort of heat exchanger PV/T collector has been designed, constructed and outdoor tested in Karabuk, Turkey which called serpentine type heat exchanger (PV/Ts). The coolants used in this study are Hybrid nanofluid, and graphene nanoplatelets dispersed in water as a base fluid with a concentrations of 0.5 wt%. In this study.

Many experiments have been conducted with distilled water, Hybrid-water nanofluid, and graphene-water nanofluid at flow rates of 0.5 L/min. The results of these experiments revealed that the 0.5 L/min is the optimum flow rate for the system. Based on the results of 0.5 wt% nanofluid concentrations, the higher concentrations of nanofluids the better enhancement in PV/T electrical efficiency. Also, graphene nanoplatelets reveled better electrical efficiency increment and higher thermal efficiency. Based on energetic and exergetic comparison performed between distilled water, 0.5 wt% hybrid nanofluid and 0.5 wt% graphene nanoplatelets-water nanofluid coolants, adding thermal unit to PV module enhanced the overall energetic efficiency by 48.1% for distilled water, 53.5% for Hybrid nanofluids, and 55.8% for graphene-water. From the exergetic estimation, the increase in overall exergetic efficiency was 10.47%, 10.94, and 11.52% for PV/T collector cooled by distilled water, Hybrid-water nanofluid, and graphene-water nanofluid respectively.

Key Word : Photovoltaic/thermal system (PV/T), graphene nanoplatelets-water nanofluid, Hybrid nanofluid, Energy and exergy analysis.

Science Code : 92802

ÖZET

Doktora Tezi

HİBRİT VE GRAFEN NANO AKIŞKAN KULLANILAN PV/T SİSTEMLERİNİN DENEYSEL VE TERMODİNAMİK ANALİZİ

Omran M. H. ALSHIKHI

Karabük Üniversitesi
Lisansüstü Eğitim Enstitüsü
Enerji Sistemleri Mühendisliği Anabilim Dalı

Tez Danışmanı:
Prof. Dr. Muhammet KAYFECİ
November 2021, 98 Sayfa

Güneş enerjisi sistemlerinde kullanılan nanoakışkanlarla ilgili önemli çalışmalar ve değerli başarılar olmasına rağmen, nanoakışkanların özellikle güneş sistemlerinde kullanılmasının önemine ilişkin genel bilgileri artırmak için daha pratik ve teorik çalışmalara ihtiyaç vardır. Birçok bilimsel araştırmayı gözden geçirdikten sonra soğutucu çalışma sıvıları olarak nanoakışkanları kullanan PV/T sistemlerinin performansını artırmanın, yaklaşık son on yılda araştırmacıların ilgisini çektiği anlaşılmıştır. Ancak PV/T kollektörleri ile ilgili araştırmaların zenginleştirilmesine katkı sağlamak için özellikle deneysel çalışmaların arttırılmasına ihtiyaç vardır. Serpantin tipi ısı eşanjörü (PV/Ts) olarak adlandırılan bir tür ısı eşanjörü olan PV/T kollektörü Türkiye'nin Karabük ilinde tasarlanmış, inşa edilmiş ve dış ortamda test edilmiştir.Bu çalışmada kullanılan soğutucular, Hibrit nanoakışkan ve ağırlıkça %0.5 konsantrasyonlu bir baz akışkan olarak suda dağılmış grafen nanoplateletlerdir.

Damıtılmış su, Hibrit-su nanoakışkanı ve grafen-su nanoakışkanı ile 0,5 L/dk akış hızlarında birçok deneyler yapılmıştır. Bu deneylerin sonuçları sistem için en uygun akış hızının 0,5 L/dk olduğunu ortaya çıkarmıştır. Ağırlıkça %0.5 olan nanoakışkan konsantrasyonlarının sonuçlarına göre, nanoakışkanların daha yüksek konsantrasyonları PV/T elektrik verimliliğinde daha iyi artış sağlamıştır. Ayrıca, grafen nanoplateletler daha iyi elektriksel verimlilik artışını ve daha yüksek termal verimliği sağlamıştır. Damıtılmış su, ağırlıkça %0.5 olan hibrit nanoakışkan ve ağırlıkça %0.5 grafen nanoplatelet-su nanoakışkan olan soğutucular arasında gerçekleştirilen enerjik ve ekserjetik karşılaştırmaya dayalı olarak, PV modülüne termal ünite eklenmesi genel enerji verimliliğini damıtılmış su için %48,1, hibrit nanoakışkanlar için %53,5 ve grafen-su için %55.8 artırmıştır. Ekserjetik tahmine göre genel egzergetik verimdeki artış damıtılmış su, hibrit-su nanoakışkanı ve grafen-su nanoakışkanı ile soğutulan PV/T toplayıcı için sırasıyla %10.47, %10.94 ve %11.52 dir.

Anahtar Kelimeler : PV/T sistem, grafen nano pelet, Hibrit, nanoakışkanlar, enerji ve ekserji analizi, güneş enerjisi, termal verim.

Bilim Kodu **:** 92802

ACKNOWLEDGMENT

First and foremost, I feel always indebted to ALLAH, the kindest and most merciful, who gave me the ability and strength to complete this work.

I'd like to express my respectful thanks and profound gratitude to my supervisor Prof. Dr. Muhammet KAYFECİ. For his keen guidance, kind supervision, valuable advice and continuous encouragement, which made possible the completion of this work.

I express my deepest gratitude to my family; especially my father and my mother for their prayers which opened my vision to follow a better path to complete my study and extraordinary support and constant encouragement.

I am also delighted to express my deepest gratitude and thanks to Prof. Dr. Mehmet ÖZKAYMAK, for his kind care, assistance, valuable instructions and cooperation throughout this work.

I would like to thank the staff of Energy labs at Karabuk University for their help during the preparation of experimental setup and testing period. Also, I am really grateful to the Unit of Scientific Research Projects Coordination at Karabuk University for the funding awarded under the number of KBÜ-BAP-17-DR-262.

Finally, I am greatly thankful to the team an Energy Systems Engineering laboratory at Karabük University who have been a great source of support during the preparation of experimental setup and testing period.

CONTENTS

Page

APPROVAL ii
ABSTRACT iv
ÖZET vi
ACKNOWLEDGMENT viii
CONTENTS ix
LIST OF FIGURES xii
LIST OF TABLES xv
SYMBOLS AND ABBREVITIONS INDEX xvi

CHAPTER 1 2
INTRODUCTION 2
1.1. BACKGROUND 2
1.2. AIMS AND OBJECTIVES 4
1.3. METHODOLOGY 5

CHAPTER 2 6
LITERATURE REVIEW 6
2.1. PV/T COLLECTORS OVERVIE 6
2.1.1. PV/T Collector Technologies 6
2.1.2. Classification of PV/T collectors 7
2.1.3. PV/T Applications by Temperature Range 9
2.2. SPECTRAL SPLITTING PHOTOVOLTAIC/THERMAL HYBRID SYSTEM PV/T COLLECTORS 9
2.3. USING NANOFLUIDS AS A COOLING FLUID IN FLAT PV/T SYSTEMS 13
2.3.1. The Preparation Methods of Nanofluids Utilized In PV/T Systems 13
2.3.2. Experimental Setup Configurations Used in PV/T Systems 18
2.3.3. Performance Enhancements of Using Nanofluids in Flat PV/T Systems 33

Page

CHAPTER 3 38
ENERGETIC AND EXERGETIC EFFICIENCY OF PV/T COLLECTOR 38
3.1. ENERGY BALANCE FOR A PV/T COLLECTOR 38
3.2. THERMAL PROPERTIES OF NANOFLUIDS 40
3.3. OVERALL ENERGETIC EFFICIENCY 43
3.4. EXERGETIC EFFICIENCY 44

CHAPTER 4 46
EXPERIMENTAL SETUP 46
4.1. CONSTRUCTION OF A PV/T COLLECTOR 46
4.2. CONFIGURATION AND COMPONENTS OF THE EXPERIMENTAL SETUP 49
4.2.1. Components of the Experimental Setup 52
4.2.1.1. The Main Frame 52
4.2.1.2. Heat Exchanger with Cooling Coil 52
4.2.1.3. Storage Tank of Nanofluid 53
4.2.1.4. The Circulation Pump 54
4.2.1.5. The Air Outlet Vent 55
4.2.1.6. The Connection Method to Link the Components of the Experimental Setup 56
4.2.2. The Data Logging and Measuring System 56
4.2.2.1. Flow Rate Measurement 56
4.2.2.2. Temperature Measurement 57
4.2.2.3. Data Acquisition Board 57
4.2.2.4. The Incident of Solar Radiation Measurement 58
4.2.2.5. Resistor Load 59
4.2.2.6. Voltage and Current Measurements 59
4.2.3. Experimental Setup Operation 60
4.2.3.1. Measurement Devices Calibration 59
4.2.3.2. The Main Steps to Operate the Experimental Setup 61
4.3. NANOFLUIDS 62

CHAPTER 5 65
RESULTS AND DISCUSSION 65

Page

5.1. CALIBRATIONS 65
5.2. THERMAL PROPERTIES OF NANOFLUID 67
5.3. TESTING PROCEDURE 67
5.4. INITIAL EXPERIMENTS WITH 0.5 L/M, 1.5 L/M, AND 2. L/M FLOW RATES BY USING CITY WATER 68
5.5. EXPIREMENTAL RESULTS AND DISCUSSION 71
5.5.1. Solar Irradiance and Ambient Temperature 73
5.5.2. The Surface Temperature Measurements 75
5.5.3. Electrical Efficiency 77
5.5.4. Electrical Efficiency Increment 80
5.5.5. Thermal and Overall Energetic Efficiency 81
5.5.6. Exergetic Efficiency 85

CHAPTER 6 89
CONCLUSIONS AND RECOMMENDATIONS 89
6.1. CONCLUSIONS 89
6.2. RECOMMENDATIONS 91

REFERENCES 92

RESUME 98

LIST OF FIGURES

Page

Figure 1.1. Classification of solar energy systems. 3

Figure 1.2. Schematic diagram of a commercial PV/T collector..... 4

Figure 2.1. WISC (Wind and infrared sensitive collector) PV/T collector's cross section equipped with a sheet-and-tube heat exchanger. 6

Figure 2.2. Schematic diagram of a typical liquid-cooled uncovered PV/T flat-plate collector..... 8

Figure 2.3. Schematic diagram of a typical liquid-cooled covered PV/T flat-plate collector. 8

Figure 2.4. PV modules convert part of the solar spectrum into electricity and the residual energy into thermal energy 10

Figure 2.5. Spectral splitting PV/T system: a) Fluid-based filter, b) Thin film-based filter 12

Figure 2.6. Electromagnetic solar spectrum utilization by a PV/T collector..... 13

Figure 2.7. Experimental setup configuration by Alous et al. 19

Figure 2.8. Experimental setup configuration by Al-Waeli et al. 20

Figure 2.9. Experimental setup configuration by Hussein, H.A., et al. 20

Figure 2.10. Experimental setup configuration by Sardarabadi et al. 21

Figure 2.11. Indoor experimental setup configuration by Ghadiri et al. 22

Figure 2.12. Experimental setup configuration by Al-shamani et al..... 23

Figure 2.13. Indoor experimental setup configuration by Al-Waeli et al. 23

Figure 2.14. Indoor experimental setup configuration by Al-Waeli et al. 24

Figure 2.15. Experimental setup configuration by Hosseinzadeh et al. 24

Figure 2.16. Experimental setup configuration by Ebaid et al. 25

Figure 2.17. Indoor solar simulator: a) photo of the simulator, b) schematic diagram. of the simulator details by Al-Waeli et al 26

Figure 2.18. Schematic diagram by Vakili et al.. 27

Figure 2.19. Indoor solar simulator by Fayaz et al. and Nasrin et al. 28

Figure 2.20. Experimental setup configuration Abdallah et al. 29

Figure 2.21. Schematic diagram by Sangeetha et al. 30

Figure 2.22. Experimental setup by Sangeetha et al. 30

Figure 2.23. Schematic diagram by Iranmanesh et al. 31

Page

Figure 2.24. Experimental setup Hassan et al. 32

Figure 3.1. Energy balance for a PV/T collector. 38

Figure 4.1. PV/T heat exchanger with serpentine design. 46

Figure 4.2. Schematic diagram for a serpentine heat exchanger. 47

Figure 4.3. Collecting PV/T: a) Distribution method of thermal paste. b) Metallic enclosure. c) Close PV/T collector. 48

Figure 4.4. Thermal paste. 49

Figure 4.5. Schematic diagram of the experimental setup. 50

Figure 4.6. A view of experimental setup. 51

Figure 4.7. The main frame of experimental setup. 52

Figure 4.8. Storage tank: a) Tank assembly design. b) Coil heat exchanger design. c) Manufactured storage tank. 53

Figure 4.9. Nanofluid tank: a) Design. b) Manufacturing. 54

Figure 4.10. Circulation pump installed and used in the setup. 55

Figure 4.11. Air vent. 55

Figure 4.12. Flow rate measuring system: a) Flow meter b) LED screen. 56

Figure 4.13. Temperature data logger: a) Pico USB TC-08. b) Position in the setup 57

Figure 4.14. a) Screen and Arduino card, b) Data collecting board. 58

Figure 4.15. Pyranometer used to measure the incident solar radiation. 58

Figure 4.16. (a) Resistor load (b) fin-fan system for cooling 59

Figure 4.17. a) Graphene nanoplatelets TEM image, b) Nanofluid sample. 63

Figure 4.18. a) TEM image for AL_2O_3 nanoparticles. b) Nanofluid sample. 63

Figure 4.19. Sample of hybrid nanofluid (HyNF) 64

Figure 5.1. Flow rate calibration. 66

Figure 5.2. Solar radiation calibration. 66

Figure 5.3. Average daily variation of electrical efficiency for different flow rates. 69

Figure 5.4. Average daily efficiencies of the system over the flow rates.0.5, 1.0, 2.0 L/min. 69

Figure 5.5. Average daily variation of thermal efficiency for different flow rates. 70

Figure 5.6. Average daily thermal power for different flow rates. 70

Figure 5.7. Measured parameters for distilled water after every 12 seconds. 72

Figure 5.8. Measured parameters for hybrid nanofluid after every 12 seconds. 72

Page

Figure 5.9. Measured parameters for graphene nanoplatelets nanofluid after every 12 seconds. 73

Figure 5.10. Daily average solar radiation and ambient temperature when distilled water is used. 74

Figure 5.11. Daily average of solar radiation and ambient temperature when a hybrid nanofluid is used. 74

Figure 5.12. Daily average of solar radiation and ambient temperature when graphene nanofluid is used. 75

Figure 5.13. Daily average variations in surface temperature for PV, PV/T using distilled water. 76

Figure 5.14. Daily average variations in surface temperature for PV and PV/T for GNP. 76

Figure 5.15. Daily average variations in surface temperature for PV and PV/T for HyNF. 77

Figure 5.16. Electrical efficiency and power production using PV/T and PV collectors for distilled water. 78

Figure 5.17. Electrical efficiencies and power production using PV/T and PV collectors for graphene nanoplatelets-water nanofluid. 78

Figure 5.18. Electrical efficiencies and power production using PV/T and PV collectors for a hybrid nanofluid. 79

Figure 5.19. Daily average variations in electrical efficiency increment. 80

Figure 5.20. Average daily variation in thermal efficiencies for PV and PV/T. 82

Figure 5.21. The variation in overall energetic efficiency for PV and PV/T. 82

Figure 5.22. Variations in the exergy efficiency for PV module and PV/T using distilled water. 87

Figure 5.23. Variations in the exergy efficiency for a PV module and PV/T using graphene nano-platelets nanofluid. 87

Figure 5.24. The variations in the exergy efficiency for PV module and PV/T using a hybrid nanofluid. 88

LIST OF TABLES

Page

Table 2.1. Some performance enhancements using nanofluids of PV/T collectors. 33

Table 4.1. Heat exchanger design specifications. 47

Table 4.2. PV panel specifications. 48

Table 4.3. Circulation pump specifications. 54

Table 4.4. Thermal properties of water and nanoparticles [32,64]. 63

Table 5.1. Thermal properties of graphene nanoplatelets and hybrid nanofluids. ... 67

Table 5.2. Experimental days. 68

Table 5.3. Dates of initial experimental days. 68

Table 5.4. The percentage of thermal power, thermal efficiency, and electrical efficiency during the experiment days. 71

Table 5.5. The average daily weather conditions, electrical increment, and cell temperature during the day-long experiment. 79

Table 5.6. Average daily weather conditions, electrical increment, and cell temperature during the peak period. 79

Table 5.7. Daily overall and thermal energetic efficiencies for PV/T using different coolants. 83

Table 5.8. The performance of energetic efficiency compared with other works. .. 84

Table 5.9. Thermal energetic performance comparison for graphene with different studies. 85

Table 5.10. Daily average of overall exegetic efficiency for PV and PV/T with different working fluids. 86

Table 5.11. The enhancement of overall exergy efficiency for PV and PV/T. 88

SYMBOLS AND ABBREVITIONS INDEX

LATIN SYMBOLS

GNP : Graphene nanoplatelets

HyNF : Hybrid nanofluid

Al_2O_3 : Aluminum dioxide

A_c : PV/T collector surface area (m^2)

A_{PV} : PV surface area (m^2)

C_f : Thermal – electrical conversion factor

C_p : Specific heat (kJ/kg K)

$C_{p,f}$: Specific heat of base fluid (kJ/kg K)

$C_{p,n}$: Specific heat of nanoparticles (kJ/kg K)

$C_{p,nf}$: Specific heat of nanofluid (kJ/kg K)

$\dot{E}_{el}$: Rate of electrical energy output (W)

$\dot{E}_{el,th}$: Thermal power converted from electrical power (W)

$\dot{E}_{in}$: Rate of energy input (W)

$\dot{E}_{loss}$: Rate of energy loss (W)

$\dot{E}_{out}$: Rate of energy output (W)

$\dot{Ex}_{el}$: Rate of electric exergy output(W)

$\dot{Ex}_{sun}$: Rate of solar exergy input (W)

$\dot{Ex}_{th}$: Rate of thermal exergy output (W)

FF : Filling factor

I_R : Solar radiation incident on surface (W/m^2)

I_m : Maximum current generated by PV cells (A)

I_{sc} : Short circuit current generated by PV cells (A)

k_f : Thermal conductivity of base fluid (W/m K)

k_n : Thermal conductivity of nanoparticles (W/m K)

k_{nf} : Thermal conductivity of nanofluid (W/m K)

$\dot{m}$: Mass flow rate of working fluid (kg/s)

m_f : Mass of base fluid (kg)

m_n : Mass of nanoparticles (kg)

N : Number of measurements of certain quantity

P_m : Maximum electrical power generated by PV cells (W)

$\dot{Q}_u$: Useful thermal power collected by working fluid in PV/T collector (W)

r : Packing factor of the PV cells

T_{amb} : Ambient temperature (°C)

T_c : PV cells temperature (°C)

T_i : PV/T collector inlet temperature (°C)

T_o : PV/T collector outlet temperature (°C)

T_r : PV reference temperature (°C)

T_{sun} : Solar radiation temperature (K)

V_m : Maximum voltage generated by PV cells (V)

V_{oc} : Open circuit voltage generated by PV cells (V)

GREEK SYMBOLS

β : Temperature coefficient of PV cells ($°C^{-1}$)

ε_{el} : Exergetic electrical efficiency

ε_{ov} : PV/T overall exergetic efficiency

ε_{th} : Exergetic thermal efficiency

φ : Volumetric ratio of the nanofluid

η_{el} : Energetic electric efficiency

η_{ov} : PV/T overall energetic efficiency

$\eta_{PV/T,et}$: PV/T overall energetic equivalent efficiency

η_r : PV module efficiency at the reference temperature

η_{th} : Thermal energetic efficiency

ρ_f : Density of base fluid (kg/m^3)

ρ_n : Density of nanoparticles (kg/m^3)

ρ_{nf} : Density of nanofluid (kg/m^3)

CHAPTER 1

INTRODUCTION

1.1. BACKGROUND

The sun is considered as the cleanest as well as sustainable energy source abundantly available in our time, which can be used to obtain clean energy as an alternative to fossil fuels. Its radiation is termed as solar energy, which is capable of producing heat by causing interactions within the solar panels, which further lead to the generation of electrical energy. Scientific studies clearly indicate that the solar energy projected on the earth is far beyond its needs and it is necessary to optimally exploit it in order to be able to benefit from it, and since it is a clean energy, it is possible to rely on it, and pollutants, which emit out of coal, oil, and natural gas, can be completely avoided.

Basically, solar energy systems can be subdivided into two groups: The systems, which transform solar energy into thermal energy, and those, which finally transform solar energy into electricity. They can be explained as systems, which derive heat out of solar energy to obtain thermal energy for heating while others obtain it for power generation. Now, another hybrid technology is available, which is termed as Photovoltaic/Thermal Hybrid technology to serve the same purposes.

Despite changes in technology, the solar energy systems exist in two broad categories: First: Systems, which are capable and efficient to generate heat out of solar energy that is used for heating processes.

Second: Systems, which are able to generate power through solar energy.

Our study aims to shed light on the third and hybrid classification, which combines the mentioned systems, and as mentioned earlier, it is called Photovoltaic/Thermal Hybrid technology (Figure 1.1).

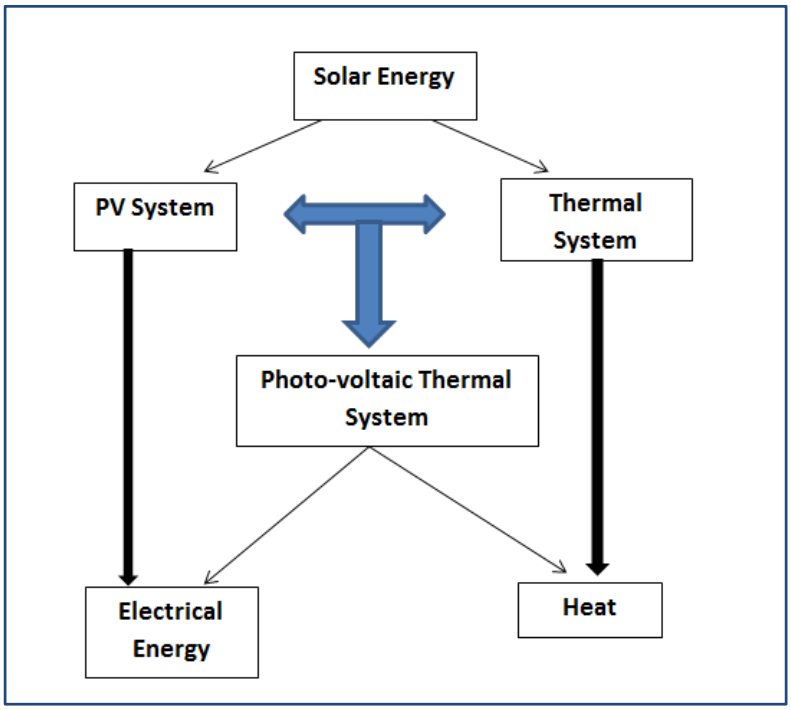

Figure 1.1. Classification of solar energy systems.

The principle that works behind solar collectors is converting incident solar radiation into thermal energy, which dissipates by a fluid, whether it is water, air or any other liquid, which is circulated through the absorber and the tubes.

The solar radiation is transformed into thermal energy, which is further used to generate electricity by using other electrical power generation methods such as steam-fed systems and others, which direct solar radiation to a point to increase the fluids' temperature, and they are used on a large-scale.

The photovoltaic modules/cells convert solar radiation into electrical power and they perform heating because they are equipped with a heat exchanger at the back of the photovoltaic (PV) cell, as Figure 1.2 shows. The PV/T collector extracts the thermal energy, and in this process, it uses the heat generated from a PV module for heating the working fluid, which passes through the PV/T heat exchanger.

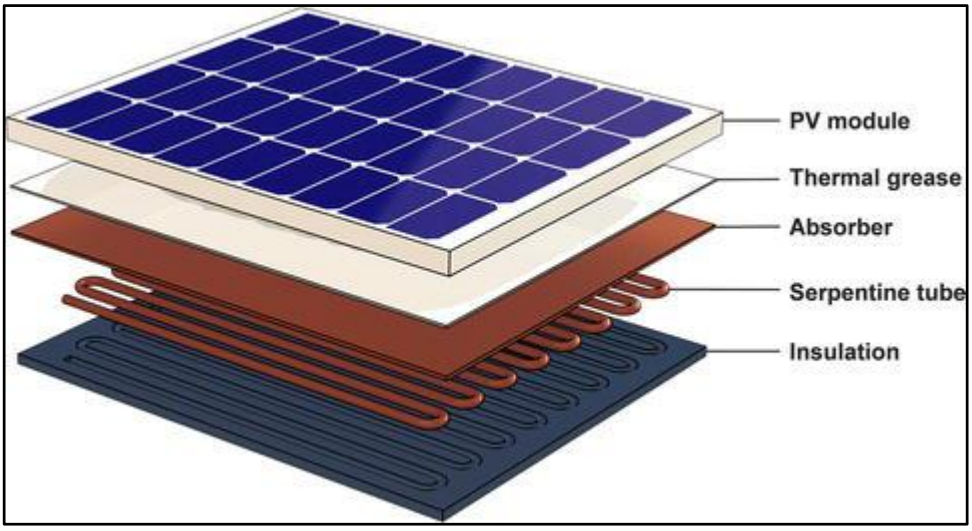

Figure 1.2. Schematic diagram of a commercial PV/T collector [1] .

It is obvious that the PV collectors' overall efficiency is likely to improve with better thermal properties, which increases the useful heat gain. This improvement can also be accomplished using fluids with better thermal properties that increase the system's efficiency.

Among the fluids, the most suitable option for improving efficiency is the use of different nanofluids, which improve the solar thermal systems' efficiencies based on the currently available studies. They consist of water, oils and/or ethylene glycol residues, which are mixed with metallic nanoparticles for enhancing the base fluid's thermal properties.

1.2. AIMS AND OBJECTIVES

The following specific objectives are focused on this study:

The aims of the study include diverting the deep attention of research communities towards the PV/T collector design, operating principles and testing the HyNF as coolants in PV/T collectors, which is still rare in the literature. To our knowledge, this study is the first attempt to conduct experimental investigations on using a hybrid nanofluid coolant of aluminum oxide and GNP in PV/T collectors. To fulfill the mentioned aims, we have taken the following steps:

- Design and construct a PV/T collector equipped with a sheet and a few tube heat exchangers. The PV/T was fixed to a serpentine-type heat exchanger.
- Calibrate and validate the component data and the system data.
- Note down the PV/T collectors' electrical as well as thermal efficiencies using nanofluids.
- Study the PV/T collectors' performances using graphene-water and Hybrid nanofluids with different 0.5 wt. %.
- Compare the results of the PV module and the PV/T collector with results of water and nanofluids.

1.3. METHODOLOGY

- Literature survey about improving the performance of PV panels by cooling them with combined heat exchangers (PV/T) and using nanofluid coolants.
- Literature inspection about the methods of acquisition of nanofluid coolants used in PV/T collectors.
- Design a test module for performance testing of the PV/T collector in the light of literature.
- Define specific components that must be available to build a test model.
- Develop the necessary plans to obtain the necessary parts from the suppliers.
- Collect the experimental module components and submit them to the Energy Department Labs at Karabuk University.
- Make the necessary calibrations to adjust all devices connected to the module.
- Start experiments under the right conditions to get good results.
- After the experiments, start the process of analyzing the results.

CHAPTER 2

LITERATURE REVIEW

2.1. PV/T COLLECTORS OVERVIE

2.1.1. PV/T Collector Technologies

PV/T collectors are also known as hybrid solar collectors, PV/T collectors, PV solar-thermal collectors, or solar cogeneration systems. They are effective power generation technologies, which transform solar radiation into utilizable electrical and thermal energies, and they combine PV solar cells, which transform solar radiation into electricity, and a solar thermal collector is also part of the equipment that transfers the PV module's waste heat to a heat transfer fluid. When electricity and heat are generated together using the same component, the systems have a higher overall efficiency as compared to solar thermal (T) or solar photovoltaic (PV)[2].

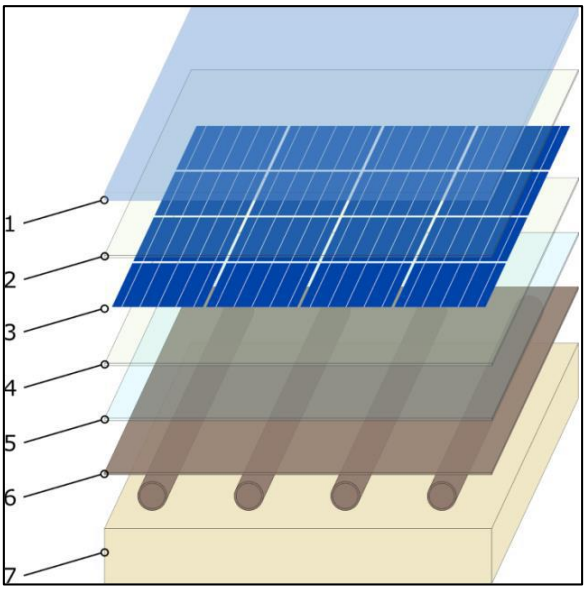

1. Encapsulant (such as EVA).
2. PV module cover glass (anti-reflective glass).
3. Solar PV cells.
4. Back sheet (PVF).
5. Thermal insulation (mineral wool/polyurethane).
6. Heat exchanger (aluminum/ copper/polymers).

Figure 2.1. WISC (Wind and infrared sensitive collector) PV/T collector's cross section equipped with a sheet-and-tube heat exchanger.

The main theory behind PV/T collectors is integrating the solar and power generation for obtaining more efficiency and for using the solar technology better than conventional PV. It converts 65-70% energy into heat and the PV cells assure 15-20% efficiency that increases the PV modules' temperature, as Figure 2.1 shows; however, for PV cells-to-fluid heat transfer, PV/T collectors are specifically designed. The heat overflow can be utilized for heating water or when a low temperature source is needed for heat pumps. Subsequently, the solar spectrum becomes useful for PV/T collectors [2].

Overall, PV/T collectors improve the heat-and-power efficiency and optimally utilize the available space, which is very significant especially in the highly populated areas [3].

Increasing cell temperatures cause a drop in photovoltaic cells' efficiency; so, extra cell temperature brings about 0.2-0.5% efficiency reduction; therefore, it is important to reduce the cell temperature so as to improve their efficiency.

2.1.2. Classification of PV/T collectors

Here, photovoltaic thermal collectors can be classified into several designs:

- Liquid-cooled covered PV/T flat-plate collectors.
- Liquid-cooled uncovered PV/T flat-plate collectors.
- Air-Cooled PV/T Flat-Plate Collectors.

1. Liquid-Cooled Uncovered PV/T Flat-Plate Collectors

As shown in Figure 2.2, it is designed by placing photovoltaic cells between the front windshield and the back foil, and a metal or plastic heat absorber filled with a coolant is installed at the back of the unit. Here, any type of heat absorber, whether roll-bonded or double-skin sheet, is installed until a good connection between the unit and the coolant is established. Good heat transfer takes place with thermal insulation in the

exchanger tubes to maintain good heat exchange. This design is one of the most common designs in use.

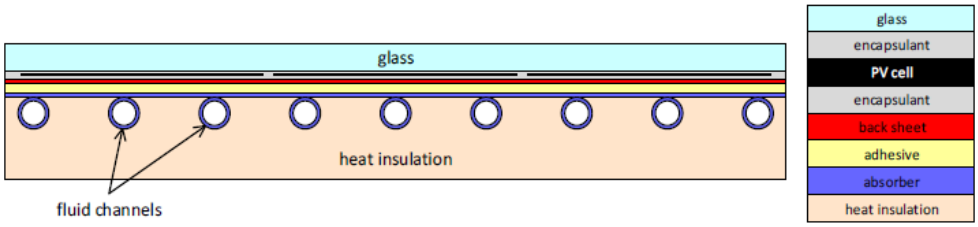

Figure 2.2. Schematic diagram of a typical liquid-cooled uncovered PV/T flat-plate collector [2].

2. Liquid-Cooled Covered PV/T Flat-Plate Collectors

This design is more similar to a solar thermal collector. In this case, photovoltaics are used instead of an absorbent spectral coating. The combination of solar cells and a heat absorber has a great similarity with the first type, which consists of a layer of glass, air pockets, heat absorber, heat exchanger, and then an insulator that maintains good heat transfer as Figure 2.3 shows. This collector is equipped with a transparent/translucent cover, which decreases the heat load and it can provide useful high temperature levels; so, it has more applications and besides, it is also used in a flat plate solar thermal collector in a similar way but it is more complex and needs high-quality materials [4].

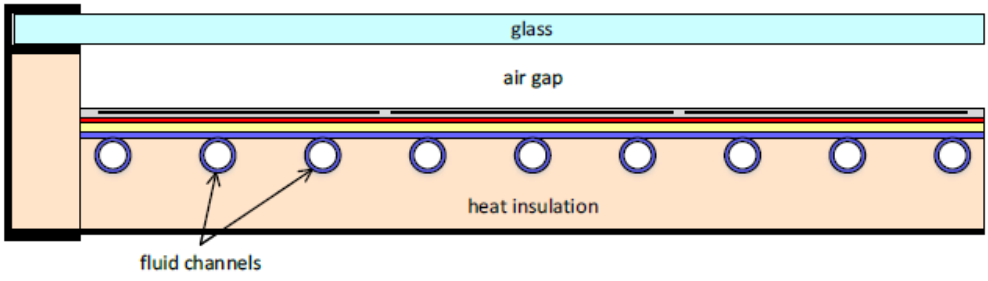

Figure 2.3. Schematic diagram of a typical liquid-cooled covered PV/T flat-plate collector.

3. Air-Cooled PV/T Flat-Plate Collectors

In this design, instead of using a coolant, air is used as a cooling medium. It was originally designed for receiving sunlight and for converting it into hot water and

electrical energy. This design releases thermal energy from the collector to the air. One of its advantages, unlike liquids, is that it does not have high-pressure steam, and its heat can also be used for heating purposes and utilized in cold places. It is cost-effective and boosts the collector's efficiency despite operating at low temperatures [2].

2.1.3. PV/T Applications by Temperature Range

The applications of PV/T and solar-thermal collectors is based on their temperatures, and they are subdivided into the following temperature categories [5].

- Applications at low temperature (up to 50 °C).
- Applications at medium temperature (up to 80 °C).
- Applications at high temperature (above 80 °C).

Applications that require low temperature are normally heat pumps, heating systems of spas and swimming pools (up to 50°C). In heat pumps, PV/T collectors either act as a low-temperature source that heats a heat pump evaporator or it heats a storage tank on the load side through supplying a medium temperature [2]. Using uncovered PV/T collectors is possible with better air-to-water heat exchange through a heat pump system. The system architecture is a combination that can operate cold storage equipment or air conditioning with WISC/air collectors [3].

2.2. SPECTRAL SPLITTING PHOTOVOLTAIC/THERMAL HYBRID SYSTEM PV/T COLLECTORS

Solar cells are made up of semiconductors. The electrical conductivity of semiconductors is low and thus absorbs energy in specific wavelengths. The solar energy converts into electricity and heat in silicon-based solar cells, as Figure 2.4 indicates. To absorb and convert photons in silicon PV cells generate electricity but the minimum force required depends on the carved weight [6]. In silicon-based photovoltaic systems, solar energy has the capacity to convert 20% energy into power while in photovoltaic components, the thermal conductivity reaches 60-70% of the

radiation incidence [7]. In a solar cell, some part of a radioactive fluid converts into heat that raises the PV system's temperature, lowers the conversion rate and eventually spreads through space. It loses heat through radiation and transports it. In the PV/T module, this high-quality material accumulates in a back-heated storage box, which raises the temperature and generates useful thermal energy. The combined system works better than the separated system PV because it has a higher efficiency to convert photovoltaic power because of low cell operating temperature, which is assured through cooling, and besides, the system gains the ability to reduce the module cost of a single system installation [8].

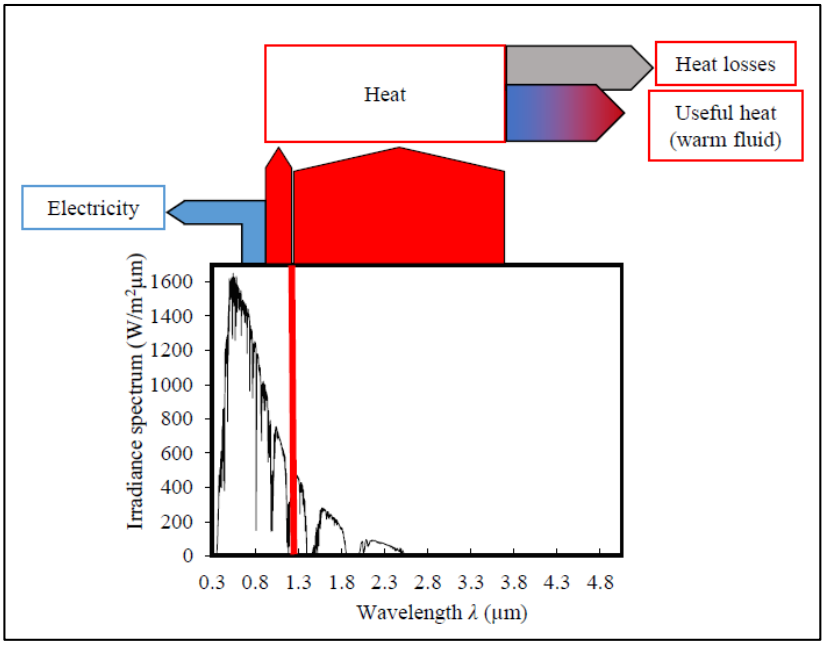

Figure 2.4. PV modules convert part of the solar spectrum into electricity and the residual energy into thermal energy [8] [9].

Conventional solar-thermal collectors have high irradiance absorption and low heat losses, and this is accomplished through applying a thin black coating layer to the metal absorber's upper surface, which has high light absorption and low mid-high infrared emissivity. Some properties of the PV modules increase the radiation losses but they improve the electrical efficiency. Consequently, a PV/T collector's thermal efficiency is limited because of the solar cells' optical properties because the absorber does not have the same spectral emissivity/absorptivity as compared to the absorbers generally used in a solar-thermal collector.

In a PV/T collector, the solar cells work better at a low temperature with more electrical efficiency as compared to a PV module where they operate without sufficient cooling. A PV's cooling takes place in a PV/T module and that depends on the inlet fluid flow rate and temperature. It also depends on the collector's material and its thermo-physical properties. In a non-cooled PV module, the liquid of PV/T collectors is at low temperature, and it operates at 20 °C lower temperature than the stabilized operating temperature [10]. The efficiency of a system in terms of converting energy into electricity largely depends on the temperature as well as supplementary factors, which include design, PV/T operation, and rise/fall in the collector's surface temperature. Thus it assures that a PV/T collector's design will result in low temperature distribution over the entire modules, which is a huge challenge [8].

Some latest studies have successfully demonstrated that the spectral splitting technology greatly contributes to several processes, which improve the PV/T. In 2.5, the PV/T design shows a nanofluid spectral splitting filter (PV/T-NSSF) that works with two distinct types of units in the light receiver, including photo-thermal and PV units. A selected absorption fluid is filled in a photo-thermal unit/fluid spectral splitting filter that absorbs solar incident of a single-junction PV cell below the band-gap energy and converts it into medium-temperature thermal energy. When an appropriate nanofluid is applied in a photo-thermal unit, this technology can give a 150-300 ^{o}C thermal output. In a traditional PV/T, it can outperform in terms of temperature and provide simultaneous supplies of electricity and thermal energy for several applications [11], including solar refrigeration, solar seawater desalination, and solar drying. Moreover, in a spectral splitting filter, the fluid is almost transparent at a PV cell's efficiency waveband. The PV cell's efficiency can be enhanced in PV/T-NSSF, and when there is a suitable spectral match, PV/T-NSSF results in effective solar energy utilization [11].

Figure 2.5 indicates two methods for using the spectral splitting technology [11]:

- Liquid-based transmission/absorption (Figure 2.4).
- Film-based transmission/reflection (Figure 2.5).

First, both heat transfer and absorption are more effective in a liquid-based spectral splitting method than the solid surfaces because in that case, solar irradiation becomes a volumetric process. A cell's radiation below the band-gap energy is both efficiently and directly transformed into heat. In addition, it assures flexible heat and power allocations for different applications, which adjusts the nanoparticles' concentration.

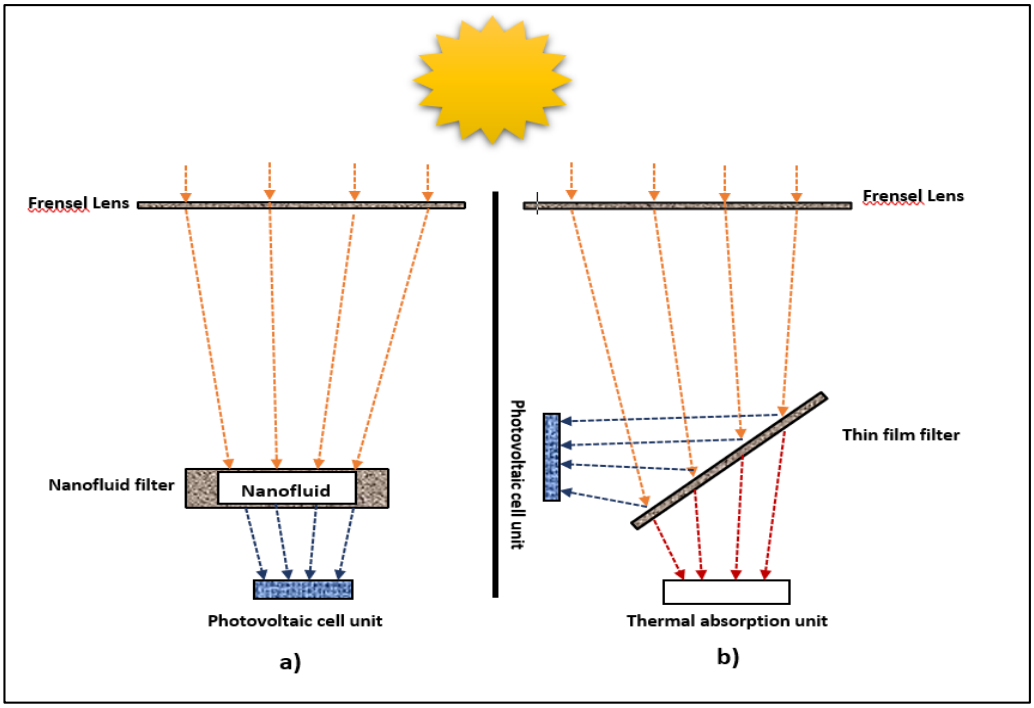

Figure 2.5. Spectral splitting PV/T system: a) Fluid-based filter, b) Thin film-based filter [11].

Moreover, a nanofluid is always isolated in tubes, and besides, traditional cleaning does not affect the filter performance; so when the outer dust affects the filter performance, the fluid-based filter is easier-to-clean as compared to the film-based filter [12]. Thus, decreasing the temperature results in increasing the cells' efficiency. Moreover, reducing the operational temperature improves the PV cells' lifetimes. In a solar spectrum, a PV/T collector's main function and power generation benefit is indicated in terms of electrical/thermal gains (see Figure 2.5).

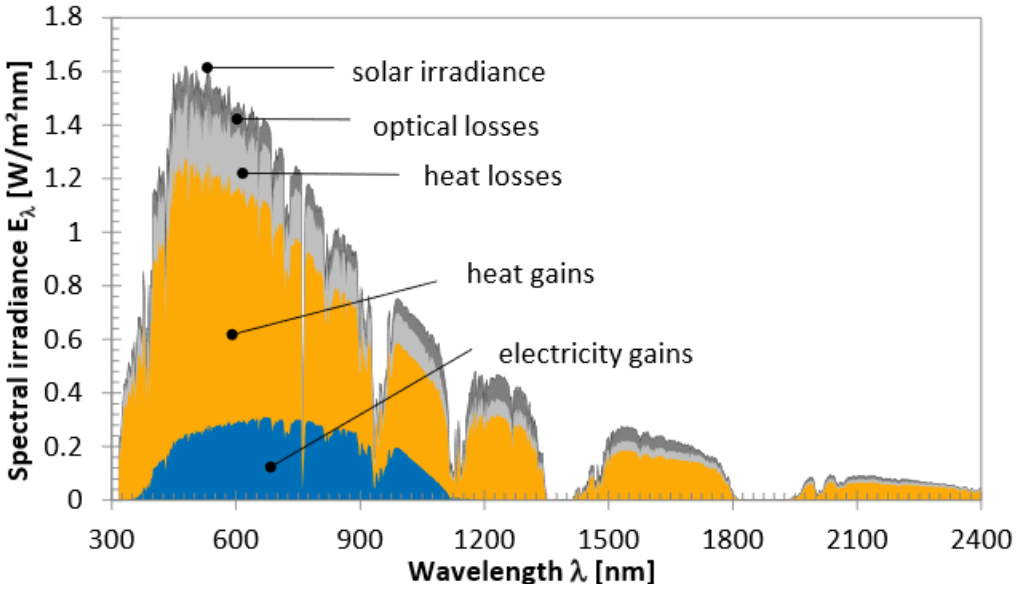

Figure 2.6. Electromagnetic solar spectrum utilization by a PV/T collector [13–15].

2.3. USING NANOFLUIDS AS A COOLING FLUID IN FLAT PV/T SYSTEMS

2.3.1. The Preparation Methods of Nanofluids Utilized in PV/T Systems

Generally, nanofluids consist of solid-liquid composite materials with nanoparticles/nanofibers, and their sizes are normally 1-100 nm, and they are suspended in a liquid [16]. The nanofluids, which have been used in the experiments, show that the fluids have substantially higher thermal conductivities as compared to the base fluids [16]. Moreover, in solar thermal systems, nanofluids are extensively used as working fluids, and they can be used as spectrum splitter filters as well. In a photo-thermal unit, if a suitable nanofluid is employed, it can lead to thermal output of 150-300 °C [11]. For a good nanofluid, the most important criteria are:

- It should be completely free from agglomerates that lead to sedimentation.
- Long continuous equilibrium of nanofluid without change in chemical properties.

Two methods are used for preparation of nanofluids [16, 17]: Single-step and two-step methods:

- Single-step/VEROS (Vacuum evaporation onto Running Oil Substrate) process: The lower agglomeration of the nanoparticle is a disadvantage of this method but on the other hand, fluids with low vapour pressure are sufficient in this process. It is a costly method and it does not allow producing nanofluids on a large scale.
- Two-step method: This method produces nanoparticles as a powder, which is later mixed with base fluids. To reduce agglomeration and evenly disperse nanoparticles in a base fluid, "ultrasonication" process is used. Adding a surfactant/dispersant to a nanofluid helps make a stable suspension.

Nowadays, the light has been shed on the nanofluid utilization in thermal applications and this topic has gained the attention of several eminent researchers, because their thermal properties are considered preferable to use instead of traditional heat transfer fluids.

Many researchers have prepared the nanofluid by different methods and followed a certain pattern in the preparation procedures. Furthermore, they have also conducted investigations to understand the nanofluids' effects as heat transfer fluids in the PV/T systems.

Alous et al. [18] conducted a study to analyze the graphene nano-platelets' performances when they are mixed in water as a base fluid (flow rate: 0.5L/min; wt. concentration: 0.5%), and they also analyzed the multi-walled carbon nanotube (MWCNT) PV/T systems. According to their findings, MWCNT-water mixture performed better for PV energy conversion when they compared it to distilled water and graphene. They reported that the graphene-water nanoplatelets have shown the highest thermal power generation efficiency. Furthermore, the results showed that the total energy efficiency improved by 57.2% for MWCNT water, 53.4% for distilled water, and 63.1% for graphene-water. The total exergy efficiency increased by 12.1%, 20.6%, and 11.2% for the PV/T collector when it was cooled using MWCNT-water nanofluid, graphene nanoplatelet-water nanofluid, and distilled water, respectively.

Sardarabadi et al. [19] prepared SiO_2/water nanofluid by dispersing between 11-14nm particle size of SiO_2 in distilled water with 1 and 3 wt.% concentration. Dispersion method was accomplished by stirring the mixture with a high-speed stirrer, and after 3 hours of continuous sonication, the fluid was processed by an ultrasonic processor. The density of SiO_2/water nanofluid was measured many times throughout the experiments, tests, and no change was observed. Also, they did not find any sedimentation even after 10 days.

Ghadiri et al. [20] in their study used ferro-fluids (Fe_3O_4 with water) at 1wt% and 3wt% concentrations. The preparation method of the magnetite nanoparticles was chemical precipitation. Fe_3O_4 nanoparticles were dispersed in distilled water using acetic acid ($C_2H_4O_2$) surfactant. After that, the mixture went through ultrasonication for 30 minutes. The nanofluid remained stable for more than a month, and its particle diameter was 45 nm.

Sardarabadi et al. [21,22] used three sorts of nano-oxide particles in their work: Al_2O_3, TiO_2 and ZnO. The nanoparticles were dispersed in the base fluid (deionized water) at 0.2wt% when a high-speed stirrer was used and suitable surfactants were added. The mixture was sonicated six times at 60 °C for 20 minutes each time. During the experiments, the researchers did not find any significant density changes but they found little sedimentation after 2 days.

Al-Waeli et al, [23] performed experimental investigation on the SiC-water nanofluid, which was prepared by dispersing (45-65nm) SiC nanoparticles in deionized water and about 0.1 ml Cetyl Trimethyl Ammonium Bromide (CTAB) was also used so as to eliminate any moisture, and an oven was used at 200 °C temperature to heat the SiC nanoparticles for 15 minutes before mixing them with CTAB-water solution. The SiC-water nanofluid was prepared with 1, 1.5, 2, 3, and 4 wt% concentrations by slowly adding the nanoparticles to a vibrating ultrasonic bath that contained CTAB-water solution. After that, the nanofluid was continuously sonicated for 5 h. It was found that 3wt% SiC nanoparticles in water improves the fluid viscosity up to 1.8% and the fluid density up to 0.0082%. For 25–60 °C temperature range, there was an 8.2% increase

in the thermal conductivity. They found the nanofluid in a stable form; however, the fluid's thermal conductivity reduced by 0.003 W/mK in six months.

Al-Waeli et al, [24] tested Al_2O_3, CuO, and SiC-based nanofluids for performance enhancement of PV/T systems at 4.0% concentration by volume. They attached a 110-watt PV panel to a solar collector to construct their PV/T. They cooled their coolant fluid by passing it over to a storage tank. According to the results, SiC nanoparticles showed considerably superior thermal conductivity and stability that further improved the PV/T performance in comparison with Al_2O_3 and CuO.

Ebaid et al. [25] used two nanofluid types in their study, which were TiO_2 dispersed in water-cetyltrimethyl ammonium bromide mixture (pH 9.7), and AL_2O_3, which was dispersed in a water-polyethylene glycol mixture (pH 5.7). To obtain a better stabilization for a while, 0.1g CTAB was added for every liter of AL_2O_3 nanofluid and 4g Polyethylene Glycol was added for every gram of TiO_2 nanoparticles. Both nanofluids were prepared with concentrations 0.01, 0.05, and 0.1wt%. The dispersion was done by mixing the nanoparticles with the base fluid and stirring it for 1h, after which, sonicating was performed at a constant temperature for 1h for several days, and the stability of the nanofluids was monitored.

Sardarabadi et al. [26] prepared a nanofluid by dispersing ZnO nanoparticles (size less than 50nm) using distilled water as a liquid with 0.2wt% concentration. Acetic acid (CH3COOH) was added to the mixture as a surfactant. Throughout the experiment, no nanofluid density changes were found. Also, after 7 days, no sedimentation was observed.

Nasrin et al. [27] dispersed MWCNT nanoparticles in deionized water and they synthesized the MWCNT powder using Carbon Chemical Vapor Deposition (CVD) method. They prepared three concentrations of nanofluid at 0.3, 0.6, and 1.0 wt.%. The combination process was achieved by stirring the mixture for 30 minutes using a high–speed shear mixing stirrer, and then sonicating the mixture continuously for four times at 70 °C for half hour each time. They could not find any density change or sedimentation during the experiments.

Hybrid nanoplatelets-water nanofluid was used in this study for the first time until now, according to a wide search and to the best of our knowledge. We applied it in a flat non-concentrating PV/T system as a working fluid and the results were compared to the outcomes of distilled water and another nanofluid (graphene nanoplatelets-water nanofluid).

Gao et al. [28] also prepared hybrid nanofluids in a two-step method. They used graphene oxide (more than 99wt% pure with more than 99.99% pure aluminum oxide nanoparticles with 30±5 nm particle size). The powder was added to deionized water to obtain hybrid nanofluids in different fractions of mass. Then an acidity meter was used to determine their pH. After half-hour stirring with a magnetic stirrer, sonication was performed for one and a half hours for obtaining a properly dispersed and stable nanofluid. WGZ-2000 Turbidimeter (Shanghai Xin Rui Instrument Co. Ltd.) was used to test the changes in the nanofluid stability. They extracted 4 mL hybrid nanofluid from the container's upper section, which was thrice diluted in deionized water. The hybrid nanofluid absorbance was calculated using a turbidimeter.

The experimental investigation by Iranmanesh et al. [29] included a graphene nano-platelet distilled water nanofluid to understand its impact on the tube solar collector water heater and its thermal performance. They selected 0.5, 1, and 2L/min flow rates for different concentrations (0.025, 0.5, 0.75 and 0.1% wt.). They reported that the mentioned nanofluid improved the solar collector's thermal efficiency up to 90.7% at 1.5L/min when it was used as an absorption medium.

A mathematical model was proposed by Al-Waeli et al, [30] in which they discussed a new nanofluid/nano-PCM PV/T system. This model was tested by conducting experiments using a silicon carbide-PCM with a silicon carbide-water nanofluid in a PV/T system, and when the results were compared, the effectiveness of the tested mathematical model was proved.

Vakili et al. [31] conducted experiments on deionized water and GNP in a solar collector. Until then, (GNP) nanofluid was never used in any volumetric solar collector as a working fluid. The results show ideal mass flow rate (0.015 kg/s) but there was

zero-loss efficiency, and the weight fractions for 0.0005, 0.001 and 0.005 were 83.50%, 89.70%, and 93.20%, respectively; however, it was 70% in case when a base fluid was applied.

2.3.2. Experimental Setup Configurations Used in PV/T Systems

During recent experiments, the researchers experimentally characterized PV/T collectors for obtaining dependable operational and performance data. So far, the investigations on PV/T collectors have been mainly performed for estimating the impact of different design parameters on the overall thermal as well as electrical efficiencies so as to identify their improvement potential.

In the literature, the basic components required for evaluating the electrical/thermal performance were analyzed using setup configurations for testing the PV/T collectors, which have the same components. These basic components are:

- A heat exchanger that removes the working fluids' heat in the PV/T collector.
- A flow meter to control the working fluids and the flow rate.
- Fluid temperature, ambient temperature, inlet/outlet and surface temperatures should be measured by using thermocouples to obtain the real data.
- Incident solar radiation, voltage and current measuring devices.
- A working fluid that circulates by using a circulation pump throughout the experimental setup.
- Nanofluids store inside the storage tank, from which it can be added to the setup or drained.

During their experiment, Alous et al. [32] constructed a 40W mono-crystalline PV and PV/T collector mounted side by side that faced towards the south at a 30° tilt angle (2.7). Then a sheet was mechanically attached to it and a tube heat exchanger was attached to the back side of a PV module that had a specific thermal insulation. The mentioned sheet-and-tube heat exchanger is in fact a copper tube, which is soldered with a thin copper plate. They used a variable-speed circulating pump to move a working fluid in the storage tank (equipped with a coil heat exchanger),

nanofluid tank, and PV/T collector. To measure the flow rate, a flow meter was installed. PV/T fluid inlet and outlet temperatures, ambient temperature, and PV and PV/T surface temperatures were measured using K-type thermocouples, which were linked to an eight-channel data logger, and that was connected with a laptop. A pyranometer measured the total incident solar radiation, which was installed at the same incidence plane with PV/T and PV panels, and all of them were linked to a computer with the help of a data collection board that transferred radiation, voltage, and current signals to the computer.

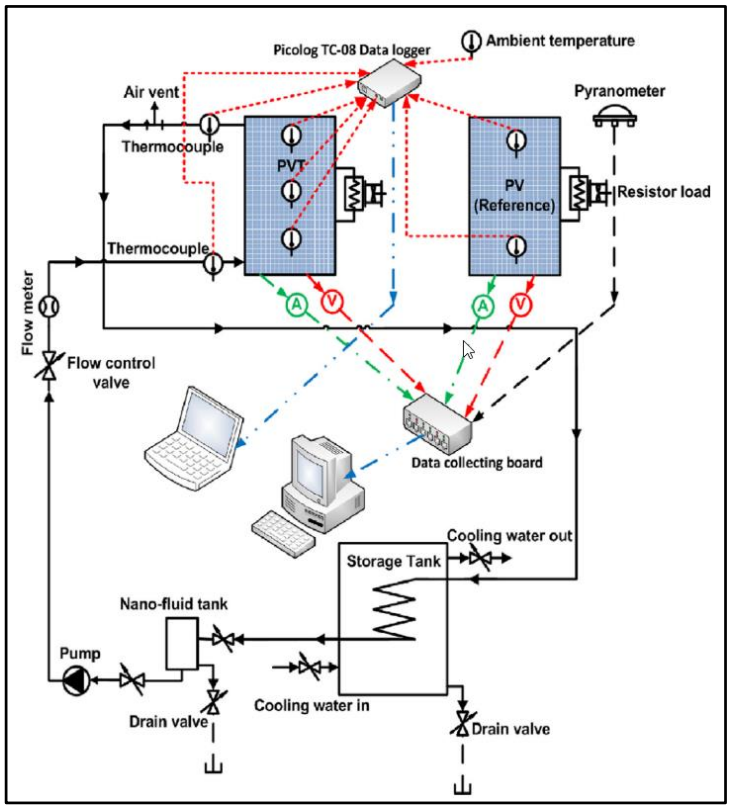

Figure 2.7. Experimental setup configuration by Alous et al. [32] .

The work by Al-Waeli et al. [30] is shown in Figure 2.7, which shows that a PV/T system is constructed using a 40 W mono-crystalline PV module that was linked to a high-heat storage tank, which contains a PCM. The tank was equipped with copper tubes, which circulate a cooling liquid, which pulls out some stored heat and later releases it to an external heat exchanger. Other major additions to the PV/T system include an external heat exchanger, water pumps, a data acquisition system, a laptop, and a nanofluid container. To store hot water that comes from the heat exchanger, a

water tank was added to the apparatus. From the sides and the base, a wax reservoir was isolated using 2cm thick glass wool that prevents heat leakage to the surroundings.

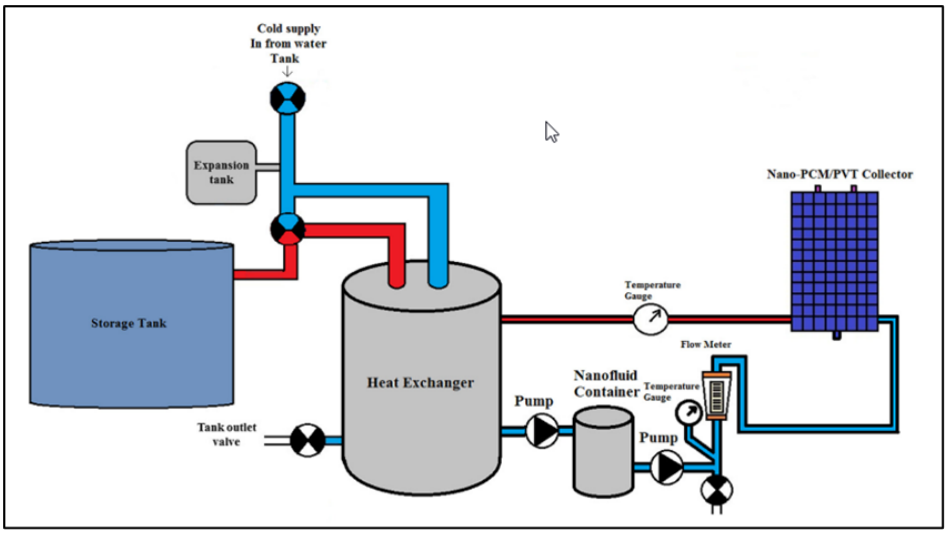

Figure 2.8. Experimental setup configuration by Al-Waeli et al. [30] .

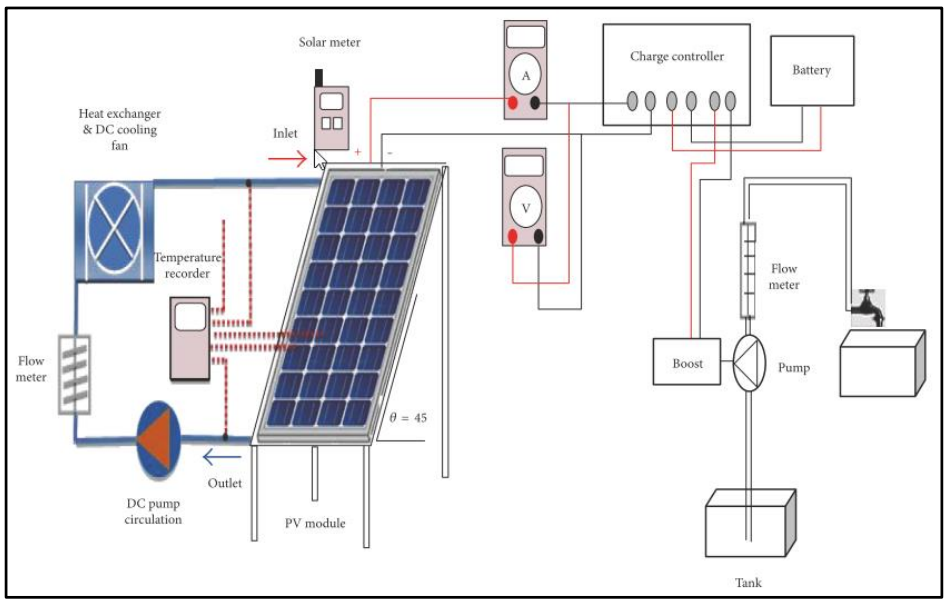

Figure 2.9. Experimental setup configuration by Hussein, H.A., et al. [33].

Hussein, H.A., et al. [33] tested an active cooling technique using a small heat exchanger equipped with a few water circulating pipes and oscillatory copper pipes on the rear surface of a PV, as Figure 2.9 shows.

Sardarabadi et al. [19] used a 40 W mono-crystalline PV in their outdoor testing stand for constructing the experimental setup. A serpentine copper tube unit was linked to a PV/T collector (Figure 2.10), and the heat exchanger was linked to a counterflow shell and tube for cooling the nanofluid. They selected city water at 40 L/h flow rate as a cooling fluid, and the flow rate of the nanofluid was 30 L/h.

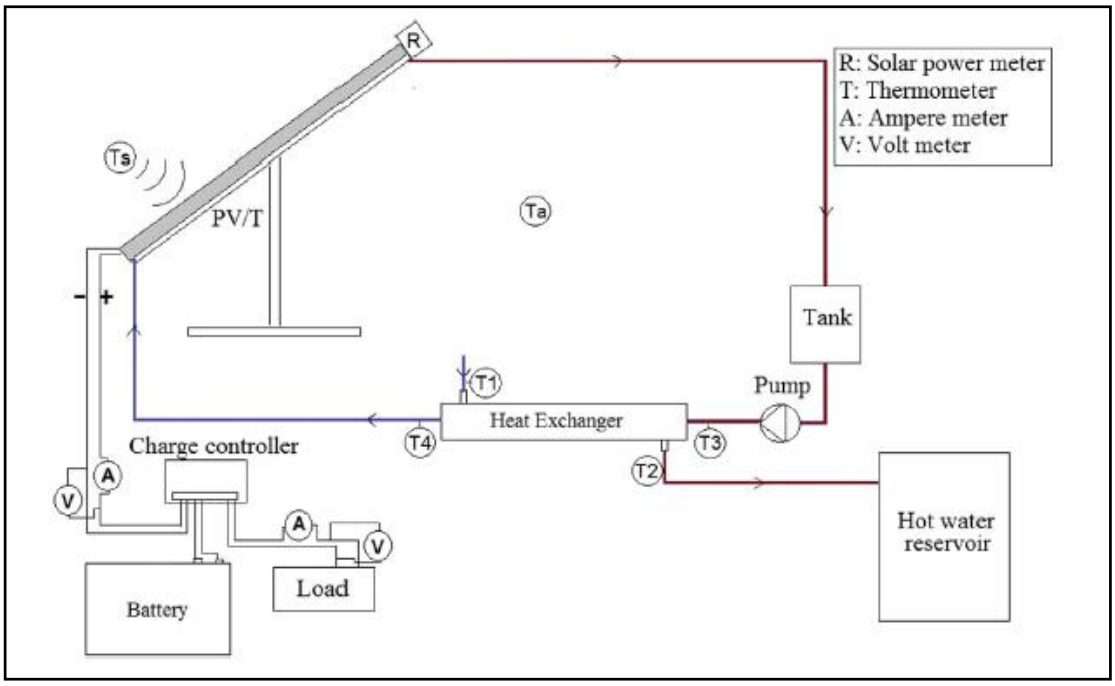

Figure 2.10. Experimental setup configuration by Sardarabadi et al [19].

Ghadiri et al. [20] constructed an indoor experimental PV/T setup using two 40 W mono-crystalline silicon PV modules, while each of them had 36 solar cells. The PV units had a sheet-and-tube collector whereas the other one had no collector. On the top of a copper plate (630 mm×540 mm), some solar cells were attached. It was welded on the back to a serpentine copper tubing that had a thermal insulation layer, as Figure 2.11 shows. The rate of cooling fluid flow was 30 L/h, which was cooled through a tube heat exchanger with 40 L/h city water on the cool side and a counterflow shell. They used 4 K-type thermocouples to measure the inlet and outlet temperatures of the mentioned heat exchanger. A circulating pump was contacted to a tank where the working fluid was stored for circulating fluid around the panel.

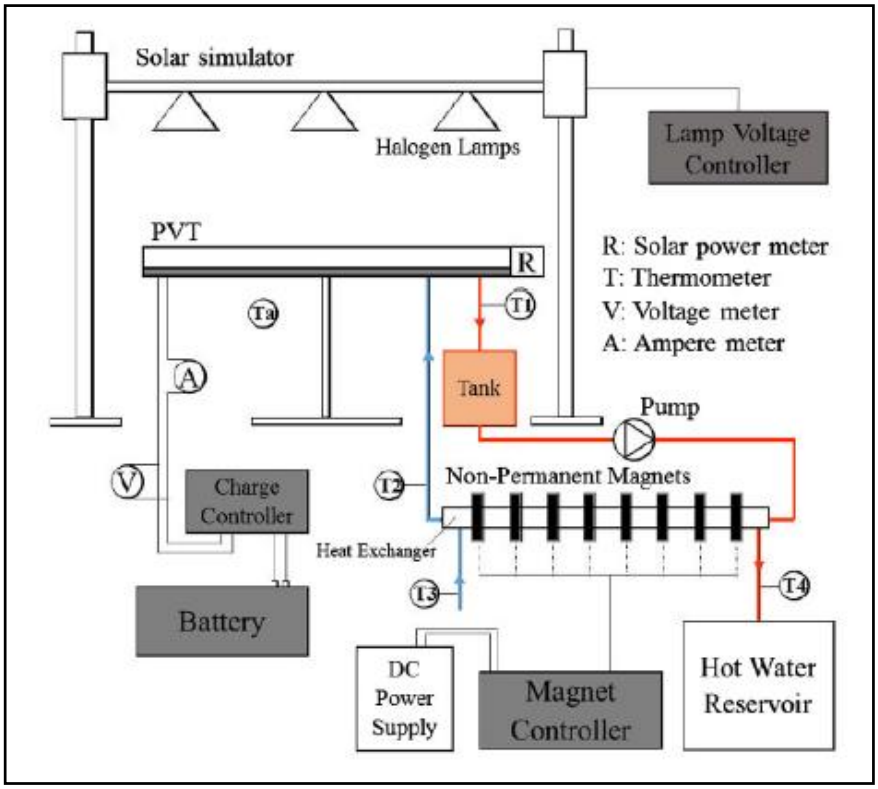

Figure 2.11. Indoor experimental setup configuration by Ghadiri et al. [20].

Al-Shamani et al. [34] utilized a 120 W Polycrystalline PV panel as a PV/T collector in an experimental setup (Figure 2.11) by attaching a rectangular stainless-steel tube with 15mm height, 1mm thickness, and 25 mm width. The PV/T collector was installed, and used, and the storage tank equipped with a coil heat exchanger was used for cooling the nanofluid. At different flow rates (0.06, 0.102, 0.136 and 0.17 kg/s), the PV/T collector's performance was estimated.

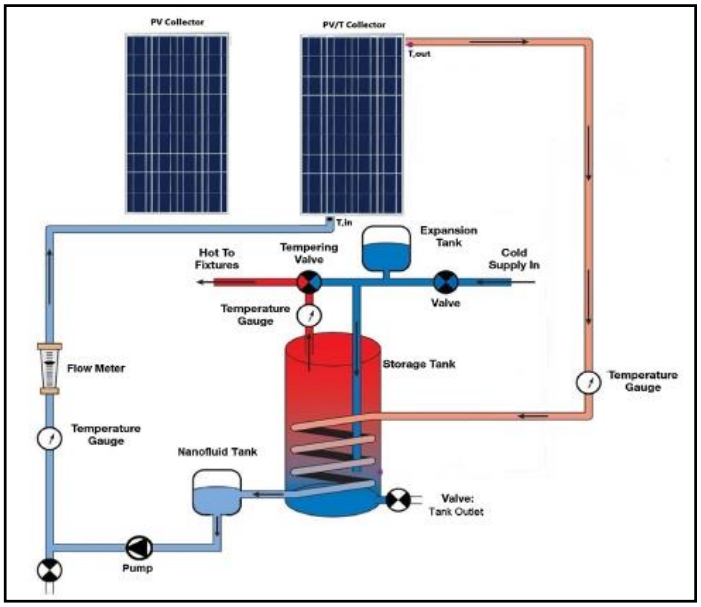

Figure 2.12. Experimental setup configuration by Al-shamani et al. [34].

In another experiment, Al-Waeli et al, [23] connected the nanofluid tank with a water storage tank. Several devices were linked to the test module, including a water pump that circulates the flow meter and a fluid for measuring the flow rate and to assess the devices, which were linked to obtain the real data. In Figure 2.12, we have shown the experiments that have been conducted at 0.068-0.170 kg/s flow rate for the nanofluid.

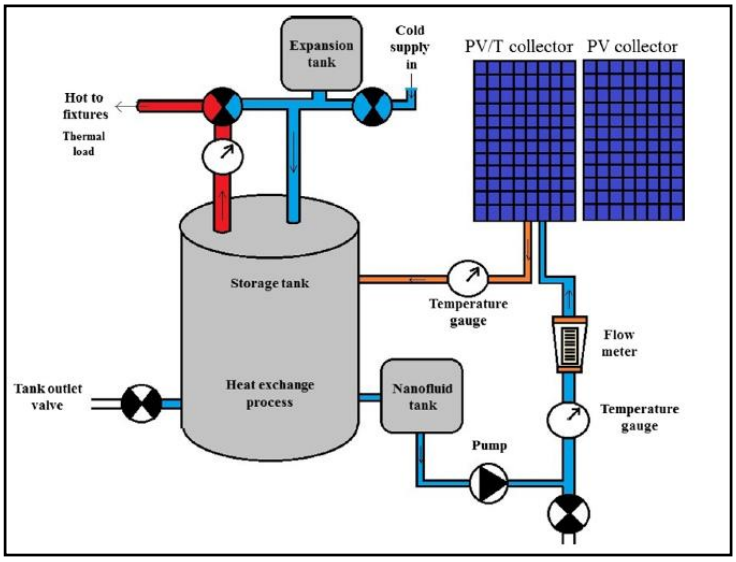

Figure 2.13. Indoor experimental setup configuration by Al-Waeli et al. [23].

Al-Waeli et al. [35] used an indoor setup to conduct an indoor solar test, as Figure 2.13 shows. The equipment called MINI-EESTC was made in Italy. They used a solar collector, which was made of tempered glass, and a copper plate replaced its surface to operate as a heat transfer medium. A copper pipe was welded to it to increase the heat transfer rate. Above the upper place, a PV collector was fixed, and fifteen lights were installed on the PV cell to provide intensities within the range 0–1500 W/m^2. A control panel operated as a solar simulator to control the process.

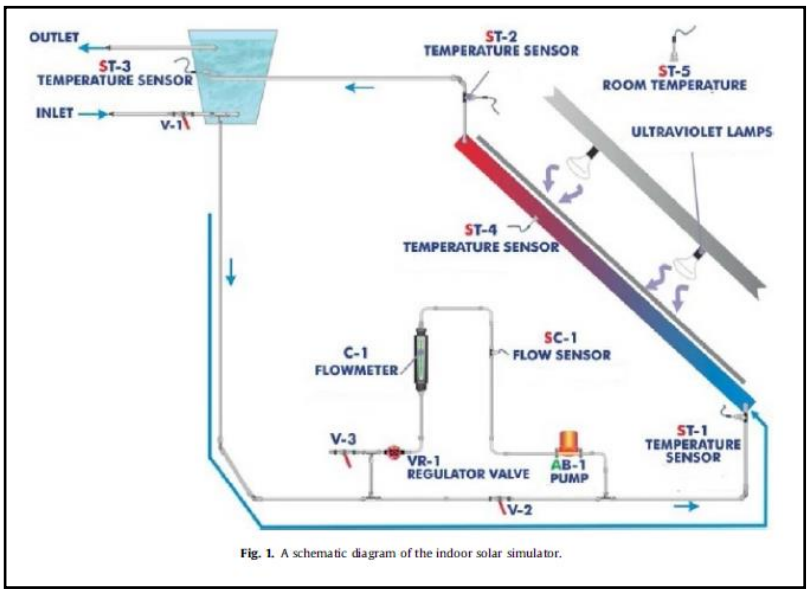

Figure 2.14. Indoor experimental setup configuration by Al-Waeli et al. [35].

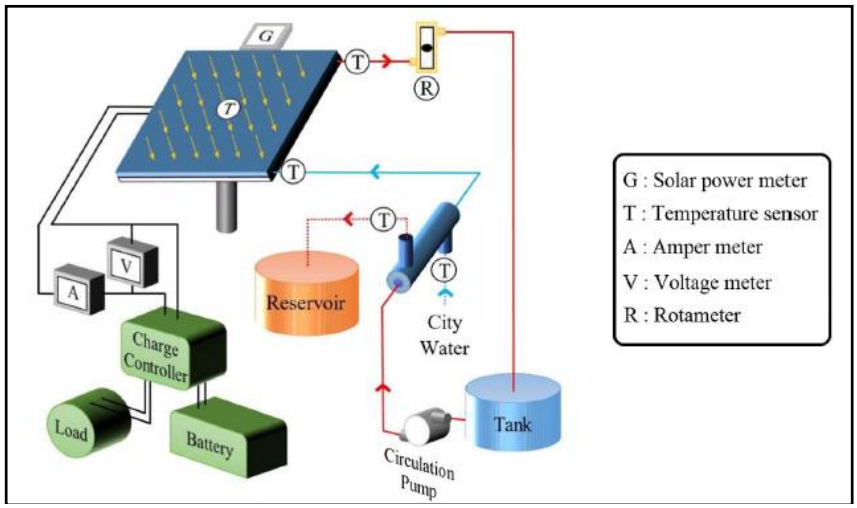

Figure 2.15. Experimental setup configuration by Hosseinzadeh et al. [36].

Hosseinzadeh et al. [36] (Figure 2.15) conducted experiments on a 40 W mono-crystalline PV/T collector that was equipped with a serpentine copper tube, which was soldered to a copper plate, and it was cooled by a shell-and-tube heat exchanger. At 30kg/h nanofluid flow rate, and at 40 L/h flow rate for the city water, the experiments were conducted, in which, the nanofluid was cooled down in a heat exchanger.

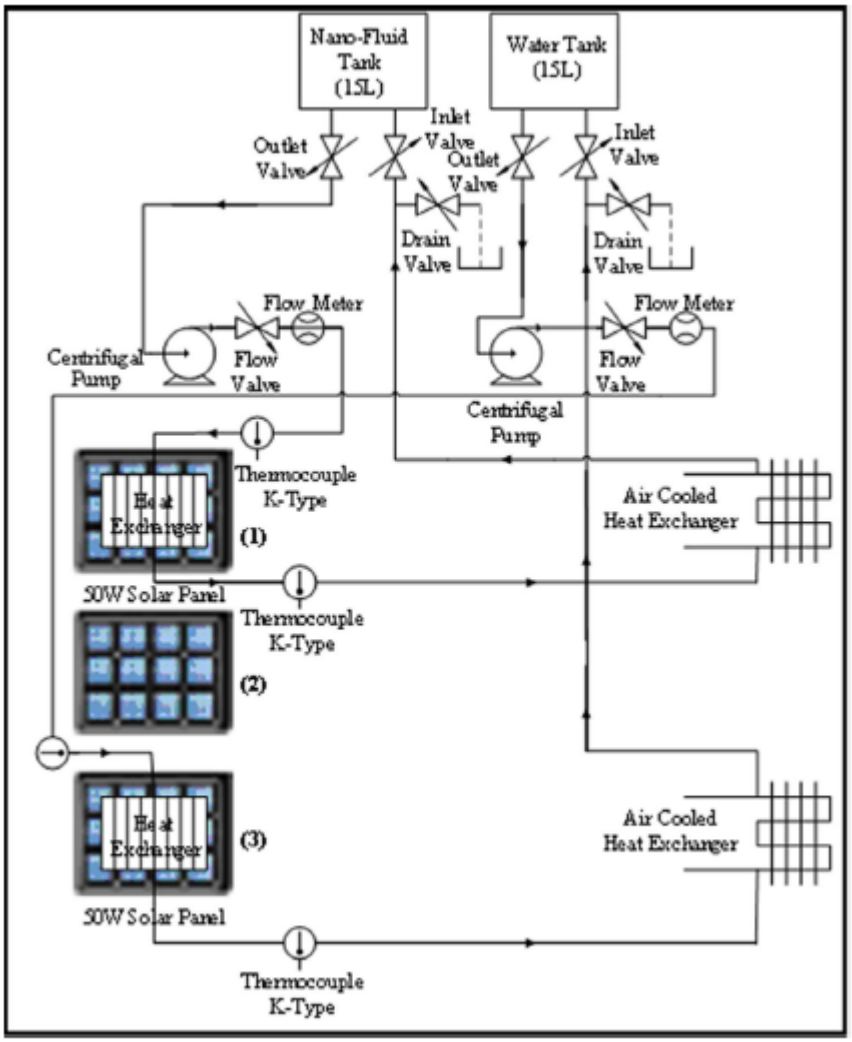

Figure 2.16. Experimental setup configuration by Ebaid et al. .

Ebaid et al. [25] formed an experimental setup, as Figure 2.16 shows, and it had three mono-crystalline silicon PV modules, which have 18x50 mm cooling area in the form of two rectangular aluminum heat exchangers, which were installed on the back side of a PV collector. To assure heat, sink material was added that assures a perfect contact between the PV collector's back surface and the aluminum heat exchanger. Moreover,

centrifugal pumps were used to circulate the cooling fluid from two 15 L insulated tanks, which were used for accumulation, and they were connected to the system by PVC pipes. Total 12 K-type thermocouples were used to measure the PV surface temperatures that contacted multiple points in the PV cell. Using two air cooling heat exchangers, the cooling fluid was cooled, and a couple of flow meters were attached at the centrifugal pumps' outlets. Other devices, which came in contact with the system, were a digital multimeter, a data logger, and a solar power meter for measuring inlet and outlet fluid temperatures of the PV module and solar irradiation intensity.

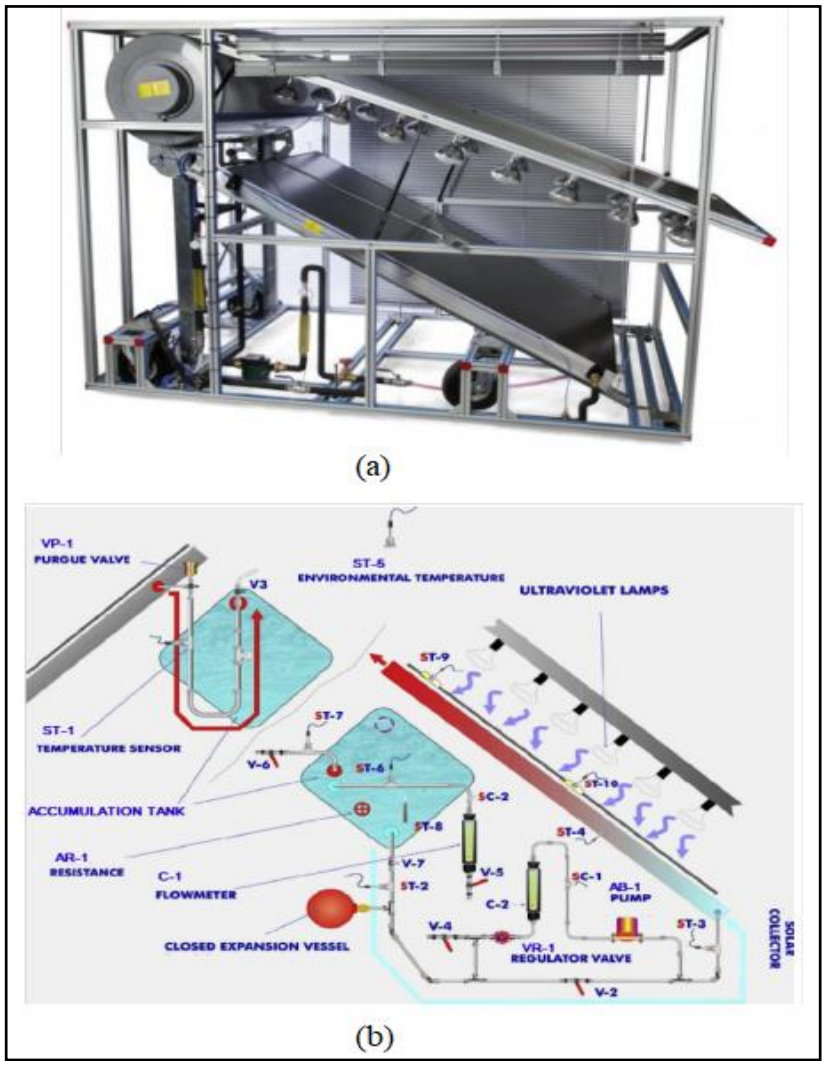

Figure 2.17. Indoor solar simulator: a) Photo of the simulator, b) Schematic diagram. of the simulator details by Al-Waeli et al [24].

In this experimental study, Al-Waeli et al [24] used two PV/T collectors. The figure of the PV/T systems shows the tests and a schematic. This study compared indoor and

outdoor testing while keeping the specifications constant by attaching a 120 W PV module to a thermal collector.

Vakili et al. [31] conducted experiments on deionized water and GNP in a solar collector. Until then, (GNP) nanofluid had never been used in a volumetric solar collector as a working fluid. Results of the experiment show an ideal mass flow rate (0.015 kg/s) with zero-loss efficiency whereas three selected weight fractions 0.0005, 0.001 and 0.005 were 83.50%, 89.70%, and 93.20% respectively, but it is only 70% in case of a base fluid (Figure 2.18).

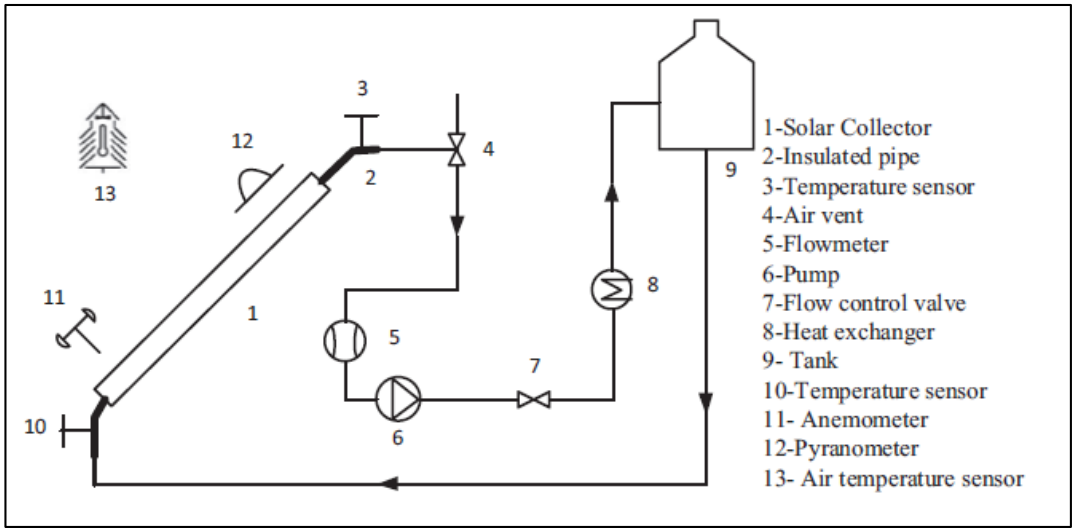

Figure 2.18. Schematic diagram by Vakili et al. [31].

Fayaz et al. [37] and Nasrin et al. [27] studied an indoor module (Figure 2.18), and their experimental setup had a PV/T, a solar simulator, a radiator, a pump, and a nanofluid tank. There were 120 halogen lamps in a solar simulator to supply the input energy. A 1.3kg/cm2 radiator was operated with forced convection, which maintained the working fluid temperature within limits that allowed it to re-enter the PV/T system. They used a centrifugal pump model MP-20RX for circulating the working fluid at 46/52 L/min pumping capacity. The pumping power consumption was 32 W. They used a 72-cell PV panel and used a sheet and tube design of serpentine aluminum pipes, which were attached to the polycrystalline back surface using a thermal paste without any absorber plate.

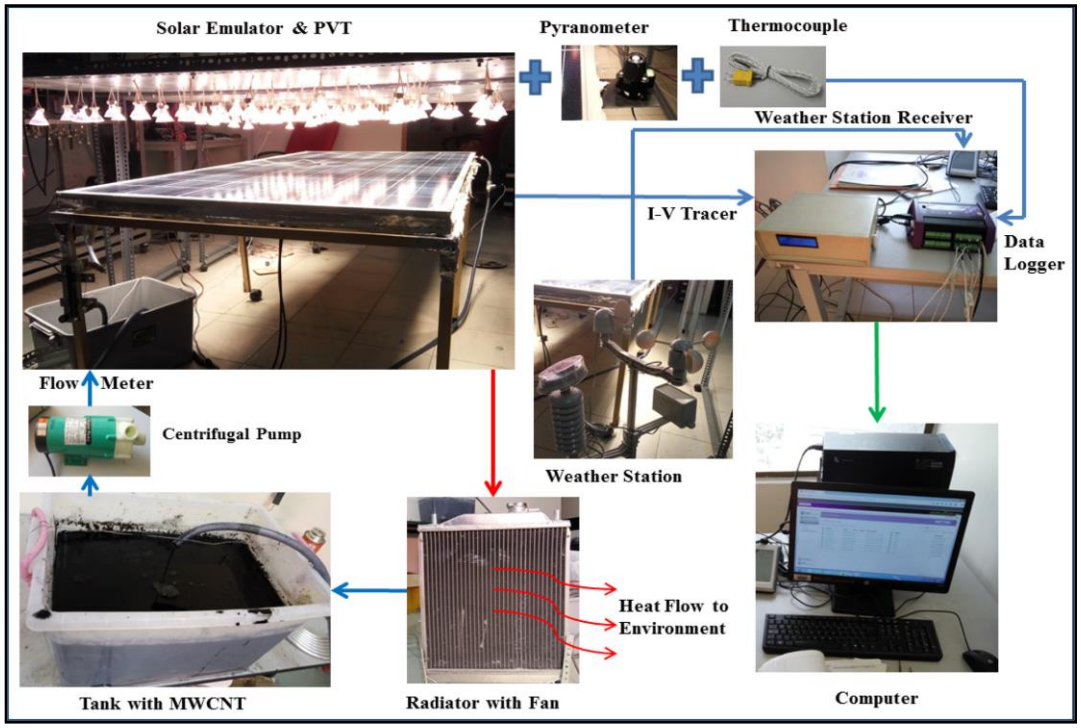

Figure 2.19. Indoor solar simulator by Fayaz et al. [37] and Nasrin et al. [27].

Abdallah et al. [38] used three identical single-crystalline solar panels in their 10 W output setup, and attached a serpentine thermal unit on the PV panel's back. The serpentine thermal unit was made up of 1/4" diameter copper tube, which was linked to a 0.3 mm copper sheet. The PV conventional panel was simultaneously tested with the PV/T water as well as nanofluid collectors in similar conditions. A circulation pump was used to circulate the cooling fluid with a 5 L tank and control valves. The flow rate of working fluids was 1.2 L/min. Eleven thermocouples were contacted with a data acquisition system in different positions and nine of them on the back surface while the rest of the two thermocouples were one each on the PV module's fluid entry and exit (Figure 2.20).

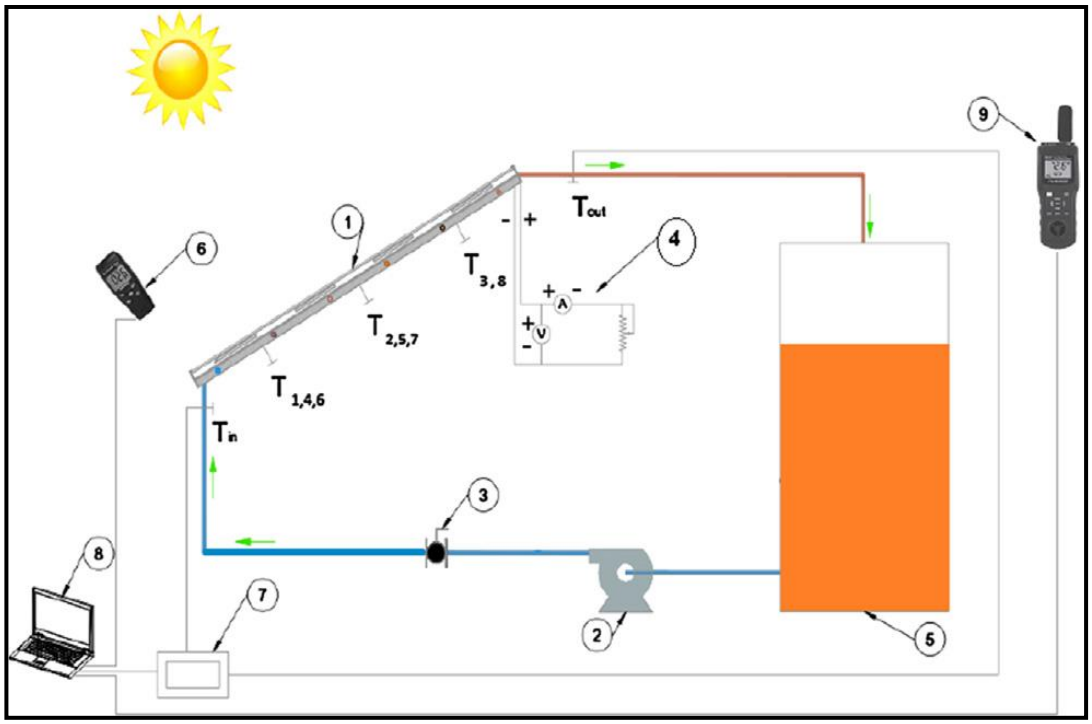

Figure 2.20. Experimental setup configuration Abdallah et al.[38].

Sangeetha et al. [39] included a monocrystalline silicon PV module in their experiment, as shown in Figure 2.20 and Figure 2.21. At 35° tilt angle, a PV/T was placed in a movable metal stand. For nanofluid storage, three different storage tanks were used and every PV module had 62*125 mm dimensions while the back side was manufactured using a tedlar, which creates resistance against impact and weathering. To improve the heat absorption in the collector, a copper pipe was installed in the collector. The tank capacity was 5 L and it was integrated using a pump. They used a shell-type heat exchanger for collecting working fluids. To measure the nanofluid stability, thermal conductivity was measured using KD-2 thermal properties analyzer, a viscometer was used to measure the viscosity, and a K-type thermocouple measured the temperature. For measuring wind speed, a digital meter was used and a voltmeter measured the current and voltage during the tests.

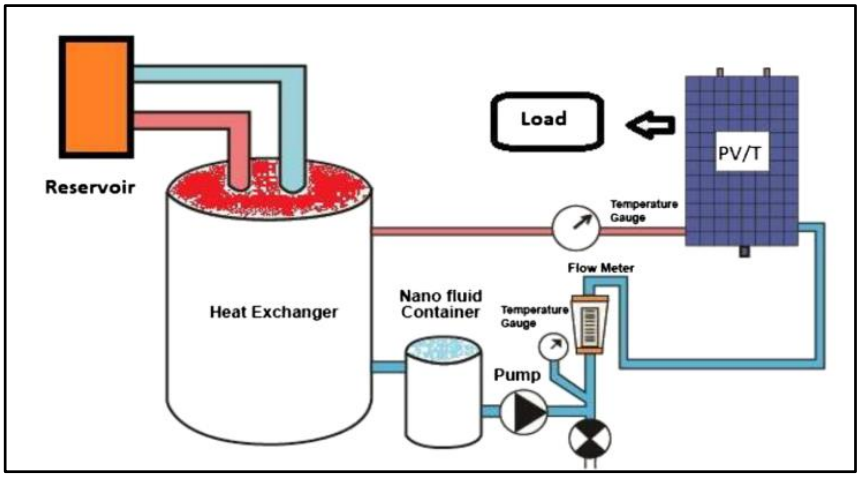

Figure 2.21. Schematic diagram by Sangeetha et al. [39].

Figure 2.22. Experimental setup by Sangeetha et al. [39].

Iranmanesh et al. [29] in their experimental study used a borosilicate glass 3.30 as a part of their experimental setup. The evacuated tube solar collector (ETSC) had 0.058m and 0.047 m outer and inner diameters. A heat pipe was linked to a curved fin, which was located in a glass tube, and its purpose is to transfer solar heat to a copper manifold, which consists of a working fluid. Hot water was obtained when the heat was transferred through fluid flow to a storage tank. Moreover, the system's other components include a nanofluid tank, circulation pump, controlling units, and cooling

water tank (capacity: 50 liters). Pyranometer and anemometer were used to measure the solar radiation and wind speed while the tilt angle was 33° to absorb maximum daily solar radiation at volumetric flow rates 0.5, 1.0 and 1.5L/min. They installed four RTD sensors (PT-100) for measuring the inlet and outlet temperatures of the storage tank and manifold besides finding the ambient temperature. They connected a 10-channel data logger to all the sensors and a computer was linked to record all the data (Figure 2.22).

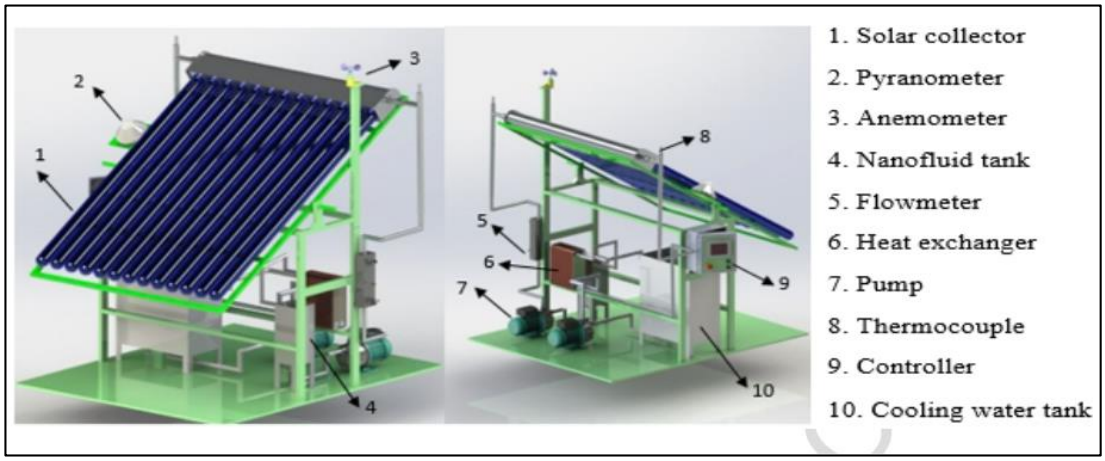

Figure 2.23. Schematic diagram by Iranmanesh et al. [29].

Hassan et al. [40] used 30W monocrystalline PV panels with 68*30cm^2 area with 34^o tilt angle for solar panel (Taxila latitude angle: 33.7^o) for collecting highest possible solar radiation when they employed a non-tracking system. Their experiments were focused on comparing between three configurations, such as a conventional PV panel, the second one was equipped with a PCM container, and the third one had a PV/T with PCM, which was equipped with copper tubes for coolant flow. It was surrounded by the PCM. Figure 2.23 indicates the mentioned experimental apparatus and its major parts.

Figure 2.24. Experimental setup Hassan et al. [40].

According to the experimental setup configurations presented above, there are two configuration options:

- A PV/T collector and another PV reference panel setup configuration.
- Two PV/T collectors and a single PV reference panel setup configuration [41].

In a single PV/T-one PV configuration system, it is possible to test a PV/T collector with PV reference panel at the same time and under the same conditions whereas, in double PV/T-one PV configuration system, it is possible to test two PV/T collectors at the same time with PV reference panel. Two PV/T-one PV configuration systems have more components since each PV/T collector has its individual thermal circuit (heat exchanger, pump, and flow meter), compared to a single PV/T-one PV setup configuration but two PV/T-one PV setup configurations have the ability to test two types of working fluids such as water and nanofluid or two types of nanofluids along with the PV reference panel, which reduce the experimental time and gives better comparison results since the two different working fluids are tested under the same conditions especially in outdoor testing conditions.

In the light of the aforementioned experimental setup configurations, an experimental setup of one PV/T-one PV configuration and PV/T collector were obtained using a serpentine thermal unit, which was constructed and appalled for studying the effects of nanofluids (MWCNT-water and graphene nano-platelets-water) in PV/T systems.

2.3.3. Performance Enhancements of Using Nanofluids in Flat PV/T Systems

Utilization of conventional working fluids to cool down the PV cells in PV/T flat collectors increases their performance but it has limitations because they have low thermal conductivities. Because of their higher thermal conductivities compared to base fluids and nanofluids, which attracted a lot of interest in thermal applications whereas a PV/T system is one of these applications. Investigations of nanofluid usage as coolants in PV/T systems in literature are still insufficient and need greater attention in future studies. Table 2.1 summarizes the performance improvements achieved by using nanofluids in a flat PV/T system.

Table 2.1. Some performance enhancements using nanofluids of PV/T collectors.

Author (s)	Type of Nanofluid	Concentration of Nanofluid	Results
Hassan et al. [40]	graphene/water, phase change material (RT-35HC) and PCM	0.05%, 0.1%, 0.15%	1. The PV temperature reduced maximum (16.1°C, 11.9°C, and 23.9°C,) using water-based PV/T/PCM system, PV/PCM system, and nanofluid-based PV/T/PCM system, respectively, when they were compared to the PV/T/PCM systems, which were integrated with water that flows through tubes in the PCM, PV/PCM system and the traditional PV. 2. Their electrical efficiencies increased by 22.7%, 9.1%, and 23.9% respectively, as compared to ordinary PV. 3. 17.5% higher thermal efficiency was observed when a nanofluid-based hybrid PV/T/PCM system was compared to a water-based hybrid PV/T/PCM system. 4. The overall efficiency enhancement was 12%.
Sardarabadi et al. [19]	SiO_2/water	1 wt% 3 wt.%	1. The overall energy efficiency increased by 3.6% in a PV/T system's output electrical energy when SiO2/water fluid was used as compared to pure water. 2. Their thermal efficiencies improved by 7.6% and 12.8% at 1wt% and 3wt% respectively as compared to PV/T-water. 3. The PV/T system's total exergy improved by 19.36%, 22.61% and

			24.31% for pure water with 1wt% and 3wt%, and silica/water.
Ghadiri et al. [20]	Ferrofluid (Fe_3O_4/water)	1 wt% 3 wt.%	1. Total 45% efficiency enhancement was observed when a PV system was used with an alternating magnetic field (Frequency: 50 Hz) that became 50% as compared to a water-cooled PV/T system. 2. A 48W rise in the total exergy was observed when a thermal collector is used in a common PV system adding 3wt% of ferrofluid applying an alternating magnetic field at 50 Hz.
Sardarabadi et al. [21]	AL_2O_3 TiO_2 ZnO All of them were dispersed in de-ionized water	0.2 wt.%	The results of this study after experimental and numerical analysis show the following: 1. The TiO_2/water and ZnO/water have higher electrical efficiencies as compared to both the deionized water and the Al_2O_3/water nanofluid. . 2. ZnO/water has shown the highest thermal efficiency as compared to the TiO_2/water, deionized water, and Al_2O_3/water.
Al-Shamani et al. [34]	Water-dispersed SiO_2 TiO_2 SiC	0.5, 1.0 and 2.0 wt% for all the nanofluids	1. SiO2 nanofluids showed the highest thermal efficiencies, which were about 81.73% while 13.52% was the highest electrical efficiency increase. The best overall energy coefficient (COE) was 0.93 as compared to the TiO_2 nanofluids and water, respectively.
Al-Waeli et al, [23]	SiC/De-ionized water	3 wt%	1. From 25 °C–60°C, the thermal conductivity enhancement was observed up to 8.2%. 2. More than 24.1% electrical efficiency improvement was observed when it was compared to a common PV system. 3. There was up to 100.19% higher thermal efficiency as compared to water. 4. The increase in the overall efficiency was 88.9% more than the PV systems.
Al-Waeli et al.[35]	Water-dispersed Al_2O_3 CuO SiC	4v%	1. Compared with the base fluid, the nanofluids increased density and viscosity by a little percentage but it increased thermal conductivity. 2. In comparison with AL_2O_3 and CuO, SiC particles were more stable and it had the highest thermal conductivity.

			3. CuO is less stable but have better thermal conductivity as compared to other nanofluids.
Ebaid et al. [25]	TiO_2/water-cetyltrimethylammonium bromide mixture. AL_2O_3/water-polyethylene glycol mixture	0.01, 0.05 and 0.1 wt% for all nanofluids.	1. AL_2O_3 and TiO_2 nanofluid reduced the PV cells temperatures better than water. 2. As compared to the TiO_2 nanofluid and water, AL_2O_3 nanofluid showed a better performance. 3. Increase in the nanofluid concentration results in a better cooling effect of a PV cell. 4. As compared to water cooling and no cooling, TiO_2 nanofluid has a higher performance.
Hosseinzadeh et al. [36]	ZnO/Deionized water	0.2 wt%	1. The thermal efficiencies of ZnO/water-cooled PV/T system improved by 16.21% when the coolant's inlet temperature reduces from 40°C to 20°C. 2. The studied parameters had a small effect on the PV/T systems' electrical efficiencies.
Al-Waeli et al. [24]	SiC/water	-	1. For performance enhancement with incremental efficiency, the indoor system's results were closer to the results of the outdoor experiment 2. The indoor system's power production is more as compared to the outdoor system by almost 4.2%. 3. They found that the outdoor system had the capability to improve the solar collectors' efficiencies. 4. The indoor system showed higher thermal and electrical energy efficiencies as compared to the outdoor system.
Fayaz et al. [37]	MWCNT/water	0.75 wt%	When solar radiation was fixed at 1000 W/m², the ambient temperature was 25 °C and the inlet temperature was 32 °C: 1. In this experimental test and numerical analysis the electrical efficiency increment of PV were 12.25% and 10.72% respectively at flow rate 120L/h. 2. The cell temperature experimentally reduced by 0.72 °C and numerically by 0.77 °C for every 10L/h. 3. There was 7.74W numerical thermal enhancement and 6.89W experimental thermal enhancement for every 10L/h. 4. There was 5.62% more numerical thermal efficiency and 5.13%

			experimental thermal efficiency for MWCNT/water in comparison with water.
Nasrin et al. [27]	MWCNT/water	0 – 1.0 wt%	1. The numerical results for this study showed a good response to the experimental measurements. 2. By experimental test, the PV performance enhanced about 9.2% with distilled water cooling. 3. By using MWCNT, the result showed that the thermal performance numerically improved by 4% and experimentally by 3.67% than water. 4. The overall efficiency numerically improved by 3.81% and experimentally by 4.11%, and the PV/T-MWCNT/water was much better than the PV/T water.
Abdallah et al.[38]	MWCNT/water	0 - 0.3 vol%	By using the optimum nanofluid concentration of 0.075 vol%: 1. The PV panel temperature reduced by 12°C at noon and 10.3°C during the daytime. 2. At noon, the overall system efficiency was 83.26% and 61.23% during the rest of the experiment day.
Al-Waeli et al. [35]	CuO, Al_2O_3, SiC in water	0.5vol%, 1vol%, 2vol%, 3vol%, and 4vol%	SiC showed the peak efficiency. Thermal efficiency: 50% Total equivalent efficiency: 16.8%
Hassan et al. [42]	SiO_2, SiC, TiO_2 in water	1wt%	Since SiC has the highest efficiency, Thermal efficiency: 85%, Overall efficiency: 97.75% Electrical efficiency: 12.75%
Salem et al. [43]	Al_2O_3/PCM mixture and/or water	0–1wt%	Pure PCM/water showed the highest efficiency
Aberoumand et al. [44]	Ag/water	2 and 4wt%	Exergy efficiency: 50% Power output enhancement: 35%
Abdallah et al. [45]	MWCNT/water	0–0.3 vol%	Total efficiency: 83.26%

Most of the references, which have been mentioned in Table 2.1 show that there is a compatibility between them and when the nanofluids are used as coolant fluids in a

PV/T system, and they improve their performances if we compare them to the PV/T collectors using conventional fluids. This kind of performance enhancement mostly relies on the base fluid type, nanoparticle shape, nanoparticle size, concentration, added surfactants and the selected mixing method. Nevertheless, there is no certain criteria so far that controls the preparation of stabilized nanofluids to identify specific methods of improvements in any PV/T system.

This study has a specific experimental setup for enhancing the PV/T collector's performance using a hybrid nanofluid as a coolant and graphene nano-platelets nanofluid. As compared to other designs [46], a sheet and tube heat exchanger (square tube serpentine type) was constructed and linked with the PV panel's backside, which formed our PV/T collector, which is used for investigations in the experiments.

CHAPTER 3

ENERGETIC AND EXERGETIC EFFICIENCY OF PV/T COLLECTOR

3.1. ENERGY BALANCE FOR A PV/T COLLECTOR

PV thermal collectors or PV/T collectors are equipped with PV thermal solar collectors and hybrid solar collectors that transform solar radiation in electrical and thermal forms of energy. They also have PV solar cells to transform solar incident into electrical and thermal forms of energy and the heat is transferred to a working fluid. This technology has the capacity to show a higher efficiency as compared to the solar-thermal (T) and solar photovoltaic (PV) systems [2]. Figure 3.1 shows the details of our system:

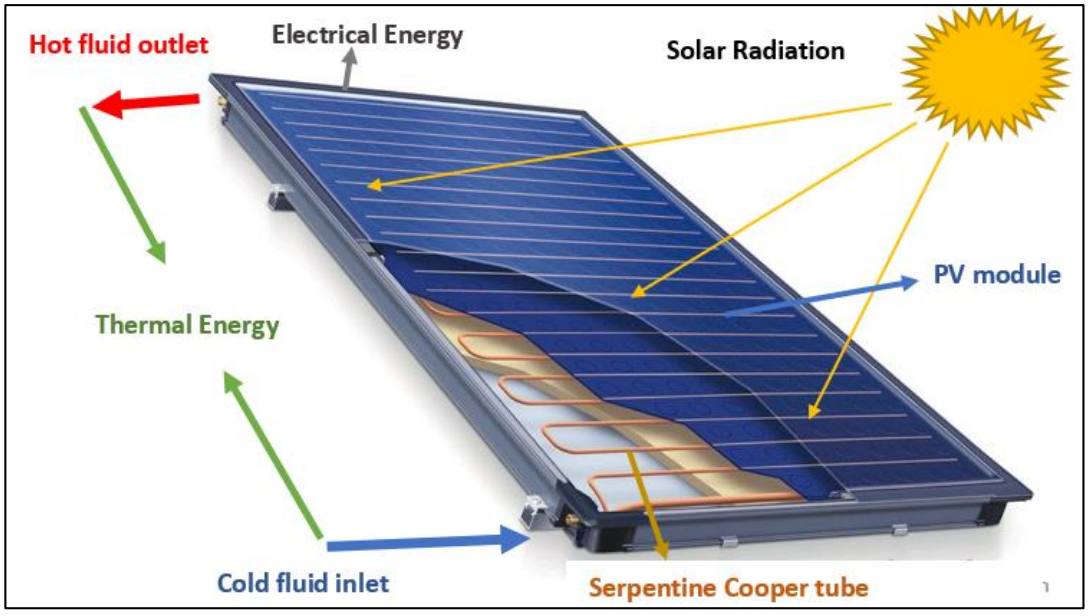

Figure 3.1. Energy balance for a PV/T collector.

$$\begin{pmatrix}\text{Rate of change in energy}\\ \text{inside}\\ \text{the control volume}\end{pmatrix} = \begin{pmatrix}\text{Rate of energy}\\ \text{entering}\\ \text{the control volume}\end{pmatrix} - \begin{pmatrix}\text{Rate of energy}\\ \text{leaving}\\ \text{the control volume}\end{pmatrix}$$

By assuming a steady-state condition, in the control volume, the rate of change in energy will be zero, and:

$$\begin{pmatrix}\text{Rate of energy}\\ \text{entering}\\ \text{the control volume}\\ \dot{E}_{in}\end{pmatrix} = \begin{pmatrix}\text{Rate of energy}\\ \text{leaving}\\ \text{the control volume}\\ \dot{E}_{out}\end{pmatrix}$$

The energy output $\dot{E}_{out}$ rate (Watt) from a PV/T collector is the summation of electrical power $\dot{E}_{el}$, power loss $\dot{E}_{loss}$ and thermal power $\dot{Q}_u$:

$$\dot{E}_{out} = \dot{Q}_u + \dot{E}_{el} + \dot{E}_{loss} \tag{3.1}$$

Because of the difference between the PV/T collector temperature and the ambient temperature, power $\dot{E}_{loss}$ dissipated as energy loss from the PV/T collector to its surroundings. For the working fluid, the rate of thermal energy output $\dot{Q}_u$ shows the useful collected power (W) in terms of temperature increase:

$$\dot{Q}_u = \dot{m} C_p (T_o - T_i) \tag{3.2}$$

Here, *Cp* = specific heat of working fluid (J/kg K), T_i and *To* = working fluid's inlet and outlet temperatures and $\dot{m}$ = the coolant mass flow rate (kg/sec). Electrical energy $\dot{E}_{el}$ (W) production rate by *PV* cells is:

$$\dot{E}_{el} = V_{oc}.I_{sc}.FF \tag{3.3}$$

Here: I_{sc} is the short circuit current (A), *Voc* is the open-circuit voltage (V), *FF* represents the filling factor that shows the PV's maximum power conversion efficiency evaluated as a ratio between the photovoltaic module's maximum power to

the open-circuit voltage. It was then multiplied by the short circuit current under the PV module's standard testing conditions [47].

$$FF = \frac{P_m}{V_{oc}.I_{sc}} \tag{3.4}$$

The PV and PV/T model's electrical power output is obtained from the following equation:

$$P = V.I \tag{3.5}$$

Here: *I* represents the output current (A) while *V* shows the output voltage (V).
Since a PV/T collector depends on solar radiation for its thermal efficiency, both thermal (η_{th}) and electrical (η_{el}) efficiencies can be expressed as:

$$\eta_{el} = \frac{P}{I_R \times A_{PV}} \tag{3.6}$$

This equation has the following variables: A_{th} shows the area (m^2) of PV/T collector, A_{PV} represents the area (m^2) of PV and I_R is the solar radiation (W/m^2).

$$\eta_{th} = \frac{Q_u}{I_R \times A_{th}} \tag{3.7}$$

The electrical efficiency increment $\Delta_{eL,}$ is obtained by Eq.

$$\Delta_{eL,} = \frac{\eta_{pvt,el} - \eta_{pv,el}}{\eta_{pv,el}} \times 100 \tag{3.8}$$

3.2. THERMAL PROPERTIES OF NANOFLUIDS

The base fluid and nanoparticles' characteristics show the thermal properties of the nanofluids [48]. The nanofluids' density can be obtained through Pak and Cho model [49], as given below:

$$\rho_{nf} = \varphi.\rho_{np} + (1-\varphi)\rho_{bf} \tag{3.9}$$

Where φ is the volume concentration of the dispersed fluid, ρ_{bf} is the base fluid density, and ρ_{np} shows the nanoparticles' density. The density of the hybrid nanofluid is obtained using the following alternative formula according to Xuan and Roetzel model:

$$\rho_{hnf} = \varphi_{np1} \cdot \rho_{np1} + \varphi_{np2} \cdot \rho_{np2} + (1 - \varphi_{tot}) \cdot \rho_{bf} \tag{3.10}$$

We can calculate the volume fraction of a nanofluid using the following formula (Xuan et al.) [50]:

$$\varphi = \frac{\frac{m_p}{\rho_p}}{\frac{m_p}{\rho_p} + \frac{m_f}{\rho_f}} \tag{3.11}$$

Here, ρ is the density in kg m^{-3} and φ is the nanoparticles' volumetric ratio in a base fluid, *m* is the mass. We used the following formula to calculate the volume fraction of a hybrid nanofluid (Nadooshan et al.) [51]:

$$\varphi = \left[\frac{\left(\frac{m}{\rho}\right)_{Al_2O_3} + \left(\frac{m}{\rho}\right)_{GNP}}{\left(\frac{m}{\rho}\right)_{Al_2O_3} + \left(\frac{m}{\rho}\right)_{GNP} + \left(\frac{m}{\rho}\right)_{EG}}\right] \times 100 \tag{3.12}$$

The following equation is used to obtain the nanofluids' heat capacity (Khanjari et al.) [52]:

$$(\rho C_p)_{nf} = (1-\varphi)(\rho C_p)_f + \varphi(\rho C_p)_p \tag{3.13}$$

Here, *Cp* represents the specific heat (kJ $kg^{-1}K^{-1}$), ρ denotes the density (kg/m^{-3}), and φ shows the volumetric ratio of nanoparticles that exists in the base fluid. The *f*, *n*, and

nf subscripts respectively show nanoparticles, nanofluid, and base fluid. The heat capacity of HyNF is obtained using the following main formula (Al-Oran et al.) [53]:

$$C_{p,hnf} = \frac{\varphi_{np1} \cdot \rho_{np1} \cdot C_{p,np1} + \varphi_{np2} \cdot \rho_{np2} \cdot C_{p,np2} + (1 - \varphi_{tot}) \cdot \rho_{bf} \cdot C_{p,bf}}{\rho_{hnf}} \quad (3.14)$$

The prepared nanofluids' thermal conductivities can be determined using the Maxwell-Garnett model [54]:

$$k_{nf} = \frac{(k_p + 2k_f + 2\varphi (k_p - k_f))}{(k_p + 2k_f - \varphi (k_p - k_f))} k_f \quad (3.15)$$

The thermal conductivity of HyNF was represented by the following equation [53]:

$$k_{hnf} = k_{bf} \left[\frac{\frac{\varphi_{np1} \cdot k_{np1} + \varphi_{np2} \cdot k_{np2}}{\varphi_{tot}} + 2 \cdot k_{bf} + 2 \cdot (\varphi_{np1} \cdot k_{np1} + \varphi_{np2} \cdot k_{np2}) - 2 \cdot \varphi_{tot} \cdot k_{bf}}{\frac{\varphi_{np1} \cdot k_{np1} + \varphi_{np2} \cdot k_{np2}}{\varphi_{tot}} + 2 \cdot k_{bf} \cdot (\varphi_{np1} \cdot k_{np1} + \varphi_{np2} \cdot k_{np2}) + \varphi_{tot} \cdot k_{bf}} \right] \quad (3.16)$$

Here, ρ, *k*, and C_p respectively represent density, thermal conductivity, and specific heat while n, nf, and f represent nano-particles, nanofluid, and base fluid. In this case, φ shows the nanoparticles' volumetric ratio of the base fluid's suspension solution, which is calculated as follows:

$$\varphi = \frac{\frac{m_p}{\rho_p}}{\frac{m_p}{\rho_p} + \frac{m_f}{\rho_f}} \quad (3.17)$$

Here, m_p and m_f show the nanoparticles' mass and base fluid's mass. We used the following formula to calculate the volume fraction of a hybrid nanofluid (Nadooshan et al.) [51]:

$$\varphi = \left[\frac{\left(\frac{m}{\rho}\right)_{Al_2O_3} + \left(\frac{m}{\rho}\right)_{GNP}}{\left(\frac{m}{\rho}\right)_{Al_2O_3} + \left(\frac{m}{\rho}\right)_{GNP} + \left(\frac{m}{\rho}\right)_{EG}}\right] \times 100 \quad (3.18)$$

3.3. OVERALL ENERGETIC EFFICIENCY

The flat PV/T system's overall efficiency (η_{ov}) equals the output-input energy ratio in a specific time period.

$$\eta_{ov} = \frac{\dot{E}_{out}}{\dot{E}_{in}} = \frac{\dot{Q}_u + \dot{E}_{el}}{\dot{E}_{in}} \quad (3.19)$$

The overall flat PV/T collector's efficiency can be obtained as a sum of thermal and electrical efficiencies (η_{th} and η_{el}, respectively) and they can be expressed as [19,55]:

$$\eta_{ov} = \frac{\dot{Q}_u}{\dot{E}_{in}} + r.\frac{\dot{E}_{el}}{\dot{E}_{in}} = \eta_{th} + r.\eta_{el} \quad (3.20)$$

Here *r* is a packing factor, which is the ratio between the PV area (A_{pv}) and the collector area (A_c); at r = 0, there is no PV cell; and r = 1 means that all the collector area is covered by PV cells.

$$r = \frac{A_{pv}}{A_c} \quad (3.21)$$

$\dot{E}_{el}$ represents rate of output electrical energy per unit PV cells' area calculated by Eq. (3.3) and Eq. (3.6), Eq. 3.2 calculates $\dot{Q}_u$ that is the rate of output thermal energy per unit area of a collector, and $\dot{E}_{in}$ represents the rate of the effective incident solar radiation per unit collector area (Eq. (3.7). The PV module's electrical efficiency is a function of the cell's temperature T_c [56], which is expressed as given below:

$$\eta_{el} = \eta_r\left[\left(1 - \beta(T_c - T_r)\right)\right] \quad (3.22)$$

In this equation:

$\beta = 0.0045°C^{-1}$ represents the temperature coefficient [57].

$T_r = 25°C$ (shows reference temperature).

η_r = the module efficiency at 25°C.

For analyzing a thermal PV/T collector, the output electrical power ($\dot{E}_{el}$) is convertible into thermal power using the following equations [56,58]:

$$\dot{E}_{el,th} = \frac{\dot{E}_{el}}{C_f} \tag{3.23}$$

Where C_f is a conversion factor, its value range is 0.35-0.40, and a value 0.38 can be used. The PV/T's overall equivalent thermal efficiency is given below:

$$\eta_{PV/T,et} = \eta_{th} + r.\frac{\eta_{el}}{0.38} \tag{3.24}$$

3.4. EXERGETIC EFFICIENCY

Exergy efficiency works using the principles mentioned in the second thermodynamics law, and it creates ready-to-use energy. Moreover, the PV/T system performance is analyzed using exergy analysis [59,60]. The exergetic efficiency shows the energy quality as well. Moreover, the quality of energy extracted by the PV/T is called the overall exergetic efficiency, which is expressed as [55,60]:

$$\varepsilon_{PV/T} = \frac{\int_{t_1}^{t_2}\left(A_c\dot{E}x_{th} + A_{pv}\dot{E}x_{el}\right)dt}{A_c\int_{t_1}^{t_2}\dot{E}x_{sun}\,dt} = \varepsilon_{th} + r.\varepsilon_{el} \tag{3.25}$$

Here $\dot{Ex}_{th}$ is the rate of the output thermal exergy per unit collector area, A_{PV} and A_c represent the PV panel and collector areas, $\dot{Ex}_{sun}$ shows the solar irradiation exergy rate per unit collector area, and $\dot{Ex}_{el}$ is the rate of electrical exergy per unit PV module area. Here r is a packing factor, which is the area between a PV panel and the collector ($r=A_{PV}/A_c$); so when the packing factor is 1, we can find the

overall exergy as the sum of thermal and electrical exergy efficiencies while the PV exergy output per unit cell area equals the electrical power [55]:

$$\dot{\mathrm{E}}\mathrm{x}_{\mathrm{el}} = \dot{\mathrm{E}}_{\mathrm{el}} \tag{3.26}$$

Here $\dot{Ex}_{th}$ is expressed as a function of the output of useful thermal exergy [55]:

$$\dot{\mathrm{E}}\mathrm{x}_{\mathrm{th}} = \dot{\mathrm{Q}}_{\mathrm{u}}\left(1 - \frac{\mathrm{T}_{\mathrm{a}}}{\mathrm{T}_{\mathrm{o}}}\right) \tag{3.27}$$

Here T_a and T_o respectively represent the ambient and the fluid outlet temperatures (K).

The solar input exergy can be determined by using Jeter's model as [61]:

$$\dot{\mathrm{E}}\mathrm{x}_{\mathrm{sun}} = \left[1 - \frac{\mathrm{T}_{\mathrm{a}}}{\mathrm{T}_{\mathrm{sun}}}\right]\mathrm{I}_{(\mathrm{t})} \tag{3.28}$$

Here T_a ambient temperature in kelvin and T_{sun} the solar radiation temperature at 6000 K [55]. Exergetic efficiency of PV/T represents the quality of the energy that PV/T collector produced from the solar radiation. It is the ratio of total exergy output to the total exergy input [62]. The overall exergetic efficiency for the PV/T collector can be written as:

$$\varepsilon_{ov} = \frac{\dot{\mathrm{E}}\mathrm{x}_{\mathrm{th}}}{\dot{\mathrm{E}}\mathrm{x}_{\mathrm{sun}} \times \mathrm{A}_{\mathrm{th}}} + \mathrm{r}\,.\frac{\mathrm{Ex}_{\mathrm{e}}}{\mathrm{Ex}_{\mathrm{sun}} \times \mathrm{A}_{\mathrm{PV}}} = \varepsilon_{\mathrm{th}} + \mathrm{r}.\varepsilon_{\mathrm{el}} \tag{3.29}$$

CHAPTER 4

EXPERIMENTAL SETUP

To accomplish this experimental study, three main activities were performed: designing and constructing a PV/T collector, building an experimental setup, which can be used to test two PV/T collectors at the same time, and purchasing two types of nanofluids.

4.1. CONSTRUCTION OF A PV/T COLLECTOR

A type of PV/T collector with serpentine heat exchanger has been built. Figure 4.1 shows the serpentine heat exchangers.

Figure 4.1. PV/T heat exchanger with serpentine design.

The serpentine heat exchanger (Figure 4.1 and Figure 4.2) is made by soldering a serpentine square copper tube with 10mm and 8mm outer and inner diameter, respectively, to a copper absorber plate with 343x419x20mm dimensions. The center-to-center tube space was 40mm [20,57,63].

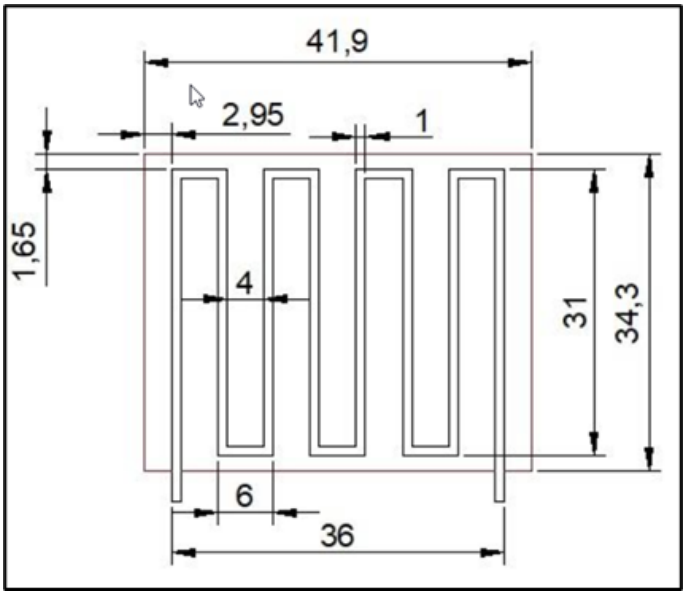

Figure 4.2. Schematic diagram for a serpentine heat exchanger.

We attached a serpentine heat exchanger on the back side of a 20-watt PV panel with 343x419x20mm dimensions, and its specifications are mentioned in Figure 4.2.

Table 4.1. Heat exchanger design specifications.

Type of collector	Head, riser and Serpentine
Tube and material	Square Copper tube
Tube dimensions	8 × 10mm
Plate material	Copper plate
Plate dimensions	39.60 × 32.80cm

Table 4.2. PV panel specifications.

Model Type	LXR-020P
Electrical Characteristics	
Rated Max. Power (P_{max})	20Wp
Power Tolerance Range	+5%
Open Circuit Voltage ($\mathbf{V_{oc}}$)	22.10V
Maximum Power Voltage ($\mathbf{V_{mp}}$)	18.00V
Maximum System Voltage	1000V
Maximum Sense Fuse Rating	10A
Dimensions	41.20×33.60cm

Thermal paste (Figure 4.3-a and Figure 4.4) were used to ensure the perfect contact between the back side of the PV panel and the serpentine heat exchanger. It was installed below the thermal barrier insulation to maintain the effectiveness of heat exchange with a 50mm thickness of glass wool layer at its back covered by metallic enclosure (Figure 4.3-b).

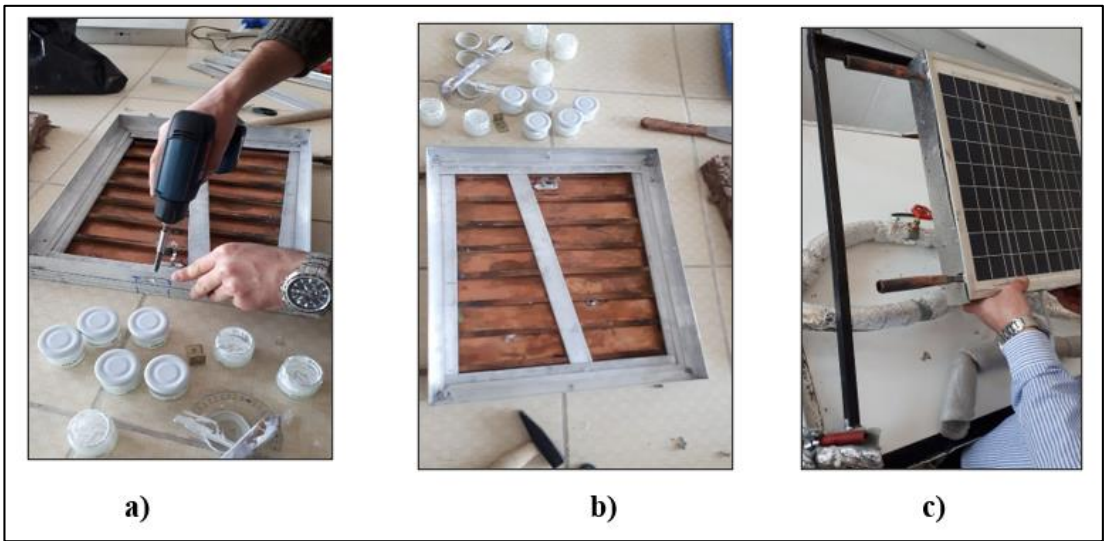

Figure 4.3. Collecting PV/T: a) Distribution method of thermal paste. b) Metallic enclosure. c) Close PV/T collector.

All the gaps and spaces between the PV panel and the insulation were closed to prevent the insulation and the thermal unit in the PV/T collector was prevented from the environmental conditions (Figure 4.3-c).

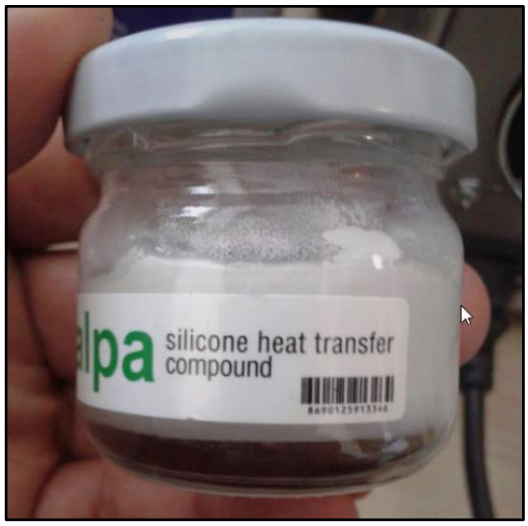

Figure 4.4. Thermal paste.

4.2. CONFIGURATION AND COMPONENTS OF THE EXPERIMENTAL SETUP

Our experimental setup has a PV/T-one PV configuration, which is shown in Figure 4.5, which is prepared for evaluating the PV/T collector's performance using a graphene nanoplatelet-water nanofluid and a hybrid-water nanofluid. The experimental setup, which is given in Figure 4.6, and was built as a complete moveable unit in the Energy Laboratory, Karabuk University. The constructed PV/T collector was mounted side by side with the PV panel on a supporting frame.

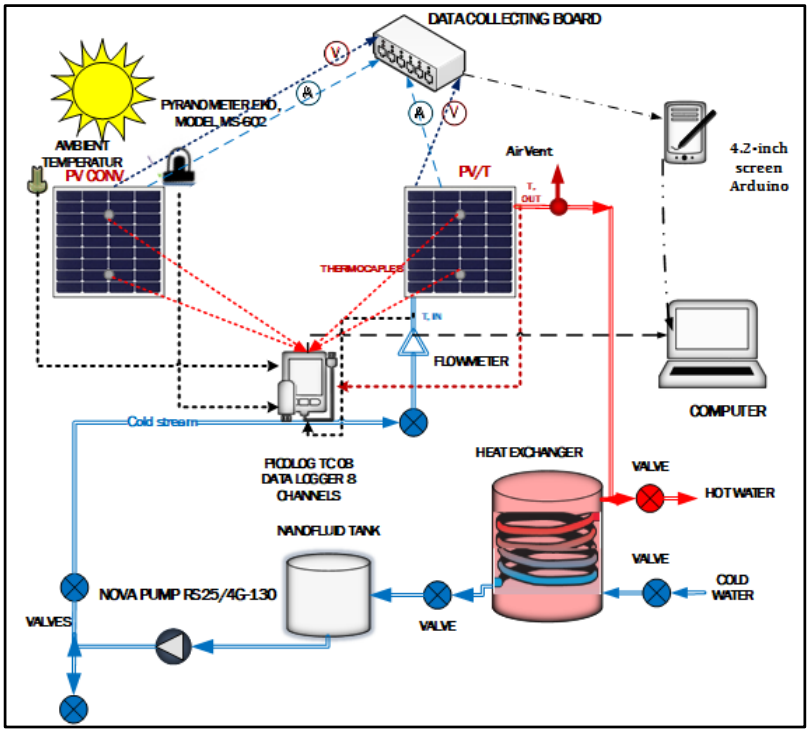

Figure 4.5. Schematic diagram of the experimental setup.

Figure 4.5 shows the main schematic of experimental setup of PV/T collectors, and it illustrates that all components are connected to a thermal cycle as a single unit, which contains:

- The running Nova RS25/4G-130 model circulating pump to circulate the coolant fluid.
- A storage tank is linked with a coil heat exchanger for extracting the heat from a coolant fluid in a PV/T collector.
- A nanofluid tank is used for adding the nanofluid to the setup or draining it from the setup.
- Air vent to remove the air from the setup pipeline.
- Control valves to control the coolant fluid flow rate.
- Connectors and flexible rubber pipe to connect the different components of the experimental setup.
- A measuring system with K-type thermocouples.

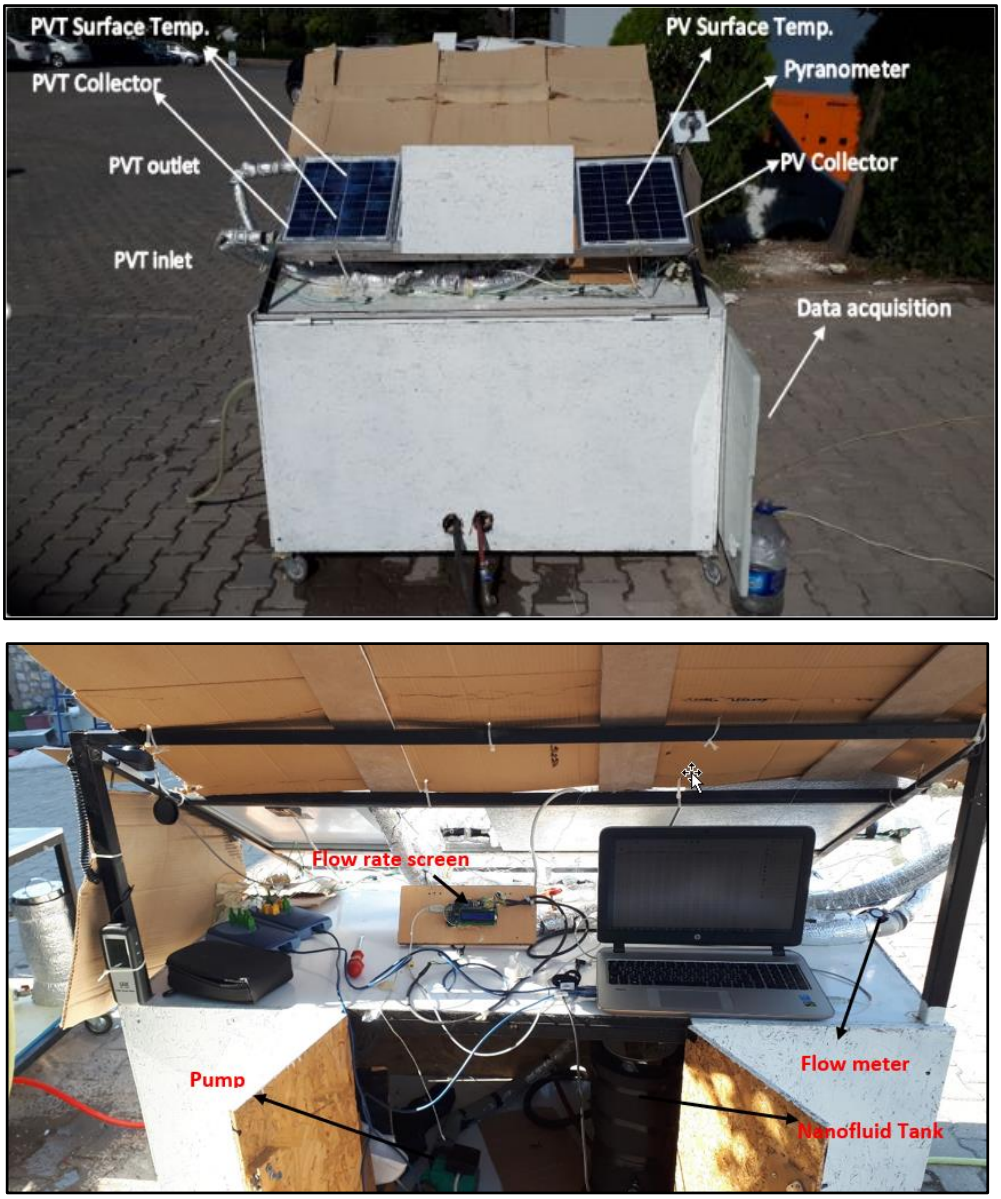

Figure 4.6. A view of experimental setup.

- K-type thermocouples for temperature measurements.
- Flow rate measuring with flow meter model YF-S201 from Sea Company.
- Solar radiation measurements with pyranometer EKO Instruments, Model: MS-602, Japan.
- Electrical resistor loads were installed and connected to data loggers to measure voltage as well as current for estimating thermal and electrical performances of a PV/T collector using different coolants.

4.2.1. Components of the Experimental Setup

4.2.1.1. The Main Frame

Figure 4.7 shows the main frame of the experimental setup of this study, which was designed and manufactured to be movable on wheels and to carry and contain all the components of the experimental setup as a single unit. Furthermore, the PV panel and PV/T collector were attached to the main frame at the same plane with a 30° tilt angle. The sides of the main frame were covered with wooden boards painted with white color.

Figure 4.7. The main frame of experimental setup.

4.2.1.2. Heat Exchanger with Cooling Coil

The storage tank is built of a metal plate (Figure 4.8-a) and copper tubes, which are arranged like a coil (Figure 4.8-b), which was designed using a solid work program and it has a capacity of about 60 liters of cooling water, for which, it may be used in a

future work. Moreover, its function is to cool the cooling fluids coming from the solar collectors, and they repeatedly return back to cool down (Figure 4.8-c).

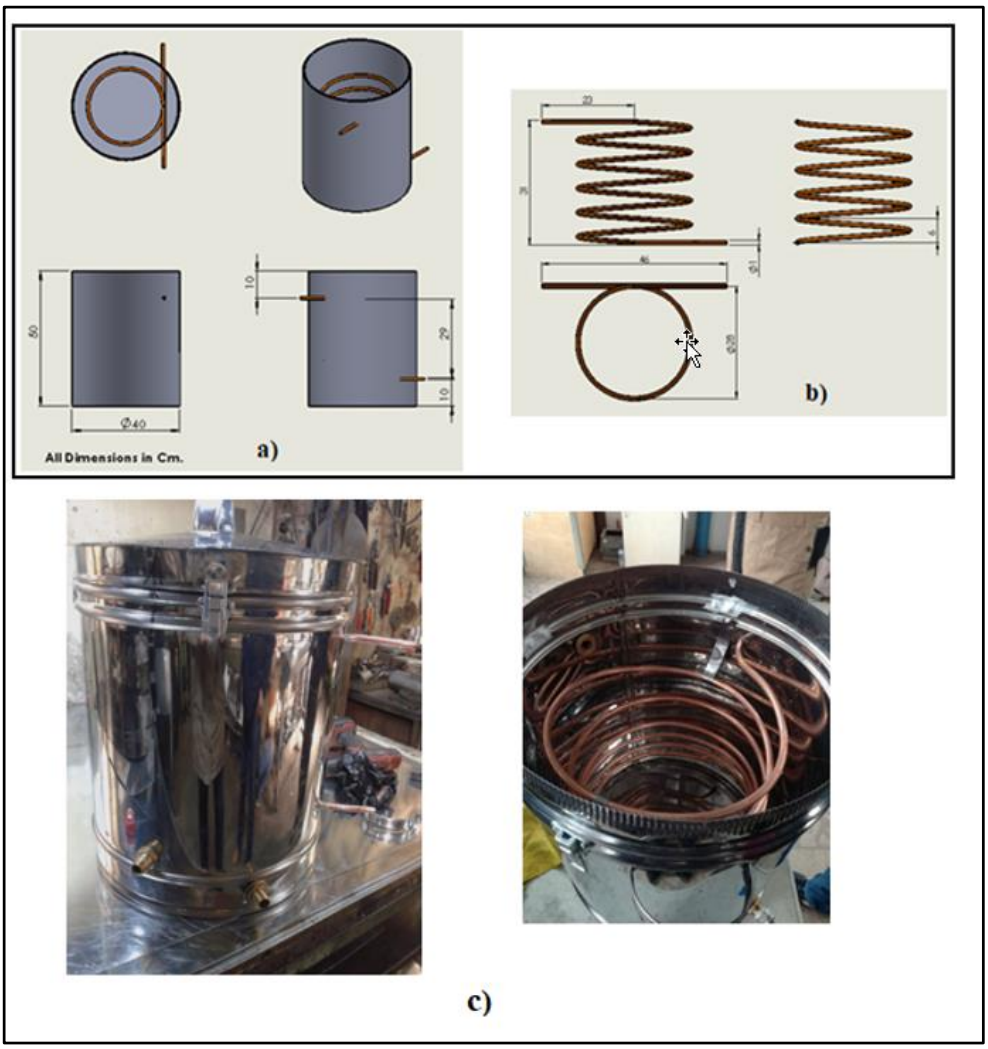

Figure 4.8. Storage tank: a) Tank assembly design, b) Coil heat exchanger design, c) Manufactured storage tank.

4.2.1.3. Storage Tank of Nano Fluid

The nanofluid tank has been designed with a capacity of about 6 liters (Figure 4.9). It facilitates the processes like filling and draining working fluids with very little fluid loss. Moreover, it was made by a sheet of metal that was assembled and welded in the university laboratories.

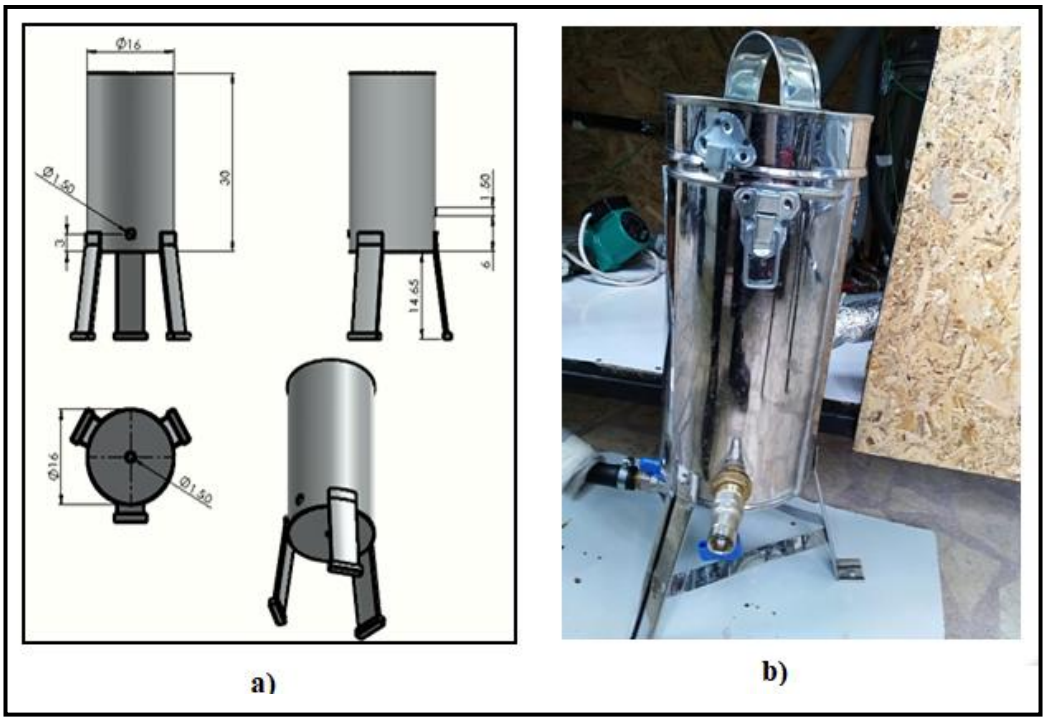

Figure 4.9. Nanofluid tank: a) Design, b) Manufacturing.

4.2.1.4. The Circulation Pump

We used a variable-speed circulating pump, which was manufactured by Nova Company (Model: RS25/4G-130), which is displayed in Figure 4.10. Its function is to circulate the selected working fluid in the experimental setup components including the PV/T collector. Table 4.3 shows the specifications of the circulating pump (power and the head at three speed levels).

Table 4.3. Circulation pump specifications.

Speed level	Power (W)	Head (m)
I	38	3
II	53	4
III	72	4.5

Figure 4.10. Circulation pump installed and used in the setup.

The pump operates when the fluid temperature ranges between -10°C to 110°C.

4.2.1.5. The Air Outlet Vent

The air vent was installed at the highest point beside the collectors in the setup to release the air in the coolant fluid.

Figure 4.11. Air vent.

4.2.1.6. The Connection Method to Link the Components of the Experimental Setup

The system components were connected by a pipe (13mm inner diameter and 21mm outer diameter) with a rubber material. The working fluid is circulated around the pipes. The PV/T collector needed nearly 4 liters to fill all the system and run the experimental system.

4.2.2. The Data Logging and Measuring System

4.2.2.1. Flow Rate Measurement

The working fluid's flow rate was measured using a flowmeter model YF-S201 manufactured by the Sea Company. It was connected to a readable LED screen. Figure 4.12 indicates the flow rate readings. The coolant fluid flow rate was controlled using a gate valve installed about 20cm before the flow meter for avoiding any fluid disorder, which may affect the flow meter reading.

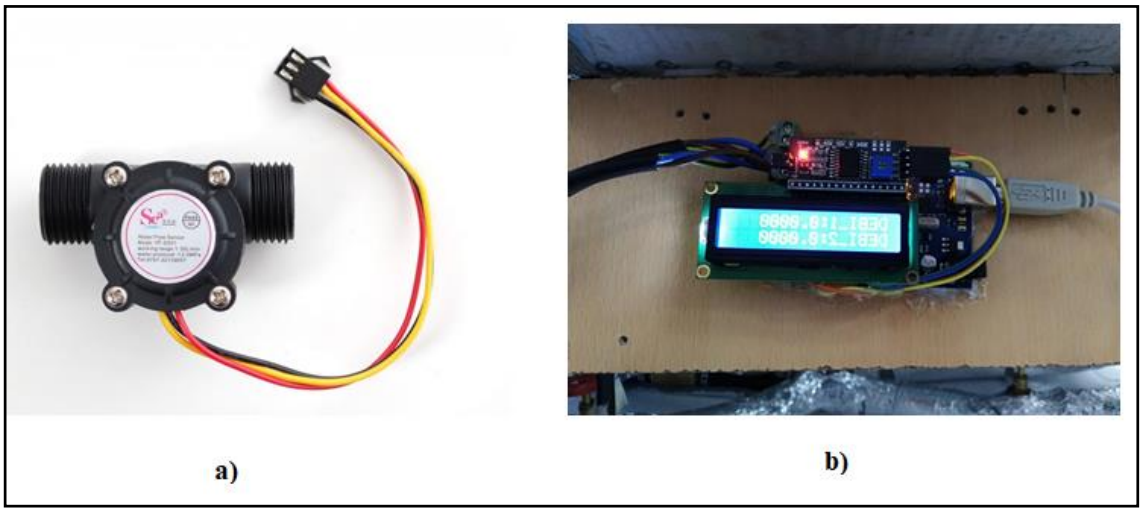

Figure 4.12. Flow rate measuring system: a) Flow meter, b) LED screen.

4.2.2.2. Temperature Measurement

All temperature points were measured by using Eight K-type thermocouples, for instance, the sheet and tube heat exchanger temperature, inlet and outlet working fluid temperatures, surface temperatures of devices like PV panel and the PV/T collector and the ambient temperature. The contact points of thermocouples are illustrated in Figure 4.6-b. All the thermocouples were linked with a Pico USB TC-08 data logger, and that was further connected with a laptop computer to easily get the data (Figure 4.13-a).

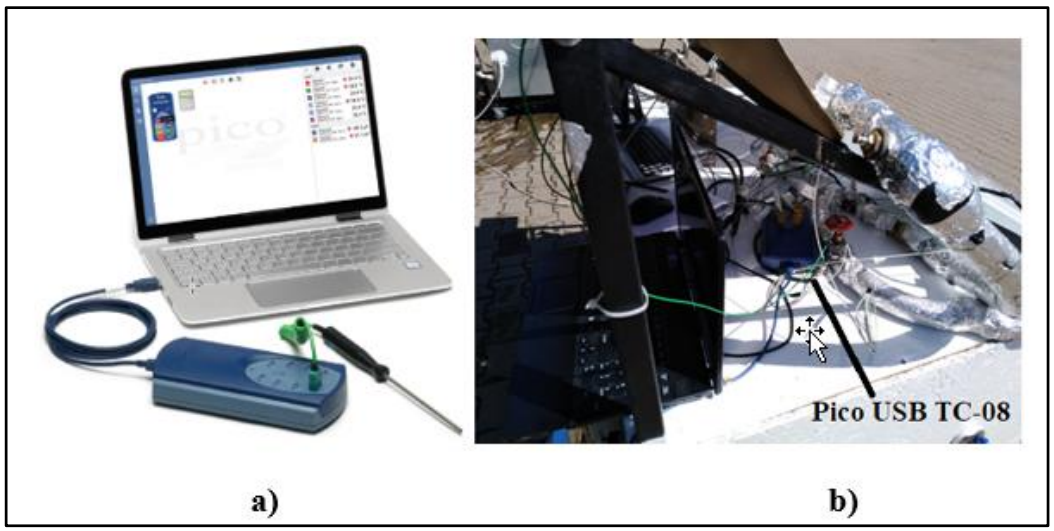

Figure 4.13. Temperature data logger: a) Pico USB TC-08, b) Position in the setup.

4.2.2.3. Data Acquisition Board

The data collecting board (Figure 4.14 b), which is considered as an electronic board, was designed and manufactured in the energy labs located at Karabuk University. The main purpose behind this board was transferring all the measured data (voltage, current, solar radiation, etc.) from the sensors of experimental setup and simultaneously transfer to a laptop computer, where it was collected and processed using a 4.2-inch screen Arduino and an SD card (Figure 4.14 a). The temperature measurements were recorded and collected by Pico USB TC-08 data logger.

a) b)

Figure 4.14. a) Screen and Arduino card, b) Data collecting board.

4.2.2.4. The Incident of Solar Radiation Measurement

We used a Pyranometer manufactured by EKO Instruments (Model: MS-602, Japan) (Figure 4.15). It measured the incident solar radiation on the PV/T collector and PV panel surfaces and it was mounted on the plane of PV as well as PV/T collectors (Figure 4.6-a). It was also connected to a data collecting board, which is connected to a laptop computer through a data cable.

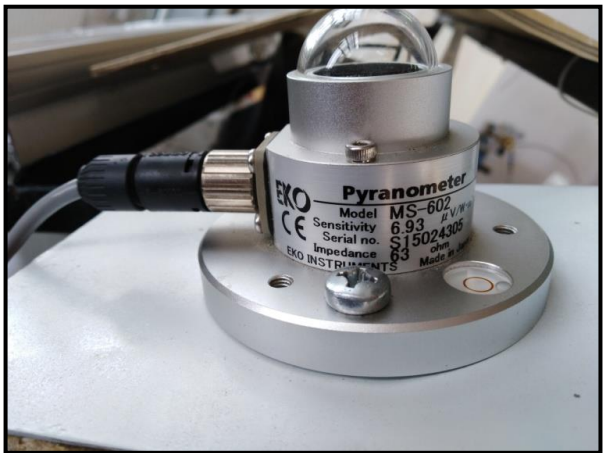

Figure 4.15. Pyranometer used to measure the incident solar radiation.

4.2.2.5. Resistor Load

Constant resistor loads were connected to a PV/T collector and a PV panel for obtaining the maximum possible electrical power and ensuring a continuous power generation through PV and PV/T panels, as shown in Figure 4.16-a. A fin-fan system was used to cool down the resistor loads and to dissipate the generated heat (Figure 4.16-b).

4.2.2.6. Voltage and Current Measurements

The voltage and current were generated using a PV panel pass and a PV/T collector through the data collecting board to the laptop computer, where they were processed by a 4.2-inch screen Arduino and SD card, which recorded and collected the data. The voltage and current measurements were calibrated to avoid the measurement errors.

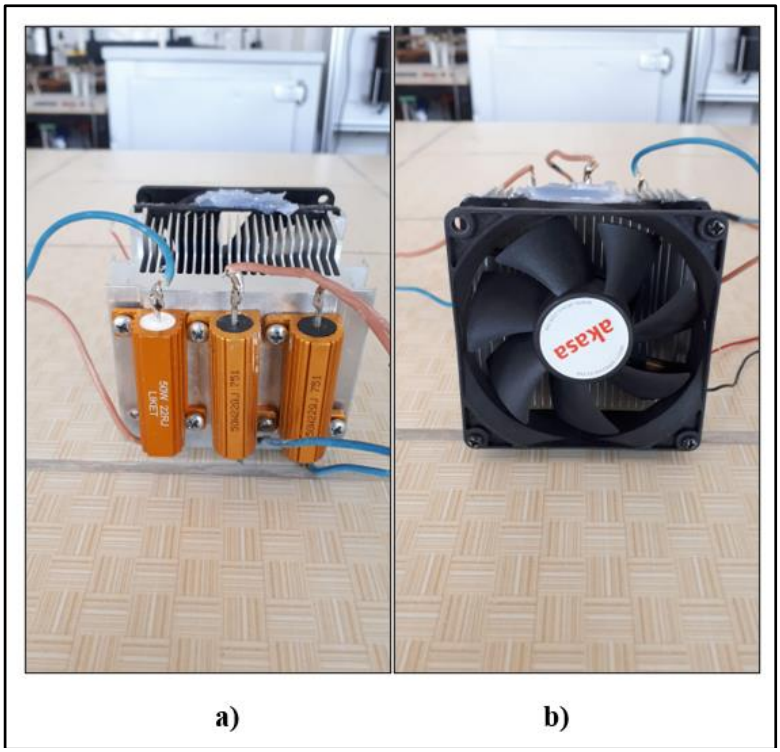

Figure 4.16. a) Resistor load, b) Fin-fan system for cooling.

4.2.3. Experimental Setup Operation

After the installation and assembling the experiment setup, several operations were carried out to start the operation, and among these operations is the calibration of measuring devices.

4.2.3.1. Measurement Devices Calibration

All devices that measure variables such as temperature, flow rate, radiation, current and voltage were calibrated using different methods explained as follows:

- Temperature

We calibrated the temperature for the temperature channels of the data collecting board. The results indicated that some of these channels did not give accurate results, which led to the use of another measuring instrument (Pico USB TC-08 temperature data logger) instead of the channels.

- Flow rate

As far as the flow rate is concerned, the process was carried out using a 1000ml scaled container with a stopwatch. This method was repeated for several readings and different values were recorded.

- Radiation

For radiation calibration, the process was carried out using a solar meter type CEM DT-1307 over the course of the experimental work.

- Voltage & Current

To assess the generated voltage and current, they were calibrated using a multimeter manufactured by the MASTECH company (model MY-68) when the PV/T collector and the PV panel were directed towards the solar radiation.

4.2.3.2. The Main Steps to Operate the Experimental Setup

It is the most important stage in obtaining the required results, so, the following procedures were followed in every experiment:

- In the early morning, always start with taking the experimental setup out of the lab to its work position facing south.
- Fill the nanofluid tank with about 4L coolant fluid in order to ensure that the whole cycle from the nanofluid tank and the pipeline to the circulation pump is filled with a coolant fluid.
- Turn on the pump releasing the air from the air vent, which may cause malfunctions and close it when the stream of working fluid is coming out without air bubbles.
- Adjust the control valve to set the required flow rate of a coolant fluid.
- Fill the storage tank with city water and then adjust the control valves to set the city water flow rate at 0.3L/min.
- Operate the system for nearly 20mins to ensure that all system components are working correctly and assure that the system is in its thermal equilibrium.
- As soon as the system starts operating, turn on the data logger Pico (USB TC-08) and for voltages, currents and solar radiation with a data collecting board and Arduino screen. After every 12 seconds, the measuring parameters were periodically taken.

The working fluid changing and cleaning method:

- Operate the pump to circulate the fluid around the whole system.
- Initiate the discharge operation for the working fluid nanofluid tank by opening the drain valve while keeping the pump at work.
- After draining the working fluid completely from the nanofluid tank, stop the pump, close the drain valve, remove the pipeline from the pump exit and open the air vent. Some air should be entered with an appropriate pressure so as to remove the rest of the working fluid from the PV/T collector and pipeline and open the drain valve and let the working fluid move out.
- To perform a good cleaning process for the system, fill the nanofluid tank with city water, operate the pump and open the drain valve to get rid of the unclean liquid. Keep the pump operating and keep the drain valve open. Then keep watching the color changes in the working fluid. When all the working fluid becomes clear and pure, turn off the pump, drain the fluid and clean the PV/T collector using the piping system.

4.3. NANOFLUIDS

The hydrous dispersion of the GNP (1 12μm diameter, 0.55 1.2nm thickness, more than 99.3wt% purity, and 500-1200m^2/g specific surface area), HyNF consisting of 1:1 0.5 GNP, 0.5 Al_2O_3 concentrations, and Al_2O_3 nanofluids with particle sizes 30 40nm with 99.9% purity were obtained from NANOGRAFI Co. Ltd. in Turkey. Table 4.4 shows the thermal properties of both nanoparticles. Scanning electron microscopy (SEM) image of GNP and Al_2O_3 nanofluids as Figure 4.17 and Figure 4.18a show. All the particles are almost spherical in shape and nano-sized within the range 10–30nm with small agglomeration. Both Figure 4.17b and Figure 4.18b shows some nanofluid samples after finishing the nanofluid preparation while sedimentation was not observed when the experiments were conducted.

In Figure 4.17 and Figure 4.18, the transmission electron microscopy (TEM) image for graphene nanoplatelets and AL_2O_3 showed no sedimentation when it was observed during and after the experimentation.

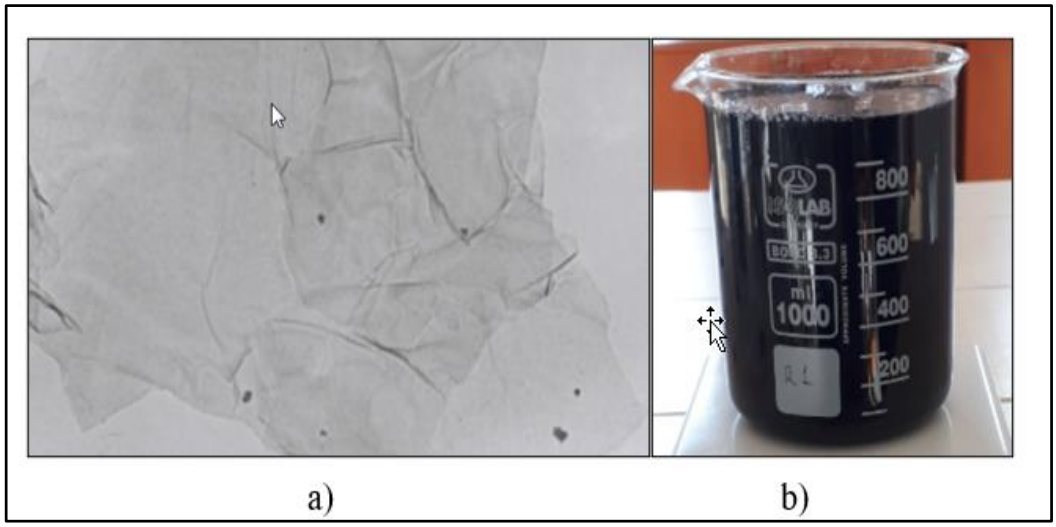

Figure 4.17. a) Graphene nanoplatelets TEM image, b) Nanofluid sample.

Table 4.4. Thermal properties of water and nanoparticles [32,64].

Property	**Water**	**Al_2O_3**	**GNP**
$\rho(kg\ m^3)$	997.1	3970	2100
Cp (kJ/kgK)	4179	765	5000
k (W/mK)	0.613	40	0.710

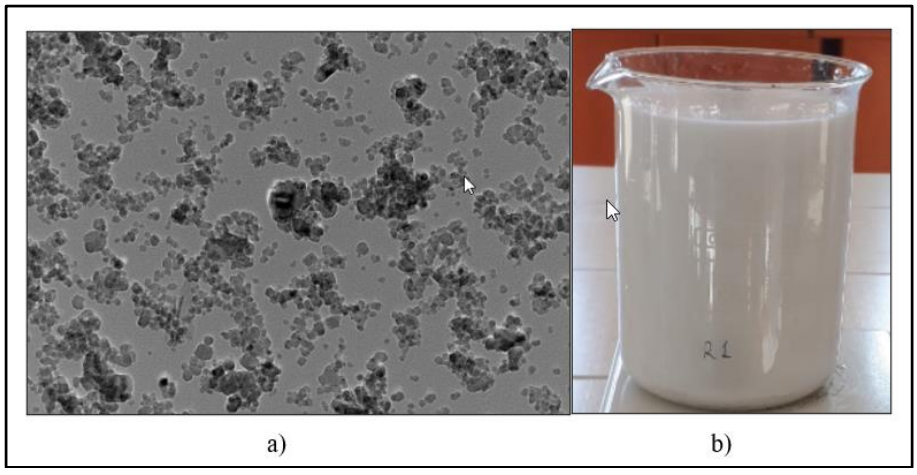

Figure 4.18. a) TEM image for AL_2O_3 nanoparticles, b) Nanofluid sample.

Figure 4.19. Sample of hybrid nanofluid (HyNF).

CHAPTER 5

RESULTS AND DISCUSSION

5.1. CALIBRATIONS

To assess the errors related to the measuring devices and data loggers used in the experimental setup, calibrations were carried out for the measuring system.

For temperature measurements, the temperature channels of the data collecting board were excluded and the Pico USB TC-08 data logger was used.

The MASTECH - MY-68 multimeter was used to calibrate the voltages and currents, which were generated by the range of experimental readings and found that the errors were negligible.

The flow rate (monitored through a flow meter and a read-out LED screen) was calibrated by a scaled container and a stopwatch. The reading of the flow meter was nearly the same as the real reading (
Figure 5.1).

The EKO MS-602 pyranometer, which was mounted on the experimental setup, has a sensitivity 6.93μV/Wm^{-2} whereas the data collecting board detects the voltage signals (V). To overcome this problem, an electrical circuit was designed, built, and installed between the data collecting board and a pyranometer was used to amplify the μV signals to V signals. This system (pyranometer, electrical amplifying circuit and data collecting board) was calibrated by a CEM DT-1307 solar meter.

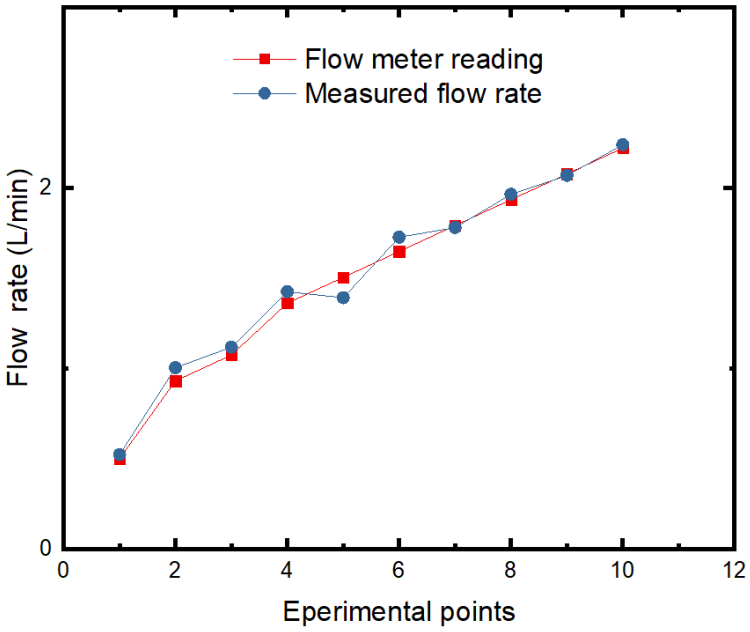

Figure 5.1. Flow rate calibration.

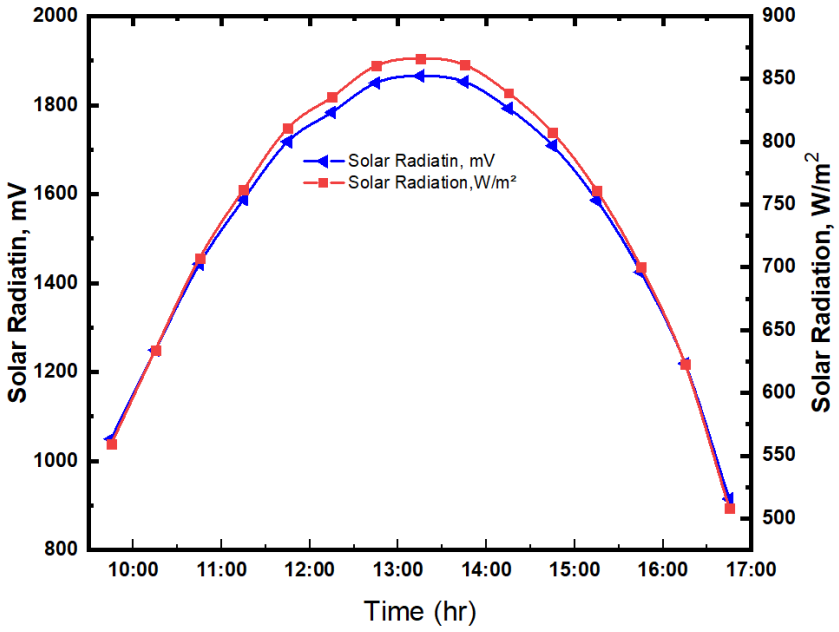

Figure 5.2. Solar radiation calibration.

A correction was done by the readings of the setup pyranometer from mV to W/m^2 I_R = R* 0.3765+163.94 (Figure 5.2).

5.2. THERMAL PROPERTIES OF NANOFLUID

The nanofluids' under-investigation thermal properties were estimated using Eq.(3.9) –(3.17) and presented in Table 5.1.

Table 5.1. Thermal properties of graphene nanoplatelets and hybrid nanofluids.

Property	**GNP**	**HyNF**
$\rho(kg/m^3)$	1259.5	1315
Cp (kJ/kg.K)	2.803	2.873
k (W/m K)	1.1755	1.0110

There is a big difference between the experimentally measured thermal properties of nanofluids and that calculated by theoretical models. However, these theoretical models are used in the literature for estimating the thermo-physical properties of nanofluids.

5.3. TESTING PROCEDURE

We conducted numerous experiments in August, September and October 2019 under consistent weather conditions, and noted the measurements. The experimental duration was 09:30-17:00 for tests pertaining to the GNP, distilled water, HyNF, and PV/T coolant inlet and outlet temperatures. We also measured solar irradiance, PV and PV/T surface temperatures, and noted the generated current and voltage for PV and PV/T simultaneously every 12 seconds with a regular flow rate (0.5L/min) during the experiment. Then, the data collected during the selected days was used to compute averages and for further calculations. We also studied and compared the performances of the nanofluid-cooled PV/T, PV modules, and the water-cooled PV/T (Table 5.2).

Table 5.2. Experimental days.

Type of coolant	No. of experiments	Dates	Flow rates
Distilled water	1	27th August 2019	0.5 L/m
Graphene nanoplatelets nanofluid	2	18th September 2019	0.5 L/m
Hybrid nanofluid	3	1st October 2019	0.5 L/m

5.4. INITIAL EXPERIMENTS WITH 0.5 L/M, 1.5 L/M, AND 2. L/M FLOW RATES BY USING CITY WATER

Several initial experiments have been conducted to experiment with several flow rates until the appropriate flow to select the optimum volume flow rate for the system by using distilled water, and the flow rates 0.5 L/m,1.5 L/m, and 2 L/m were chosen. These experiments were conducted in an appropriate weather condition from 9:30 to 16:30.

Table 5.3 Dates of initial experimental days.

Dates	Flow rates	Remarks
23.8.2019	0.5 L/m	Initial test
25.8.2019	1.5 L/m	Initial test
26.8.2019	2.0 L/m	Initial test

Figure 5.3 shows that the electrical efficiency produced by PV/T collector at flow rates 0.5 L/min is close and higher than that generated by 1.5 L/m and 2 L/m.

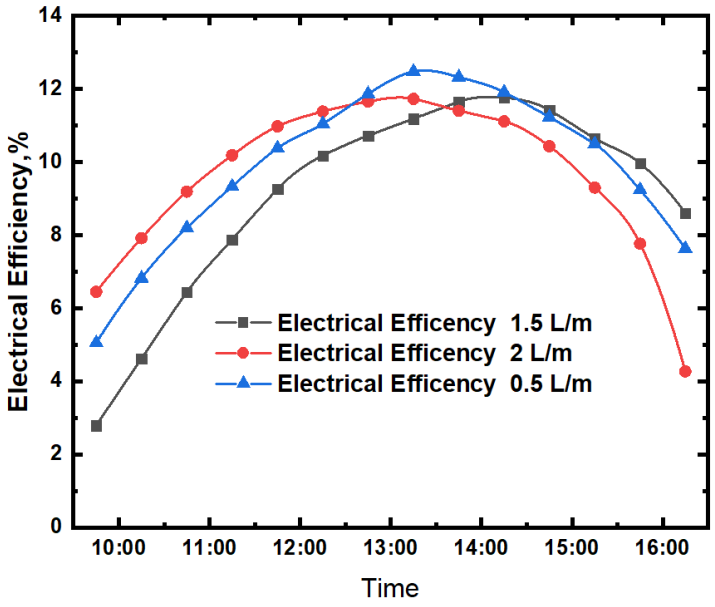

Figure 5.3. Average daily variation of electrical efficiency for different flow rates.

Thermal power and thermal efficiency are affected by the 0.5 L/m flow rate more than other flow rates, which is observed that the best thermal power and efficiency stable trends were at 0.5 L/m flow rate as shown in Figure 5.4.

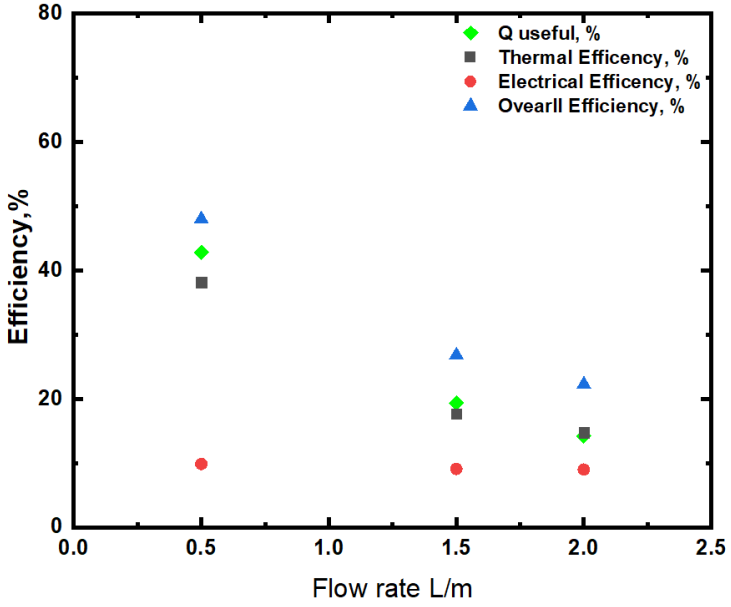

Figure 5.4. Average daily efficiencies of the system over the flow rates.0.5, 1.0, 2.0 L/min.

Figure 5.5 shows that in respect of the surrounding climate condition like wind velocity, change of the incident radiation through the experiments days thermal power does not follow a specific bath. As a result of the analysis of the initial experiment, we decided to make and reach to run all the tests at a fixed 0.5 L/m flow rate.

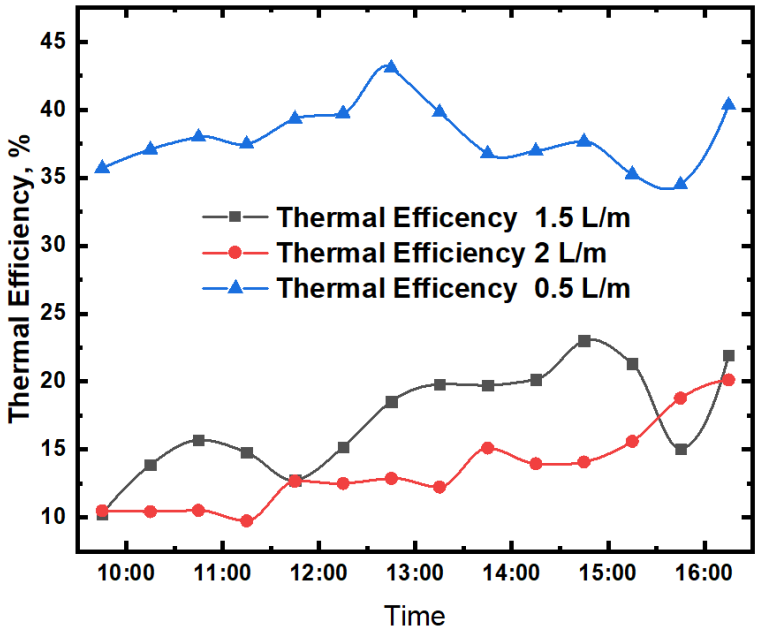

Figure 5.5. Average daily variation of thermal efficiency for different flow rates.

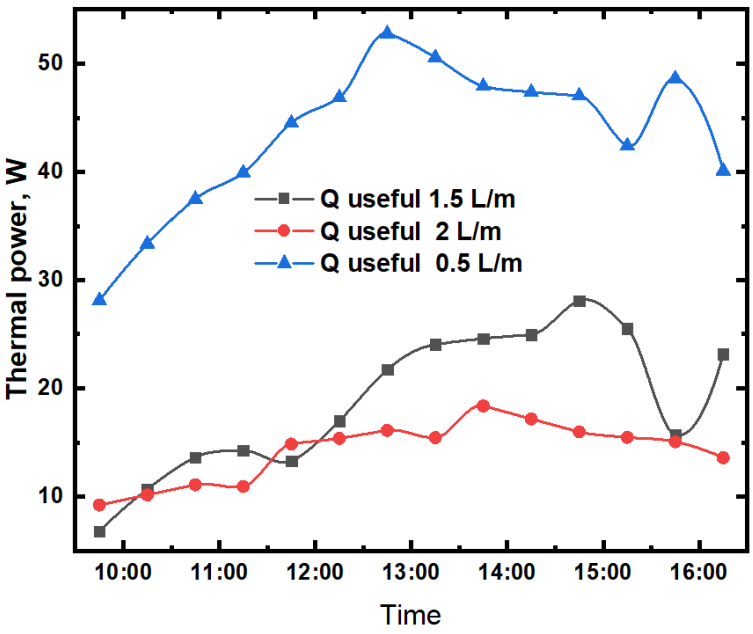

Figure 5.6. Average daily thermal power for different flow rates.

Table 5.4. The percentage of thermal power, thermal efficiency, and electrical efficiency during the experiment days.

Flow rate	Q useful, %	Thermal Efficiency, %	Electrical Efficiency, %
0.5	42.81	38.14	9.85
1.5	19.35	17.69	9.08
2	14.24	14.73	8.98

5.5. EXPIREMENTAL RESULTS AND DISCUSSION

For this study, we conducted many experiments on the PV/T modules' cooling operations. All the measurements were collected after every 12 seconds, as Figure 5.7, Figure 5.8 and Figure 5.9 indicate from 09:30 to 17:00 at 0.5 L/m flow rate and it was calculated for two time periods. The first was the all-day period from 09:30 to 17:00 and the second was the peak period from 11:15 to 15:15 for all the under-investigation coolants. First, the distilled water experiment was performed on 27 August, 2019 at 0.5 L/m flow rate under stable weather conditions and then the same experiment was conducted for the GNP on 18 September, 2019 at 0.5L/m flow rate.

Finally, the experiment using HyNF was conducted on 1 October, 2019 at 0.5L/m flow rate. Because of the unstable weather conditions on other days, we ignored the results of several experiments conducted in those days.

The nanofluids' experimental results at 0.5 wt% concentration was chosen to perform an energetic and exergetic comparison.

As mentioned earlier, we noted measurements after every 12 seconds from 9:30 am to 5:00 pm for all the working fluids at 0.5 L/min flow rate, in the chosen days of August, September and October. Figure 5.7, Figure 5.8 and Figure 5.9 show daily measured parameters every 12 seconds for experiments using distilled water and at 0.5 wt% for experiments on nanofluids. The obtained data was averaged and shown in the middle of every half hour for calculations as well as analysis.

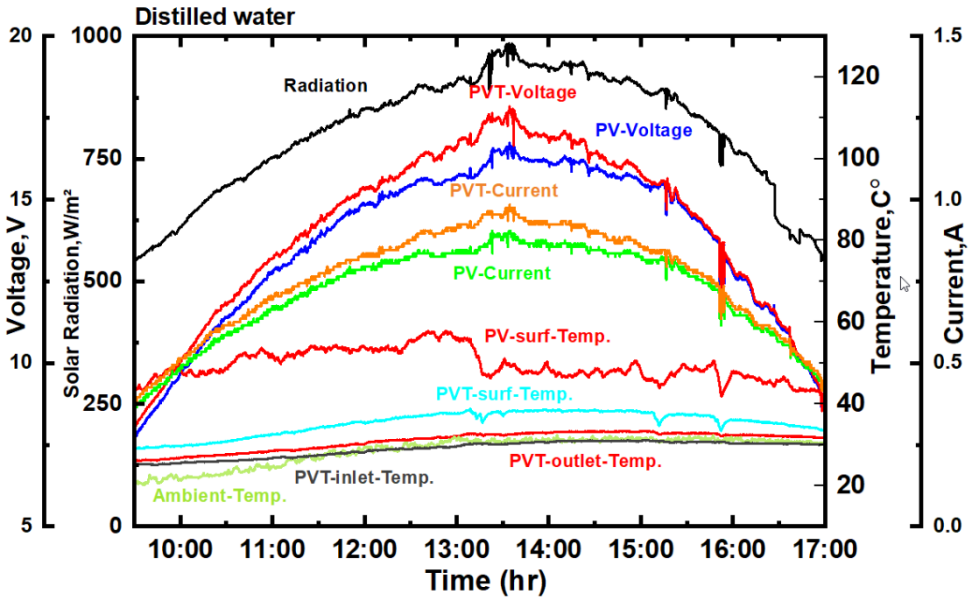

Figure 5.7. Measured parameters for distilled water after every 12 seconds.

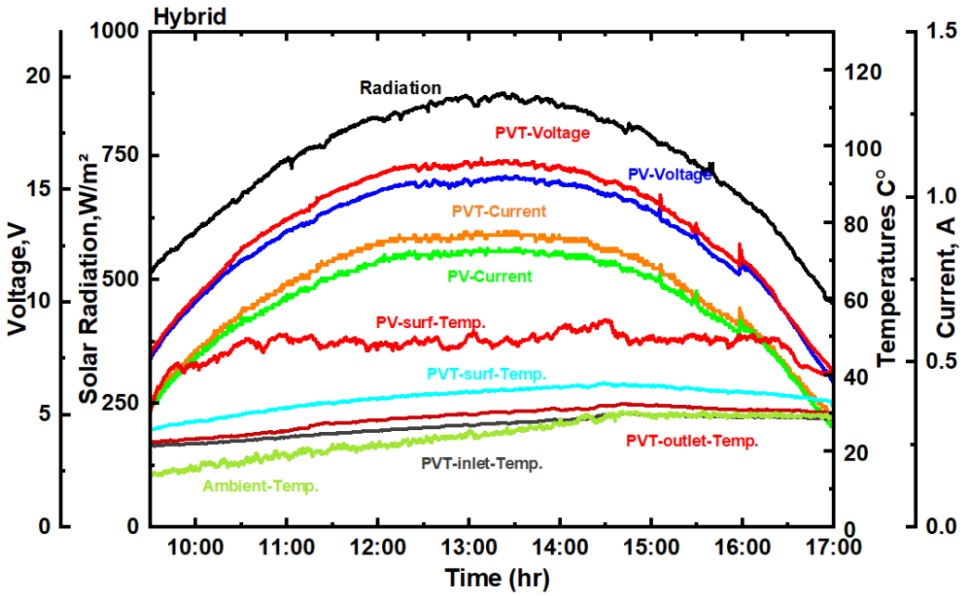

Figure 5.8. Measured parameters for hybrid nanofluid after every 12 seconds.

In the above figures, the average weather conditions, ambient temperature, and solar radiation were clarified. The average of solar radiation for each experiment forms a curve, which begins to increase when the sun rises until it reaches the mid-day and gradually begins to descend, while the maximum rate was observed as 940 W/m^2 when the time was 13:00 while it was minimum (320 W/m^2) at 9:00. We observed that it was 540 W/m^2 at the closing hour (17:00). The ambient temperature values increased

from 9:00 when the temperature was 20°C and it increased until 17:00 when the temperature was 32°C.

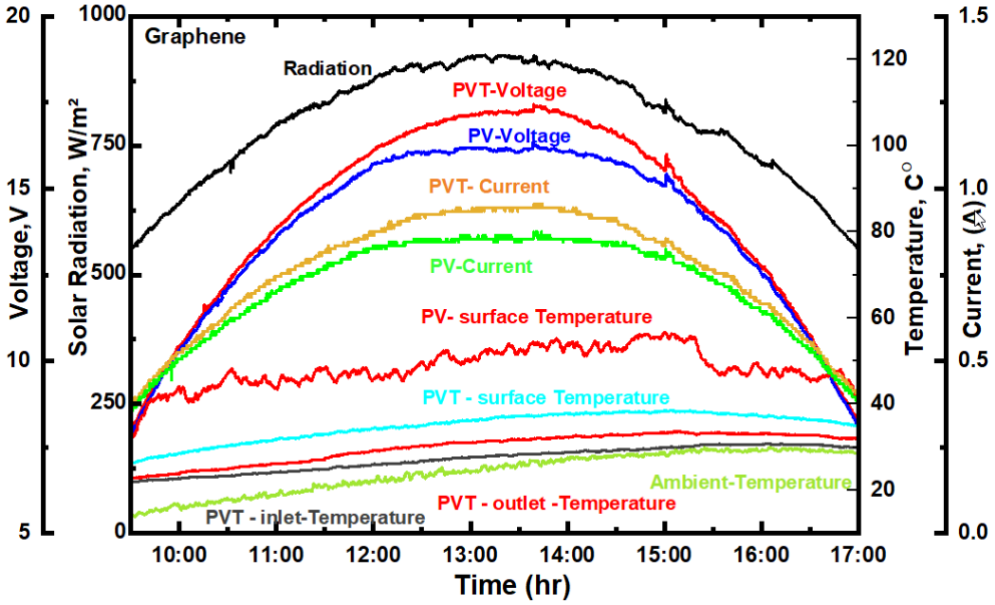

Figure 5.9. Measured parameters for graphene nanoplatelets nanofluid after every 12 seconds.

5.5.1. Solar Irradiance and Ambient Temperature

We tilted the experimental module at almost 30° towards the south, which is an appropriate direction to receive solar radiation. As we can see in Figure 6, the highest ambient temperature was observed at 15:15; after which, it started to decrease to 30°C by the end of the experiments at 17:00. Moreover, the solar radiation reached its peak at about 908 W/m^{-2} at 13:45, which gradually decreased to 530W/m^{-2} at 17:00. All data taken from the experiments was presented in Figure 5.10., Figure 5.11 and Figure 5.12.

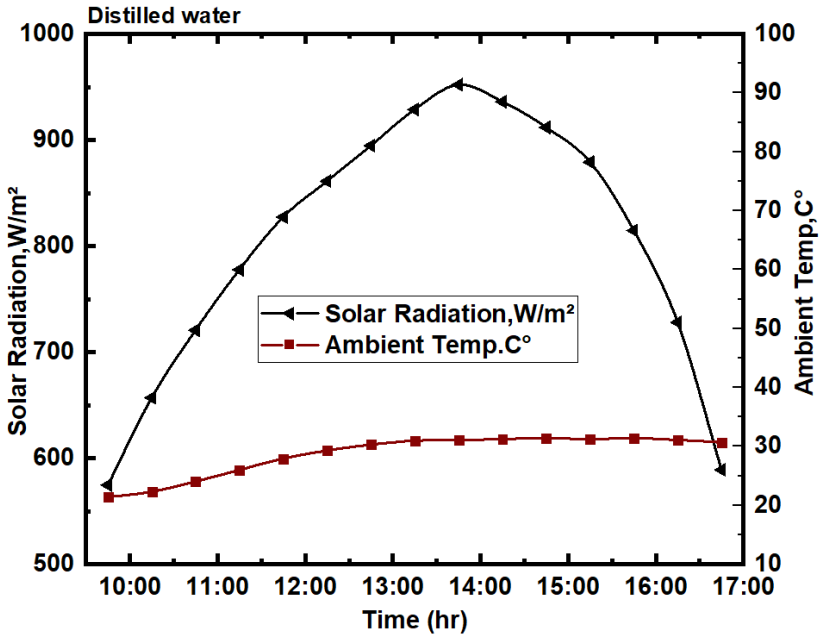

Figure 5.10. Daily average solar radiation and ambient temperature when distilled water is used.

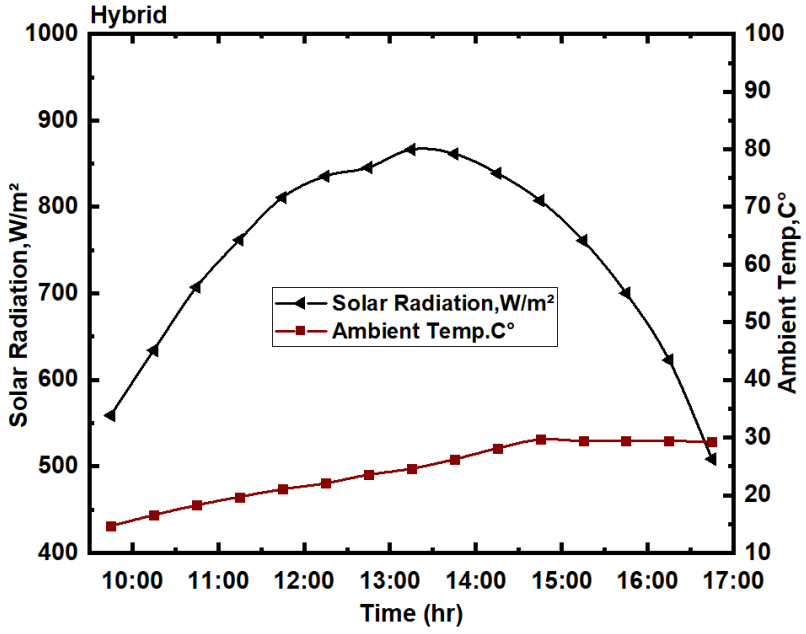

Figure 5.11. Daily average of solar radiation and ambient temperature when a hybrid nanofluid is used.

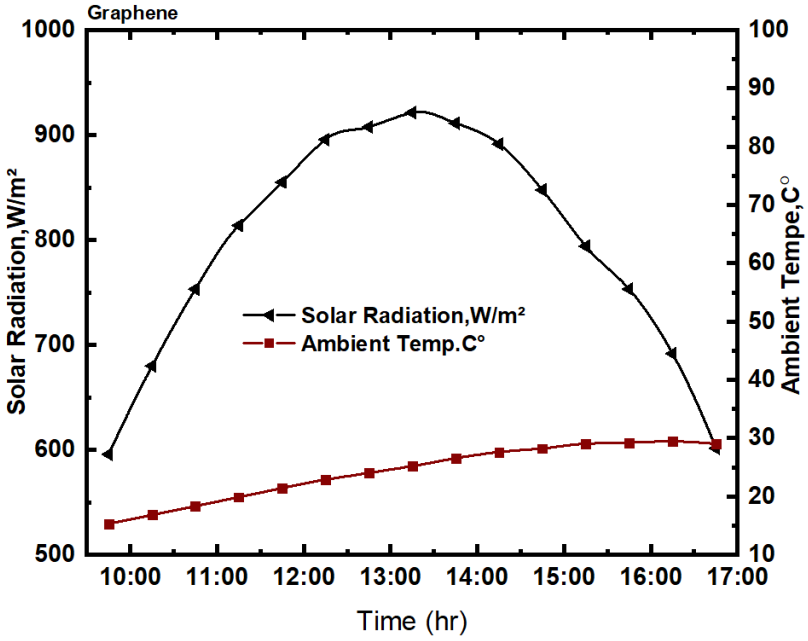

Figure 5.12. Daily average of solar radiation and ambient temperature when graphene nanofluid is used.

5.5.2. The Surface Temperature Measurements

Figure 5.13, Figure 5.14 and Figure 5.15 show the PV/T and PV collectors' surface temperatures during the cooling times for both water and nanofluids from 09:30 to 17:00. The PV/T collector's surface temperature reduced more quickly when a coolant was used.

The first experiment was conducted on 27th August, 2019 from 09:30 to 17:00 and distilled water was used for cooling when the solar radiation and ambient temperature were high, and the daylight duration was longer. Moreover, at 09:30, the PV/T and PV surface temperatures were 30℃ and 46℃, respectively, which reached maximum (38℃) for the PV/T at 14:15 and 56℃ for the PV at 13:00. After the middle of the day, the radiation was lower, which decreased the PV surface temperature; however, the inlet, outlet, and PV/T surface temperatures were not affected due to the heat gained by the coolant and there was insufficient time to respond and the temperature progressively decreased until the end of the test, which is shown in Figure 5.13.

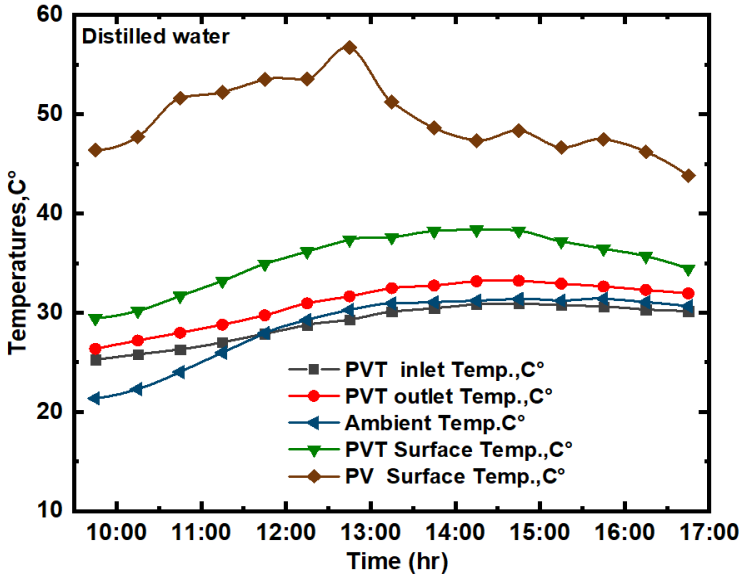

Figure 5.13. Daily average variations in surface temperature for PV, PV/T using distilled water.

The second experiment was conducted on 18th September, 2019 from 09:30 to 17:00 using the GNP fluid for cooling. As shown in Figure 5.14, the weather was steady most of the day and the surface temperatures for the PV/T and PV gradually increased from 27℃ and 39.5℃ at 09:30 to 38℃ and 54.8℃ at 14:45, respectively, which progressively decreased until 17:00.

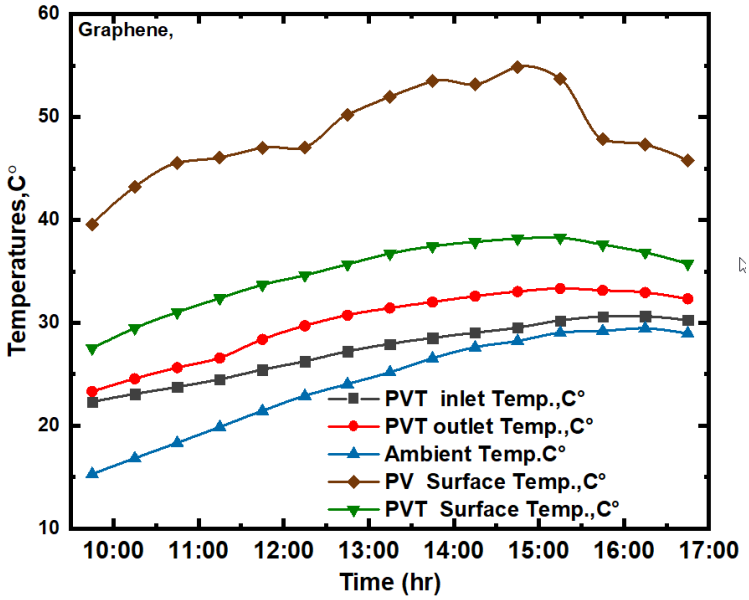

Figure 5.14. Daily average variations in surface temperature for PV and PV/T for GNP.

The third experiment was conducted on 1st October, 2019 from 09:30 to 17:00 using HyNF for cooling. As shown in Figure 5.15, the ambient temperature and solar radiation were less as compared to previous experiments and they were stable most of the test day (Figure 7c). The respective surface temperatures (PV/T and PV) were 26.8℃ and 39.8℃ at 9:30, which gradually increased to 37℃ and 52℃, respectively, at 14:15. As a result, when the solar radiation increased, the PV and PV/T surface temperatures increased as well, and the coolant fluid temperatures also increased. The maximum surface temperature values for PV/T and PV collectors using distilled water, GNP, and HyNF were 14.2℃, 14.4℃, and 14℃, respectively.

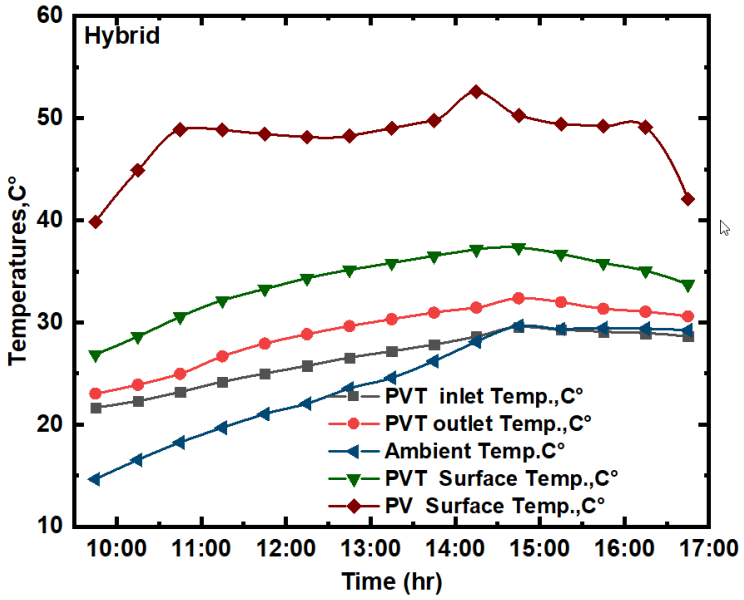

Figure 5.15. Daily average variations in surface temperature for PV and PV/T for HyNF.

5.5.3. Electrical Efficiency

As mentioned previously, we measured the surface temperature and its effects on the PV/T and PV surfaces and how to use the coolant to reduce the temperature to improve the electrical and overall energy performance. Furthermore, we have mentioned the thermal energy and the power generated by the panels in relation to PV and PV/T collectors, which depended on solar radiation. The maximum electric power generation was achieved at maximum solar radiation. Table 5.5 and Table 5.6 show

electric efficiencies of PV and PV/T, solar radiation, electrical efficiency increments, and surface temperature differences for both time periods (all day and peak periods).

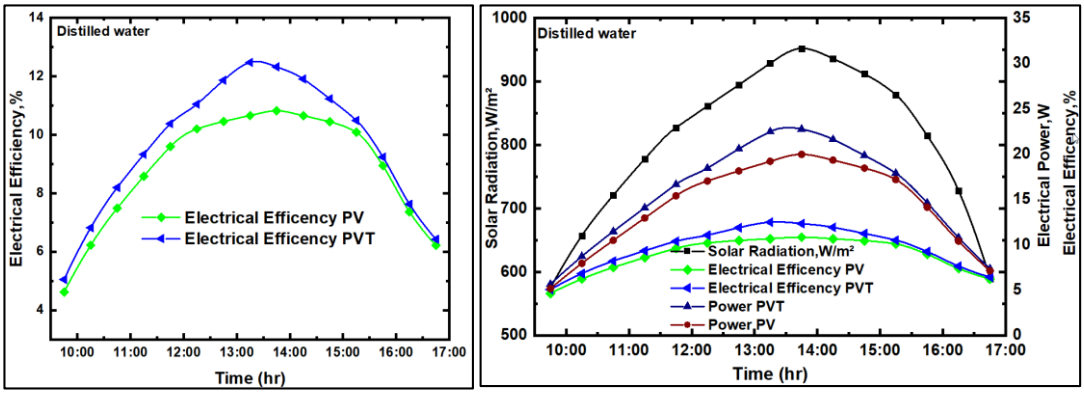

Figure 5.16. Electrical efficiency and power production using PV/T and PV collectors for distilled water.

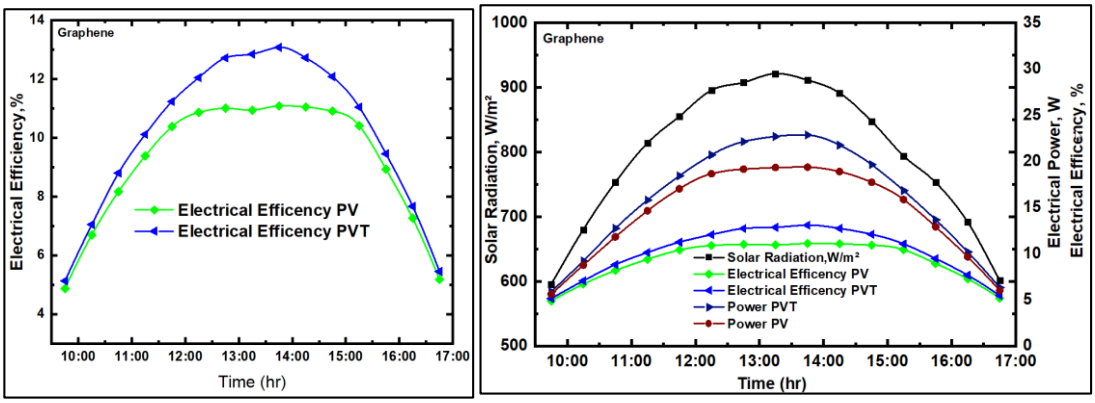

Figure 5.17. Electrical efficiencies and power production using PV/T and PV collectors for graphene nanoplatelets-water nanofluid.

Figure 5.17 clearly indicates that the electrical power increases when solar intensity rises; however, when the experiments were performed, the daily average solar radiation using GNP nanofluid, HyNF, and distilled water were 803, 794 and 742 W/m^2, respectively. Moreover, all the data was taken from the experiments in terms of ambient temperature, radiation and electrical efficiency increments, which were averaged and divided into two times, namely the day-long periods and peak periods, while we compared the performances of the coolants. Every coolant showed significant output electrical energy at 9.6%, 9.8%, and 10.2% for distilled water, HyNF, and GNP, respectively.

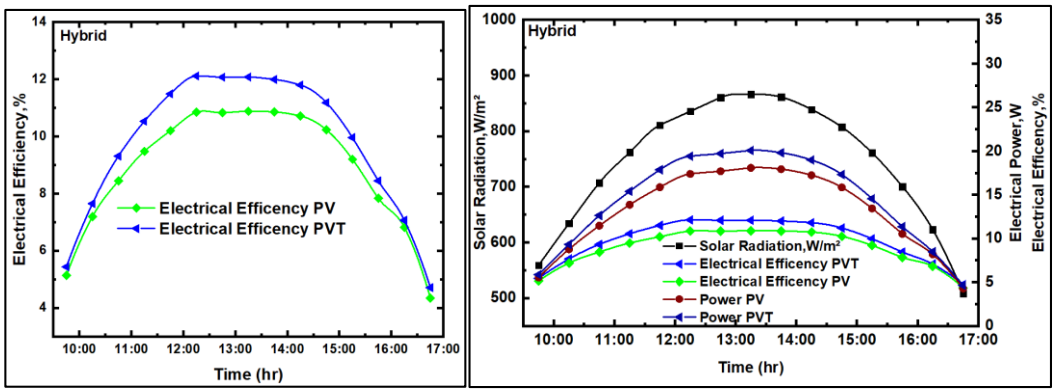

Figure 5.18. Electrical efficiencies and power production using PV/T and PV collectors for a hybrid nanofluid.

Table 5.5. The average daily weather conditions, electrical increment, and cell temperature during the day-long experiment.

Type of coolant	I_R (W m^{-2})	T_{amb} (°C)	$T_{S,PV}$ (°C)	$T_{S.PV/T}$ (°C)	$\eta_{PV,eL}$ (%)	$\eta_{PV/T,eL}$ (%)	$\Delta_{eL,in}$ (%)
Distilled. water	803	28.4	49.4	35.2	8.8	9.6	8.7
Graphene nanofluid	794	26.0	48.4	34.0	9.2	10.2	9.6
Hybrid nanofluid	742	24.5	48.0	34.0	8.9	9.8	9.2

Table 5.6. Average daily weather conditions, electrical increment, and cell temperature during the peak period.

Type of coolant	I_R (W m^{-2})	T_{amb} (C°)	$T_{S,PV}$ (C°)	$T_{S.PV/T}$ (C°)	$\eta_{PV,eL}$ (%)	$\eta_{PV/T,eL}$ (%)	$\Delta_{eL,in}$ (%)
Distilled. water	893	29.6	51.0	37.0	10.2	11.4	10.5
Graphene nanofluid	880	26.7	51.0	36.0	10.8	12.3	12.9
Hybrid nanofluid	831	25.0	49.4	35.5	10.5	11.7	11.0

5.5.4. Electrical Efficiency Increment

As mentioned previously, the PV/T and PV surface temperatures increased when the solar radiation increased from the beginning to the end of the experiments, which decreased the electric efficiency of the PV/T.

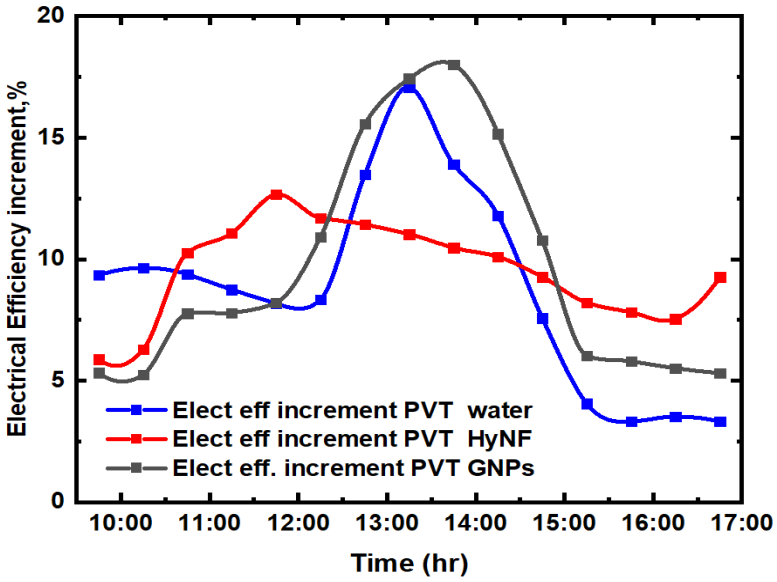

Figure 5.19. Daily average variations in electrical efficiency increment.

In such cases, the heat is gradually extracted with the coolant fluid at a high temperature, which increases the electrical efficiency. As shown in Figure 5.19, GNP is the most electrically efficient fluid coolant as compared to the rest of the coolants. This indicates that the GNP has higher thermal conductivity as compared to the other coolants, which results in faster heat disposal, which is obtained by Eq. (3.15). Table 5.5 and Table 5.6 summarize the average daily electrical increments for the day-long and peak durations.

From the results, which can be observed in Figure 5.21, we obtained the overall energetic efficiency for a photovoltaic PV/T collector and a conventional PV panel. It also shows that thermal efficiency affects the overall energetic efficiency more than the electrical efficiency. Moreover, the thermal efficiency variations during the test time did not follow any specific path, and this happened because there were variations in the experimental testing conditions such as ambient temperature, wind speed,

humidity, and solar radiation. The results are summarized in Table 5.7, which shows the average thermal and overall energetic efficiencies for a PV/T. Also, Table 5.7 shows the PV/T collector's average daily thermal efficiency when distilled water was used. It has a good agreement with the values, which Alous et al, [32] and Sardarabadi et al, [19] have reported.

5.5.5. Thermal and Overall Energetic Efficiency

In this study, we have calculated the overall energy efficiency applying Eq. (3.20) as Figure 5.21 shows. Since all the photovoltaic cells were in the collector area and they had a perfect contact, the packing factor is equal to 1. The results show that GNP are better than HyNFs and distilled water because they have higher thermal conductivity as well as overall energy efficiency. Moreover, it was noticed that during the day time, both the overall energy efficiency and the thermal efficiency increased, and it was found that the PV/T collector's energy was too close to the energy, which was generated using the values shown by GNP, which Alous et al. [18,32]have already mentioned and the values, which distilled water has shown were closer to the values, which were mentioned by Sardarabadi et al. [19]; however, several factors like wind speed, solar radiation changes, and changes in humidity affect the thermal energy efficiency and the thermal efficiency curve does not follow a specific trend, as shown in Figure 5.20. As a result, the averages of the daily overall energy efficiency for the day-long periods were 48.1%, 53.5% and 55.8% for distilled water, HyNFs, and GNP, respectively, and 50.1%, 58.9% and 64.4% respectively for distilled water, HyNF and GNP during the peak period.

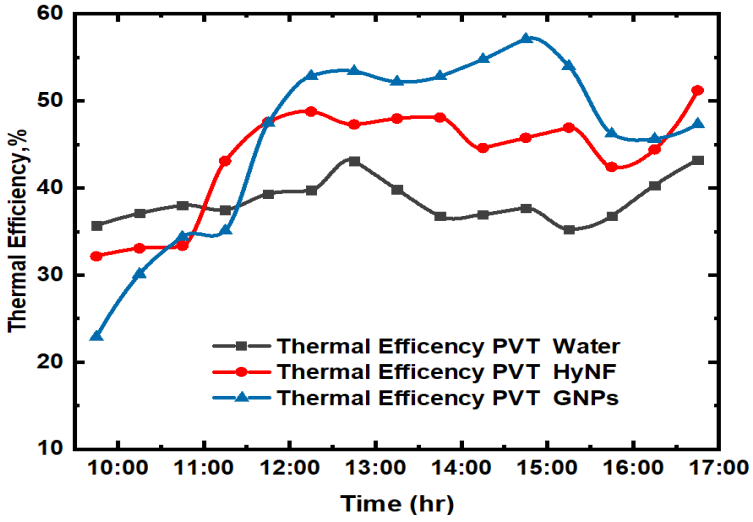

Figure 5.20. Average daily variation in thermal efficiencies for PV and PV/T.

The reference PV system showed 9.4% average overall efficiency when there was no collector (day-long period) and 10.7% for the peak period. This confirms that thermal cooling units should be used to increase the PV's overall energy efficiency. We used Eq. (3.8) to obtain the average daily thermal efficiency, which was 38.4% and 45.7% with PV/T for distilled water and GNP, respectively. These results were comparable to the values obtained in a study conducted by Alous et al. [32], who found respective values 38.8% and 47.4% for distilled water and GNP, which are compatible with the values given in Table 5.8. The result for every experiment depended on different situations like type of cooling, ambient temperature, and solar radiation intensity.

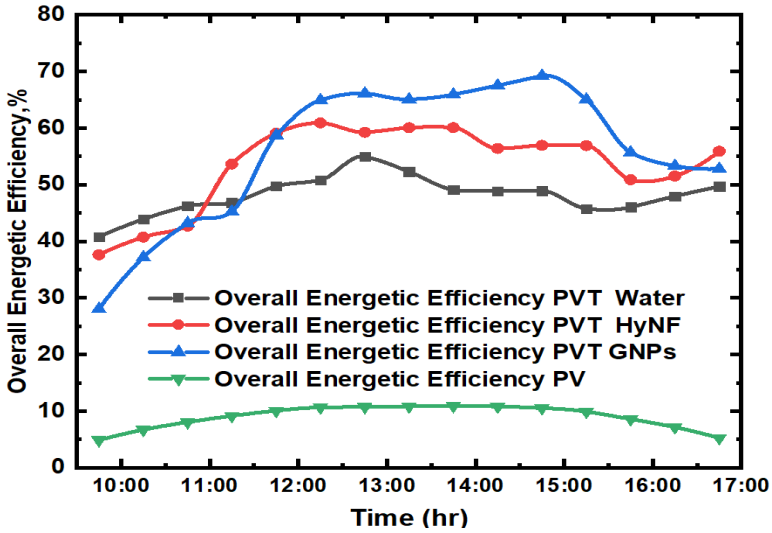

Figure 5.21. The variation in overall energetic efficiency for PV and PV/T.

In Table 5.8, we have presented a comparative summary of increments in energetic efficiencies in a hybrid nanofluid-cooled PV/T, and these values are based on the present study, which were confirmed using the previous literature. The table shows a clear and acceptable convergence between the experimental results of the current study and the previous literature. Minor differences in the results exist because of differences in experimental conditions (time and weather).

Table 5.7. Daily overall and thermal energetic efficiencies for PV/T using different coolants.

Type of Coolant	All day period		Peak period	
	η_{th} *(%)*	η_{ov} *(%)*	η_{th} *(%)*	η_{ov} *(%)*
Distilled. water	38.4	48.1	38.7	50.1
Graphene nanofluid	45.7	55.8	52.2	64.4
Hybrid nanofluid	43.7	53.5	47.3	58.9

Table 5.8 shows a comparison between the thermal efficiency found in this study and a previous study by Alous et al., who utilized a coolant consisting of graphene nanoplatelets-deionized water for a PV/T collector in the same weather conditions and location.

Furthermore, the solar collector transforms solar energy into thermal energy because of higher thermal efficiency, and it converts most of the obtained solar energy into thermal energy and the residual energy was converted into electricity.

Table 5.8 shows increment in thermal efficiency of Alous' study and in the current study, which confirms the graphene nano-platelet nanofluid, which increases the performance of a thermal-solar systems. The results obtained in our study in this context are similar to the results reported in Alous' study.

Table 5.8. The performance of energetic efficiency compared with other works.

Author:	Test conditions	The type of study	Working fluid	Electrical efficiency increments relative to PV.	Thermal/overall efficiency increment relative to PV/T-water
Alous, et all	Outdoor Test. Flow rate: 0.5L/m	Experimental	Water	8.5%	-
			Graphene-water 0.5wt%	9.0%	Improvement in thermal efficiency by 8.6% and in total efficiency by 9.7%.
This work	Outdoor Test. Flow rate: 0.5L/m	Experimental	Distilled Water	8.7%	
			Graphene-water 0.5wt%	9.6%	Improvement in thermal efficiency by 7.3% and total efficiency by 7.7%.
			Hybrid – water (GNP+Al_2O_3) 0.5wt%	9.2 %	Improvement in thermal efficiency by 5.3% and total efficiency by 5.4%.

We have conducted this investigation work because there were not many researchers who used graphene nanoplatelets nanofluid in the PV/T systems, and so far, no investigation work is based on hybrid nanofluids in PV/T systems to the best of the author's knowledge. In this case, the thermal efficiency of results of this study can be compared to another study, for which, graphene nanoplatelets-deionized water was used as a coolant in a PV solar collector. This study was conducted at 0.5L/m flow rate, at which, the thermal efficiency was 47.4% and 38.8% respectively for graphene nanoplatelets nanofluid and deionized water. This work analyzed the PV/T system's thermal efficiency when graphene nanoplatelets nanofluid and distilled water were used at 0.5 wt% concentration. The thermal efficiencies were 45.7% and 38.4% at 0.5L/m while 55.8% and 38.7% were the highest thermal efficiencies. The results of the highest thermal efficiency of this work and Alous' work agree to a certain extent.

In Table 5.9 shows the thermal energetic performance comparison between this study and Alous study, which the results revealed that the thermal efficiencies were (38.4%, 45.7%) and (38.8%, 47.4%) for distilled water and graphene nanofluid whereas the max thermal energies were (48.1%, 55.8%) and (53.4%, 63.1%) for distilled water and graphene nanofluid respectively. Moreover, the thermal efficiency increases were 7.3% for this study and 8.6% for Alous study while the max thermal energies were 7.7% for this study and 9.7% for Alous study.

Table 5.9. Thermal energetic performance comparison for graphene with different studies.

Item	This Study	Alous et al.
Setup used	PV/T collector	PV/T collector
Base fluid	Deionized water	Deionized water
Nanofluid concentration	Weight fraction 0.005	Weight fraction 0.005
Flow rate	0.5L/min	0.5L/min
Thermal efficiency Increment	1. Thermal efficiency for distilled water is 38.4%. 2. Thermal efficiency for graphene nanoplatelets nanofluid is 45.7%. 3. Thermal efficiency increase is 7.3%.	1. Thermal efficiency for deionized water is 38.8%. 2. Thermal efficiency for graphene nanoplatelets nanofluid is 47.4%. 3. Thermal efficiency increase is 8.6%.
Max. thermal efficiency	1. Max. thermal efficiency for distilled water is 48.1%. 2. Max. thermal efficiency for graphene nanofluid is 55.8%. 3. Max. thermal efficiency increase is 7.7%.	1. Max. thermal efficiency for distilled water is 53.4%. 2. Max. thermal efficiency for graphene nano-platelets nanofluid is 63.1%. 3. Max. thermal efficiency increase is 9.7%.

5.5.6. Exergetic Efficiency

It means the quality of energy the PV/T produces and it is considered as a significant improvement. The PV module and PV/T collector have shown certain exergetic efficiencies, which were calculated using Eq. (3.25) and Eq. (3.26). The daily electrical and thermal output exergy variations of the PV and PV/T using graphene nanoplatelets

nanofluid, distilled water, and hybrid nanofluid are displayed in Figure 5.22, Figure 5.23 and Figure 5.24. The figures clearly depict that the system's output thermal exergy is lower as compared to its output electrical exergy. This means that output quality of the system's thermal power is lower as compared to the PV/T's output exergetic efficiency. It happened because of a small difference, which happened between the coolant's outlet temperature (heat source) and the ambient temperature (heat sink). Furthermore, the obtained electrical energy has a higher quality because it can be transformed into work, which is unaffected by the surroundings when thermal energy is unable to produce the work, except for the situation when there is a temperature difference between the heat source and heat sink. During the experiment and peak periods, the average daily exergetic efficiency has been summarized in Table 5.10.

Table 5.10. Daily average of overall exegetic efficiency for PV and PV/T with different working fluids.

Type of coolant	All day period	Peak period
Distilled water	10.47%	12.4%
Graphene nanofluid	11.52%	14.0%
Hybrid nanofluid	10.94%	13.0%
PV	9.44%	11.14%

Table 5.10 illustrates that when a heat exchanger contacts with the absorber to the PV/T panel's backside and nanofluids are used as coolant fluids with proven high-thermal properties, it improves the energy quality and increases the energy efficiency, and that is shown through rise in the overall exergy efficiency. In this case, the results show that PV/T with GN/P has considerably higher exergy performance as compared to distilled water and HyN/F. In Table 5.10, it is obvious that the GN/P's overall exergy improvement for both all-day and peak periods exceeded HyN/F and distilled water in a conventional PV module.

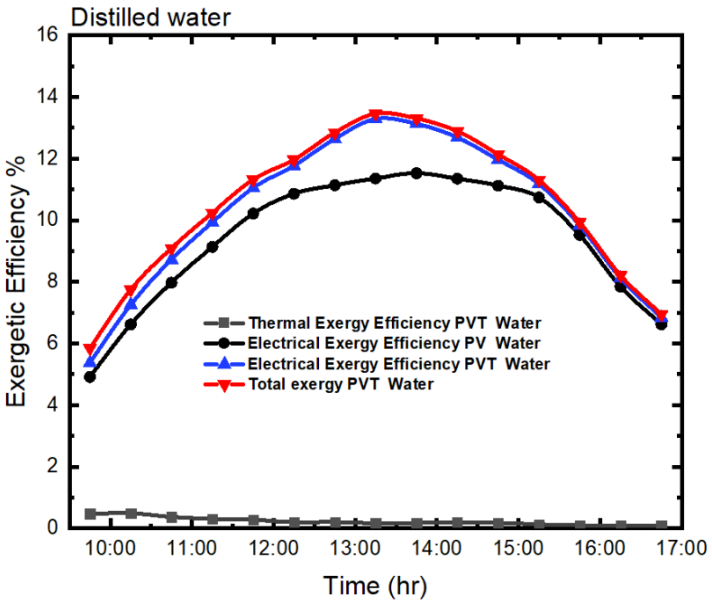

Figure 5.22. Variations in the exergy efficiency for PV module and PV/T using distilled water.

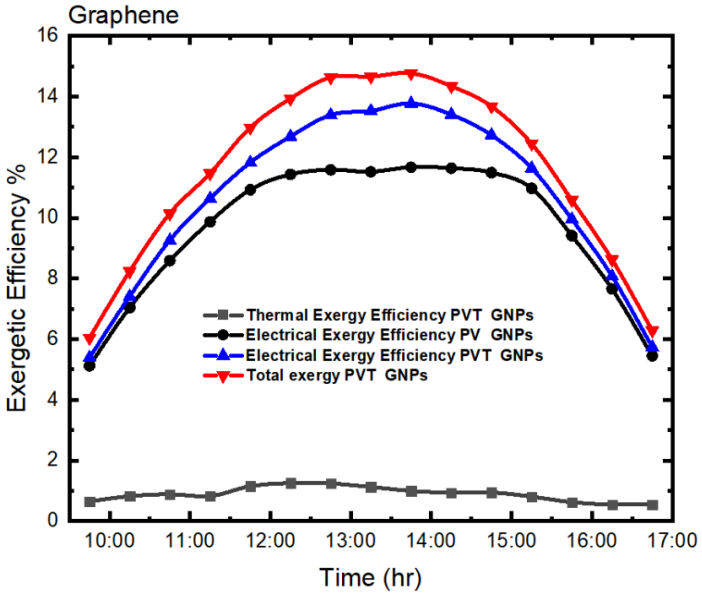

Figure 5.23. Variations in the exergy efficiency for a PV module and PV/T using graphene nano-platelets nanofluid.

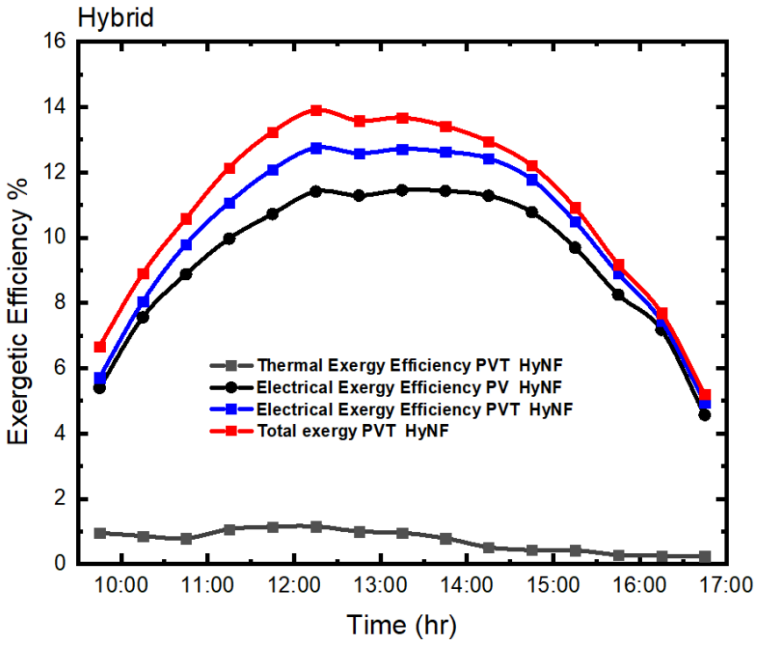

Figure 5.24. The variations in the exergy efficiency for PV module and PV/T using a hybrid nanofluid.

Table 5.11 clearly indicates the results of overall exergy enhancements through the all-day experiment and the peak period when there was a conventional PV module and a PV/T was used applying distilled water as a coolant. The enhancements were 21% and 15.6% for the graphene nanoplatelets nanofluid and hybrid nanofluid relative to the PV module and 9.8% and 4.4% relative to the PV/T distilled water module. Consequently, we found that the graphene nanofluid performs better than the hybrid nanofluid.

Table 5.11. The enhancement of overall exergy efficiency for PV and PV/T.

Type of Coolant.	All day period		Peak period	
	PV	PV/T-water	PV	PV/T-water
PV/T – distilled water	11.2%	-	11.0%	-
PV/T - GNP	21.0%	9.8%	24.0%	13%
PV/T - HyNF	15.6%	4.4%	14.7%	3.7%

CHAPTER 6

CONCLUSIONS AND RECOMMENDATIONS

6.1. CONCLUSIONS

This study was conducted with a main objective of providing in-depth comprehension on how to obtain substantial benefit from the PV/T systems and collector devices keeping in view changes in time, weather, and demand for renewable energies. We designed an experimental setup, and some parts of the apparatus were manufactured at the Energy Labs, Karabuk University for investigating the impact of using hybrid as well as graphene nanoplatelets-water nanofluids as coolants, and then we tested the performances of PV/T collector and the results of the experiments were compared to the results of PV/T water collector and conventional PV module. The photovoltaic collector and PV/T were built with serpentine heat exchanger and a square-shaped tube, which were installed in an experimental test setup. All data like flow rate, voltage, current, temperatures (surface temperature, inlet & outlet temperatures), and solar radiation for PV conventional and PV/T collector were measured and analyzed to obtain the required results. On the other hand, the comparison was conducted between coolants, which were used in this study. They include distilled water, 0.5wt% graphene nano-platelet-water nanofluid concentration, and 0.5wt% hybrid-water nanofluid.

After conducting all the experiments for all the coolants with 0.5wt% concentration and 0.5L/m flow rate, the obtained results are as follows:

- 0.5 L/min flow rate for initial tests showed better stability for thermal power during the period of experiment, for which we are chosen to be the main flow rate used in the all experiments.

- Several experiments have been neglected due to unstable climatic conditions, for example, clouds and rains. Some malfunctions were detected in some devices, which were connected to the system, and they lost some results that should have been obtained but there were some critical problems.
- Coolant fluids were tested, including nanofluids and distilled water through a cooling module, which reduced the maximum cell temperature for a PV/T system by approximately 14.2°C, 14.4°C and 14°C for distilled water, HyNF and GNP, respectively.
- The overall energy efficiency was enhanced by 5.4% and 7.7% for the HyNF and GNP nanofluid as compared to the distilled water.
- The highest electrical power generation level was observed when GNP nanofluid was used for cooling.
- A PV/T system's thermal efficiency increased by nearly 5.3% and 7.3% more than the distilled water for HyNF and GNP nanofluids, respectively. It showed that the graphene nano-platelet nanofluid is better than the thermal efficiency of the other two fluids.
- In PV/T systems, the nanotechnology is in the form of nanoparticles, which is useful for hybrid systems as a coolant in comparison with distilled water.
- In PV panels, the cooling apparatus is installed in the heat exchanger on the back side of a PV panel, which improved the overall exergy efficiencies of PV/T-distilled water, GNP, and HyNF by 11.2%, 21%, and 15.6% respectively.
- After completing the study that was carried out to emphasize the importance and effectiveness of using nanofluids in cooling PV/T collectors compared to other cooling methods (water and air). It was found that nanofluids increase the efficiency of solar collectors at a high rate and they have the ability to reduce the surface temperature by extracting heat from the collectors; so, studying the effects of nanofluids will cover the PV/T collectors more extensively and provide sources to fill the knowledge gap.

6.2. RECOMMENDATIONS

Keeping in view the results obtained in this study, other aspects of power generation and efficiency should be studied to improve the knowledge and to increase the efficiency and performance of solar collectors, which are mentioned as follows:

- The use of other types of nanofluids especially with high thermal properties may provide better results.
- The use of different configurations of heat exchangers improves the conductivity of cooling fluids, which leads to getting the best results.
- Adding fins with the heat exchanger enhances the performance of the solar collector, which might improve efficiency.
- There is a possibility to use other types of the heat exchanger materials such as quartz, stainless steel, and Pyrex glass, which should be considered.
- 0.5% concentration was used in this study, so in future work, different other concentrations could be studied to achieve higher efficiency of solar collectors.
- Continuing to do laboratory experiments using nanotechnology expands the understanding of the importance of using nanofluids in solar collectors.
- Making new sorts of hybrid nanofluids by using different types of materials with high thermal properties enhance efficiencies of the PV/T collectors.

REFERENCES

1. Senniangiri, N., Bensam Raj, J., and Sunil, J., "Effects of Temperature and Particles Concentration on the Dynamic Viscosity of Graphene-NiO/Coconut Oil Hybrid Nanofluid: Experimental Study", ***International Journal Of Nanoscience***, 1950016 (2019).

2. Zenhäusern, D., Bamberger, E., Baggenstos, A., and Häberle, A. %J F. R., "PV/T Wrap-Up: Energy Systems with Photovoltaic-Thermal Solar Collectors", 31: (2017).

3. Lämmle, M., Oliva, A., Hermann, M., Kramer, K., and Kramer, W. %J S. E., "PV/T collector technologies in solar thermal systems: A systematic assessment of electrical and thermal yields with the novel characteristic temperature approach", 155: 867–879 (2017).

4. Brottier, L., "Optimisation biénergie d'un panneau solaire multifonctionnel: du capteur aux installations in situ", ***Université Paris-Saclay***, (2019).

5. Kalogirou, S. A., "Solar Energy Engineering: Processes and Systems", ***Academic Press***, (2013).

6. Santbergen, R., van Zolingen, R. J. C. %J S. energy materials, and cells, solar, "The absorption factor of crystalline silicon PV cells: A numerical and experimental study", 92 (4): 432–444 (2008).

7. Dupeyrat, P., Ménézo, C., Fortuin, S. %J E., and Buildings, "Study of the thermal and electrical performances of PV/T solar hot water system", 68: 751–755 (2014).

8. Guarracino, I., "Hybrid photovoltaic and solar thermal (PV/T) systems for solar combined heat and power", (2017).

9. Imenes, A. G., Mills, D. R. %J S. energy materials, and cells, solar, "Spectral beam splitting technology for increased conversion efficiency in solar concentrating systems: a review", 84 (1–4): 19–69 (2004).

10. Sandnes, B. and Rekstad, J. %J S. E., "A photovoltaic/thermal (PV/T) collector with a polymer absorber plate. Experimental study and analytical model", 72 (1): 63–73 (2002).

11. An, W., Zhang, J., Zhu, T., and Gao, N. %J R. energy, "Investigation on a spectral splitting photovoltaic/thermal hybrid system based on polypyrrole nanofluid: preliminary test", 86: 633–642 (2016).

12. Pang, W., Cui, Y., Zhang, Q., Wilson, G. J., Yan, H. %J R., and Reviews, S. E., "A comparative analysis on performances of flat plate photovoltaic/thermal collectors in view of operating media, structural designs, and climate conditions", 119: 109599 (2020).

13. Lämmle, M., Herrando, M., and Ryan, G., "Basic Concepts of PV/T Collector Technologies, Applications and Markets IEA SHC Task 60/Report D5", (2021).

14. Lämmle, M., Kroyer, T., Fortuin, S., Wiese, M., and Hermann, M. %J S. E., "Development and modelling of highly-efficient PV/T collectors with low-emissivity coatings", 130: 161–173 (2016).

15. Dupeyrat, P., "Experimental development and simulation investigation of a Photovoltaic-Thermal hybrid solar collector", ***Lyon, INSA***, (2011).

16. Sridhara, V. and Satapathy, L. N. %J N. research letters, "Al 2 O 3-based nanofluids: a review", 6 (1): 1–16 (2011).

17. Akoh, H., Tsukasaki, Y., Yatsuya, S., and Tasaki, A. %J J. of C. G., "Magnetic properties of ferromagnetic ultrafine particles prepared by vacuum evaporation on running oil substrate", 45: 495–500 (1978).

18. Alous, S., Kayfeci, M., and Uysal, A., "Experimental study about utilization of MWCNTs and graphene nanoplatelets water-based nanofluids in flat non-concentrating PV/T systems", ***Thermal Science***, (00): 337 (2019).

19. Sardarabadi, M., Passandideh-Fard, M., and Heris, S. Z., "Experimental investigation of the effects of silica/water nanofluid on PV/T (photovoltaic thermal units)", ***Energy***, 66: 264–272 (2014).

20. Ghadiri, M., Sardarabadi, M., Pasandideh-fard, M., and Moghadam, A. J., "Experimental investigation of a PV/T system performance using nano ferrofluids", ***Energy Conversion And Management***, 103: 468–476 (2015).

21. Sardarabadi, M. and Passandideh-Fard, M., "Experimental and numerical study of metal-oxides/water nanofluids as coolant in photovoltaic thermal systems (PV/T)", ***Solar Energy Materials And Solar Cells***, 157: 533–542 (2016).

22. Sardarabadi, M., Hosseinzadeh, M., Kazemian, A., and Passandideh-Fard, M. %J E., "Experimental investigation of the effects of using metal-oxides/water nanofluids on a photovoltaic thermal system (PV/T) from energy and exergy viewpoints", 138: 682–695 (2017).

23. Al-Waeli, A. H. A., Sopian, K., Chaichan, M. T., Kazem, H. A., Hasan, H. A., and Al-Shamani, A. N., "An experimental investigation of SiC nanofluid as a base-fluid for a photovoltaic thermal PV/T system", ***Energy Conversion And Management***, 142: 547–558 (2017).

24. Mat, S. and Ruslan, M. H., "Comparison study of indoor/outdoor experiments of a photovoltaic thermal PV/T system containing SiC nanofluid as a coolant", ***Energy***, (2018).

25. Ebaid, M. S. Y., Ghrair, A. M., and Al-Busoul, M., "Experimental investigation of cooling photovoltaic (PV) panels using (TiO2) nanofluid in water-polyethylene glycol mixture and (Al2O3) nanofluid in water-cetyltrimethylammonium bromide mixture", ***Energy Conversion And Management***, 155: 324–343 (2018).

26. Sardarabadi, M., Passandideh-Fard, M., Maghrebi, M.-J., and Ghazikhani, M., "Experimental study of using both ZnO/water nanofluid and phase change material (PCM) in photovoltaic thermal systems", ***Solar Energy Materials And Solar Cells***, 161: 62–69 (2017).

27. Nasrin, R., Rahim, N. A., Fayaz, H., and Hasanuzzaman, M., "Water/MWCNT nanofluid based cooling system of PV/T: Experimental and numerical research", ***Renewable Energy***, 121: 286–300 (2018).

28. Gao, Y., Xi, Y., Zhenzhong, Y., Sasmito, A. P., Mujumdar, A. S., and Wang, L., "Experimental investigation of specific heat of aqueous graphene oxide Al2O3 hybrid nanofluid", ***Thermal Science***, (00): 381 (2019).

29. Iranmanesh, S., Ong, H. C., Ang, B. C., Sadeghinezhad, E., Esmaeilzadeh, A., and Mehrali, M., "Thermal performance enhancement of an evacuated tube solar collector using graphene nanoplatelets nanofluid", ***Journal Of Cleaner Production***, 162: 121–129 (2017).

30. Al-Waeli, A. H. A., Chaichan, M. T., Sopian, K., Kazem, H. A., Mahood, H. B., and Khadom, A. A. %J S. E., "Modeling and experimental validation of a PV/T system using nanofluid coolant and nano-PCM", 177: 178–191 (2019).

31. Vakili, M., Hosseinalipour, S. M., Delfani, S., Khosrojerdi, S., and Karami, M., "Experimental investigation of graphene nanoplatelets nanofluid-based volumetric solar collector for domestic hot water systems", ***Solar Energy***, 131: 119–130 (2016).

32. Alous, S., Kayfeci, M., and Uysal, A., "Experimental investigations of using MWCNTs and graphene nanoplatelets water-based nanofluids as coolants in PV/T systems", ***Applied Thermal Engineering***, 162: 114265 (2019).

33. Hussein, H. A., Numan, A. H., and Abdulrahman, R. A., "Improving the Hybrid Photovoltaic/Thermal System Performance Using Water-Cooling Technique and Zn-H2O Nanofluid", ***International Journal Of Photoenergy***, 2017: (2017).

34. Al-Shamani, A. N., Sopian, K., Mat, S., Hasan, H. A., Abed, A. M., and Ruslan, M. H., "Experimental studies of rectangular tube absorber photovoltaic thermal collector with various types of nanofluids under the tropical climate conditions", ***Energy Conversion And Management***, 124: 528–542 (2016).

35. Al-Waeli, A. H. A., Chaichan, M. T., Kazem, H. A., and Sopian, K., "Comparative study to use nano-(Al2O3, CuO, and SiC) with water to enhance photovoltaic thermal PV/T collectors", ***Energy Conversion And Management***, 148: 963–973 (2017).

36. Hosseinzadeh, M., Salari, A., Sardarabadi, M., and Passandideh-Fard, M., "Optimization and parametric analysis of a nanofluid based photovoltaic thermal system: 3D numerical model with experimental validation", ***Energy Conversion And Management***, 160 (October 2017): 93–108 (2018).

37. Fayaz, H., Nasrin, R., Rahim, N. A., and Hasanuzzaman, M., "Energy and exergy analysis of the PV/T system: Effect of nanofluid flow rate", ***Solar Energy***, 169: 217–230 (2018).

38. Abdallah, S. R., Saidani-Scott, H., and Abdellatif, O. E. %J S. E., "Performance analysis for hybrid PV/T system using low concentration MWCNT (water-based) nanofluid", 181: 108–115 (2019).

39. Sangeetha, M., Manigandan, S., Chaichan, M. T., and Kumar, V., "Progress of MWCNT, Al2O3, and CuO with water in enhancing the photovoltaic thermal system", ***International Journal Of Energy Research***, (2019).

40. Hassan, A., Wahab, A., Qasim, M. A., Janjua, M. M., Ali, M. A., Ali, H. M., Jadoon, T. R., Ali, E., Raza, A., and Javaid, N., "Thermal management and uniform temperature regulation of photovoltaic modules using hybrid phase change materials-nanofluids system", ***Renewable Energy***, 145: 282–293 (2020).

41. Lari, M. O. and Sahin, A. Z., "Effect of retrofitting a silver/water nanofluid-based photovoltaic/thermal (PV/T) system with a PCM-thermal battery for residential applications", ***Renewable Energy***, 122: 98–107 (2018).

42. Daverat, C., Pabiou, H., Menezo, C., Bouia, H., and Xin, S., "Experimental investigation of turbulent natural convection in a vertical water channel with symmetric heating: Flow and heat transfer", ***Experimental Thermal And Fluid Science***, 44: 182–193 (2013).

43. Salem, M. R., Elsayed, M. M., Abd-Elaziz, A. A., and Elshazly, K. M. %J R. E., "Performance enhancement of the photovoltaic cells using Al2O3/PCM mixture and/or water cooling-techniques", 138: 876–890 (2019).

44. Aberoumand, S., Ghamari, S., and Shabani, B. %J S. E., "Energy and exergy analysis of a photovoltaic thermal (PV/T) system using nanofluids: An experimental study", 165: 167–177 (2018).

45. Abdallah, S. R., Elsemary, I. M. M., Altohamy, A. A., Abdelrahman, M. A., Attia, A. A. A., and Abdellatif, O. E., "Experimental investigation on the effect of using nano fluid (Al2O3-Water) on the performance of PV/T system", ***Thermal Science And Engineering Progress***, 7: 1–7 (2018).

46. Ibrahim, A., Othman, M. Y., Ruslan, M. H., Mat, S., Sopian, K. %J R., and reviews, sustainable energy, "Recent advances in flat plate photovoltaic/thermal (PV/T) solar collectors", 15 (1): 352–365 (2011).

47. Hu, C. and White, R. M., "Solar cells: from basic to advanced systems", (1983).

48. Drew, D. A. and Passman, S. L., "Classical Theory of Solutions", Theory of Multicomponent Fluids, ***Springer***, 59–61 (1999).

49. Pak, B. C. and Cho, Y. I., "Hydrodynamic and heat transfer study of dispersed fluids with submicron metallic oxide particles", ***Experimental Heat Transfer An International Journal***, 11 (2): 151–170 (1998).

50. Xuan, Y. and Roetzel, W., "Conceptions for heat transfer correlation of nanofluids", ***International Journal Of Heat And Mass Transfer***, 43 (19): 3701–3707 (2000).

51. Nadooshan, A. A., Eshgarf, H., and Afrand, M., "Measuring the viscosity of Fe3O4-MWCNTs/EG hybrid nanofluid for evaluation of thermal efficiency: Newtonian and non-Newtonian behavior", ***Journal Of Molecular Liquids***, 253: 169–177 (2018).

52. Khanjari, Y., Pourfayaz, F., and Kasaeian, A. B., "Numerical investigation on using of nanofluid in a water-cooled photovoltaic thermal system", ***Energy Conversion And Management***, 122: 263–278 (2016).

53. Al-Oran, O., Lezsovits, F., and Aljawabrah, A., "Exergy and energy amelioration for parabolic trough collector using mono and hybrid nanofluids", ***Journal Of Thermal Analysis And Calorimetry***, 1–18 (2020).

54. Maxwell-Garnett, J. C., " Colours in metal glasses and in metallic films", ***Fill. Trans***, 203: 385–420 (1904).

55. Chow, T. T., Pei, G., Fong, K. F., Lin, Z., Chan, A. L. S., and Ji, J., "Energy and exergy analysis of photovoltaic–thermal collector with and without glass cover", ***Applied Energy***, 86 (3): 310–316 (2009).

56. Tiwari, A. and Sodha, M. S. %J S. energy, "Performance evaluation of solar PV/T system: an experimental validation", 80 (7): 751–759 (2006).

57. Zondag, H. A., de Vries, D. W. de, Van Helden, W. G. J., van Zolingen, R. J. C., and Van Steenhoven, A. A. %J S. energy, "The thermal and electrical yield of a PV-thermal collector", 72 (2): 113–128 (2002).

58. Kumar, R. and Rosen, M. A. %J A. T. E., "Performance evaluation of a double pass PV/T solar air heater with and without fins", 31 (8–9): 1402–1410 (2011).

59. Y.A. Çengel, M. A. B., "Thermodynamic: An Engineering Approach.", ***Mc Graw-Hill Education***, (2015).

60. Farzanehnia, A. and Sardarabadi, M., "Exergy in Photovoltaic/Thermal Nanofluid-Based Collector Systems", Exergy and Its Application-Toward Green Energy Production and Sustainable Environment, ***IntechOpen***, (2019).

61. Jeter, S. M., "Maximum conversion efficiency for the utilization of direct solar radiation", ***Solar Energy***, 26 (3): 231–236 (1981).

62. Hepbasli, A., "A key review on exergetic analysis and assessment of renewable energy resources for a sustainable future", ***Renewable And Sustainable Energy Reviews***, 12 (3): 593–661 (2008).

63. De Vries, D. W., "Design of a photovoltaic/thermal combi-panel", (1998).

64. Jia, Y., Ran, F., Zhu, C., and Fang, G., "Numerical analysis of photovoltaic-thermal collector using nanofluid as a coolant", ***Solar Energy***, 196: 625–636 (2020).

RESUME

Omran Alshikhi completed primary and elementary education in the Alasaba city in the Western Mountain. In 2004, he graduated from Marine Engineering Department, Arab Academy for science and technology and maritime transport, in Alexandria, Egypt. In 2005, he started master degree in same Academy. In 2009 he a master's degree in (Computerized maintenance management system (CMMS)). In the period 2010-2015 he worked as full-time lecturer at Tripoli University in Marine and offshore Department, faculty of Engineering, from which he got a scholarship to continue his PhD education. In 2016 he commenced his PhD academic program at Karabuk University in Department of Energy Systems and started his PhD thesis research.